

## Liquid-liquid extraction systems types

Liquid–liquid extraction, also known as solvent extracting, is a well-established separation technique that depends on the unequal distribution of a solute between two immiscible liquids. The initial feed liquid containing the solute is brought into contact with a solvent that is selected to have a greater affinity for the solute. The partition of the solute can be enhanced by adding a chemical extractant to the solvent; this practice is widespread in the hydrometallurgical and nuclear industries. Most industrial extractors operate continuously with a countercurrent flow of the two phases. In mixer–settlers, the phases are contacted as a well-agitated dispersion of drops, which are then sent to settling tanks for phase disengagement. In extraction columns, the dispersed drops move counter currently against the flow of the second (continuous) phase. The physics, chemistry, and practice of extraction, with brief descriptions of important industrial extraction processes and equipment, are presented. Research on hydrodynamic aspects of process design, eg, axial mixing, drop dispersion, and coalescence, is reviewed.

### Commercial Extractors

Extractors can be classified according to the methods applied for interdispersing the phases and producing the countercurrent flow pattern. Figure 1 summarizes the classification of the principal types of commercial extractors; Table 1 summarizes the main characteristics. [1]

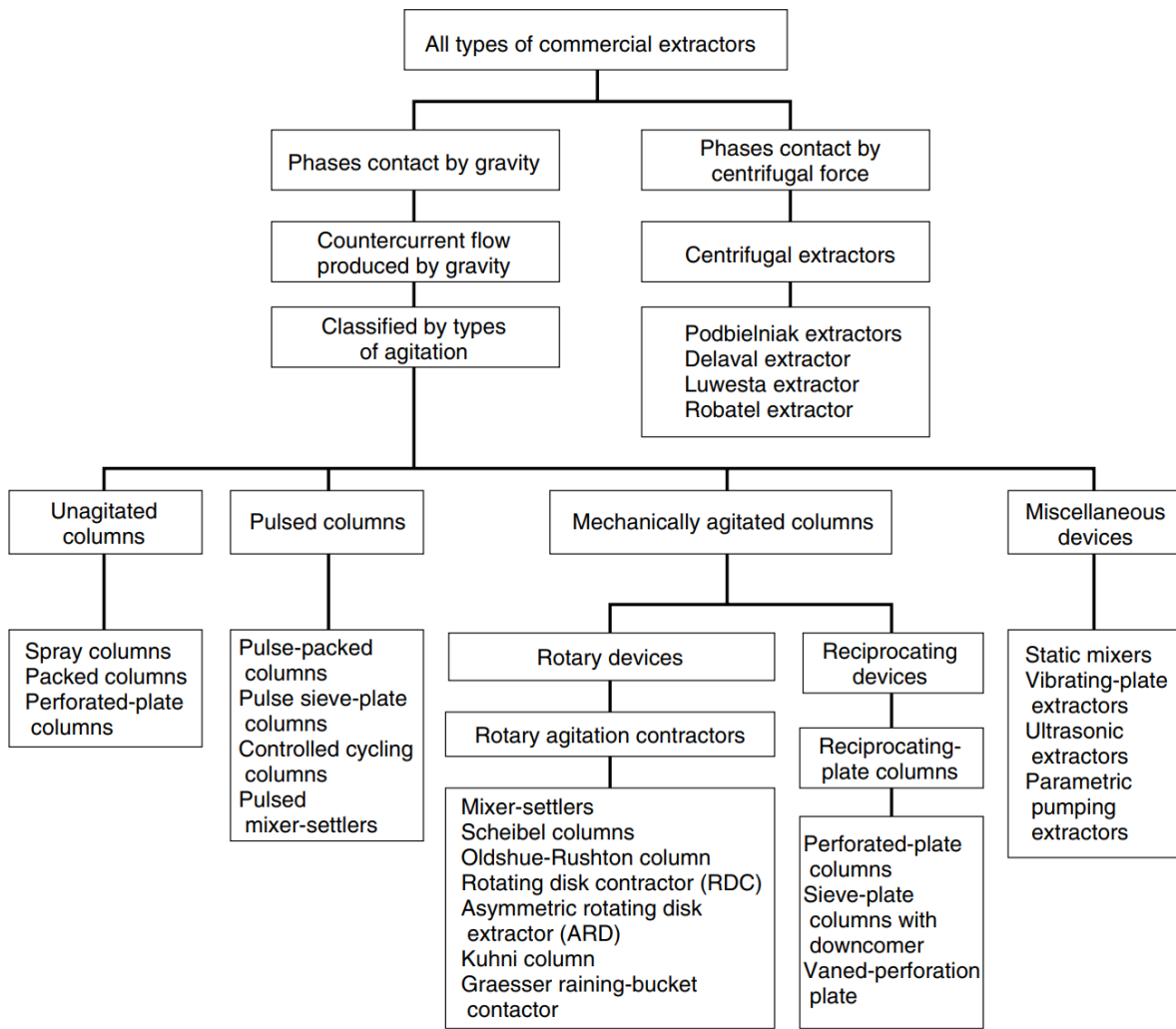


Fig. 1. Classification of commercial extractors.[1]

Table 1. Summary of Commercial Extractors[1]

Types of extractor	General features <sup>a</sup>	Fields of industrial application
unagitated columns	low capital cost, low operating and maintenance cost, simplicity in construction, handles corrosive material	petrochemical, chemical
mixer-settlers	high stage efficiency, handles wide solvent ratios, high capacity, good flexibility, reliable scale-up, handles liquids with high viscosity	petrochemical, nuclear, fertilizer, metallurgical
pulsed columns	low HETS, no internal moving parts, many stages possible	nuclear, petrochemical, metallurgical
rotary agitation columns	reasonable capacity, reasonable HETS, many stages possible, reasonable construction cost, low operating and maintenance cost	petrochemical, metallurgical, pharmaceutical, fertilizer
reciprocating-plate columns	high throughput, low HETS, great versatility and flexibility, simplicity in construction, handles liquids containing suspended solids, handles mixtures with emulsifying tendencies	pharmaceutical, petrochemical, metallurgical, chemical
centrifugal extractors	short contacting time for un-stable material, limited space required, handles easily emulsified material, handles systems with little liquid density difference	pharmaceutical, nuclear, petrochemical

<sup>a</sup>Height of an equivalent theoretical stage = HETS.

New extraction techniques, eg, membrane extraction, supercritical extraction, and two-phase aqueous extraction, are that in this research has been evaluated two-phase aqueous extraction or liquid-liquid extraction in Mechanically Agitated Columns.

### Mechanically Agitated Columns

#### Rotary Agitated Columns

Because of the mechanical advantages of rotary agitation, most modern differential contactors employ this method. The best known of the commercial rotary agitated contactors are shown in Figure 2. Features and applications of these columns are given in Table 1. In the Scheibel column, developed in 1948, every alternate compartment is agitated by an impeller, and the

unagitated compartments are packed with open woven wire mesh. Capacity and mass-transfer data are given in the literature. A newer type of Scheibel column (Fig. 2) using horizontal baffles with or without wire mesh packing was developed in 1956. Performance data for a 30.5-cm column, with or without wire mesh packing, have shown that the HETS varies as the square root of diameter. A third design is similar, but a pumping impeller instead of a turbine is used in the mixing stage. Scale-up and performance of a 1.47-m Scheibel column have been reported, as have detailed description and design criteria for the Scheibel column and scale-up procedures.[1]

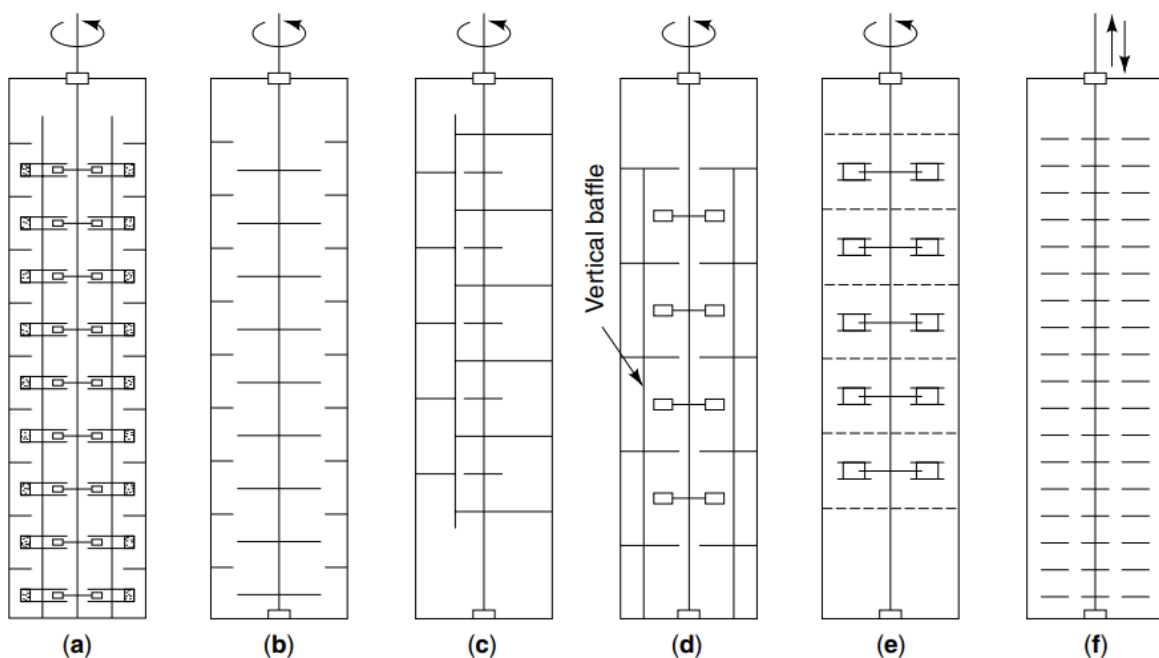


Fig. 2. Mechanically agitated columns: (a) Scheibel column; (b) rotating-disk contactor (RDC); (c) asymmetric rotating-disk (ARD) contactor; (d) Oldshue–Rushton multiplemixer column; (e) Kuhni column; and (f) reciprocating-plate column.[1]

### Studies of Drop Behavior and Prediction of Sauter Mean Drop Diameter in Various Rotary Agitated Extraction Columns

Knowledge of droplet behavior is one of the most important criteria for determination of mass transfer kinetics for choosing the type of liquid-liquid extraction columns. Mean drop size data

of dispersed phase droplets in continuous phase were obtained for various rotary agitated liquid-liquid extraction columns. The effects of operational variables such as rotor speed and dispersed and continuous phase velocities were investigated. In addition, the effect of mass transfer direction was studied on the Sauter mean drop diameter. The Sauter mean drop diameter was influenced mainly by mass transfer direction and agitation speed. In this research work, previous experimental works in agitated extraction columns (RDC, ARDC, PRDC, Scheibel, Oldshue-Rushton and Kühni columns) are reviewed. Calculations with the literature correlations cannot predict experimental data, thus unified correlations considering the physical properties, operating conditions and geometric parameters were provided to predict the mean drop size ( $d_{32}$ ). The results of the proposed correlation were compared with the experimental data obtained from the literature and the present investigation. This correlation covers several physical systems for various rotary agitated extractors. Findings of this study demonstrated that the proposed correlation leads to an accurate prediction for the Sauter mean drop diameter in rotary extraction columns. [2]

In the industry, a great variety of different equipment designs is used in extraction processes. Mixing in these columns generates a large interfacial area with efficient mass transfer of the desired solute between the two immiscible liquids. The rotating disc contactor (RDC) consists of a number of compartments formed by a series of stator rings, with a rotating disk centered in each compartment and supported by a common rotatingshaft. A modification of this design is the asymmetrical rotating disc contactor (ARDC). The asymmetrical stator consists of trays and baffles to divide the column into extraction zones and linked transfer zones. The extraction zone is limited by the stator partition and is separated by the trays into chambers. Phase transport and separation takes place in the settling zone behind the partition. The other modification of the RDC column was investigated using sieve discs in the column. The effect of perforation in these columns leads to a better performance and better liquid–liquid dispersion

in comparison with RDC columns. The Scheibel column extractor consists of a vertical shell divided into a number of compartments by annular partition discs. A set of double bladed paddle or turbine impellers was used as a central agitator shaft. The Oldshue-Rushton column consists of a number of compartments separated by horizontal stator-ring baffles, each fitted with vertical baffles and turbine type impeller mounted on a central shaft. The Kühni column is also similar to the Scheibel column, but does not contain any packing. The principal features of the column are the use of a shrouded turbine impeller to promote radial discharge within the compartments. Knowledge of droplet behavior is one of the most important criteria for determination of mass transfer kinetics for choosing the type of extraction equipment. In addition, viscosity and surface tension are the criteria for the agitation energy needed to disperse a phase and these parameters have main effect on the droplet size in agitation extraction columns. A number of correlations have been proposed to predict the mean drop size in liquid–liquid extraction columns using different columns and systems. Kumar and Hartland suggested two correlations for low and high rotor speed for RDC column. A unified correlation for prediction of the drop size in mechanically agitated columns, namely Kühni, rotating disc, asymmetric rotating disc and Wirtz-II was reported by Kumar and Hartland [3]. Different correlations for Sauter mean drop diameter are shown in Table 2. However, no reliable equation for the prediction of drop diameter in all agitated contactors has been proposed so far. The aim of this research work is to acquire a sufficient understanding of drop behavior in rotary agitated columns in order to obtain basic data required for design of extraction columns. Drop size in two rotary agitated columns (OldshueRushton and Kühni columns) has been studied by changing the operating parameters such as disperse and continuous phase flow rates and agitation speed. The results are discussed and compared with the predicted values from several available data and correlations in the literature for rotary agitated columns. Finally, two correlations are proposed for prediction of Sauter mean drop diameter with the experimental

data from Oldshue-Rushton and Kühni columns and other experimental data in the literature.[2]

TABLE 2. Unified correlations for prediction of the drop size in mechanically agitated columns[2]

Equation	Column type
Tsouris et al., 1990 [19] (1) $\frac{d_{32}}{d_R} = 90.7 \left( \frac{h_c}{H} \right)^{-0.13} \left( \frac{V_i^2 d_R \rho_m}{\sigma_i} \right)^{-0.39} \left( \frac{V_k}{V_i} \right)^{0.4} \varphi^{-0.31}$	Oldshue-Rushton column
Moreira et al., 2005 [20] (2) $d_{32} = 1.858 + 13631 Q_d - 0.676 h^2 + 27.36 (Q_d h)^{0.2} - 0.0667 (Nh)^{1.3} + \frac{3.871}{h + 10^6 Q_d}$	RDC column
Al-Rahawi et al., 2008 [21] (3) $d_{32} = 0.705 \left( \frac{\sigma}{g \Delta \rho} \right)^{0.5} \frac{D_h^{0.8} (Q_c / Q_d)^{0.15}}{N^{0.185} (Q_c + Q_d)^{0.1}}$	RDC column
Oliveira et al., 2008 [22] (4) $d_{32} = (5.43 \pm 0.35) - (1.38 \pm 0.22) N_R + [(0.57 \pm 0.15) - (0.1 \pm 0.02) E] Q_c N_R$	Kühni column
Kadam et al., 2009 [10] (5) $d_{32} = 0.194 \left( \frac{P}{V} \right)^{0.45} \sigma^{0.77} (\rho_c \mu_c)^{-0.3} \left( \frac{\mu_d}{\mu_c} \right)^{0.07}$	ARDC column
Yuan et al., 2012 [23] (6) $\frac{d_{32}}{D_b} = 0.51 \left( \frac{Q_d}{ND_b^3} \right)^{0.09} \left( \frac{\mu_c}{\mu_d} \right)^{0.25} \left( \frac{\Delta \rho}{\rho_d} \right)^{-2.4} \left( \frac{ND_d^2 \rho_d}{\mu_d} \right)^{-0.63} \left( \frac{\sigma}{ND_b \mu_d} \right)^{0.46}$	Scheibel column
Yuan et al., 2014 [24] (7) $\frac{d_{32}}{D_b} = 4.65 \left( \frac{Q_d}{ND_b^3} \right)^{0.26} \left( \frac{\mu_c}{\mu_d} \right)^{0.33} \left( \frac{\Delta \rho}{\rho_d} \right)^{-1.35} We^{-0.79} \quad Re \geq 2500$ $\frac{d_{32}}{D_b} = 4.03 \left( \frac{Q_d}{ND_b^3} \right)^{0.151} \left( \frac{\mu_c}{\mu_d} \right)^{0.01} \left( \frac{\Delta \rho}{\rho_d} \right)^{-0.371} Re^{-0.05} We^{-0.714} \quad 0 \leq Re \leq 2500$	Scheibel column
Hemmati et al., 2015 [25] (8) $d_{32} = 10 \left( \frac{N^4 d_R^4 \rho_c}{\sigma g} \right)^{-0.3} \left( \frac{\mu_c^4 g}{\Delta \rho \sigma^3} \right)^{0.09} \left( 1 + \frac{V_c}{V_d} \right)^{-0.4}$	PRDC column

## **Case study (n-butanol–water, n-butyl acetate–water and toluene–water systems)**

Studied systems were n-butanol–water, n-butyl acetate–water and toluene–water in the experiments without mass transfer. Two systems involving toluene-acetone (3.5%)-water and n-butyl acetate–acetone (3.5%)-water were used in the experiments with two directions of mass transfer. The data analysis was divided into three cases: no solute transfer; solute transfer from the continuous (c) to the dispersed (d) phase, and solute transfer from the (d) to the (c) phase. These liquid–liquid systems have been recommended by the European Federation of Chemical Engineering as official test systems for investigation of extraction. Distilled water was used as the continuous phase and technical grade of toluene; n-butyl acetateand n-butanol were used as the dispersed phase. The physical properties of the chemical systems are given in Table 3.

TABLE 3. Physical properties of systems studied at 20 °C [2]

<b>Physical property</b>	<b>Toluene-Water</b>	<b>n-Butyl acetate-Water</b>	<b>n-Butanol-Water</b>
$\rho_c$ [kg/m <sup>3</sup> ]	998.2	997.6	985.6
$\rho_d$ [kg/m <sup>3</sup> ]	865.2	880.9	846.0
$\mu_c$ [mPa.s]	0.963	1.027	1.426
$\mu_d$ [mPa.s]	0.854	0.734	3.364
$\gamma$ [mN/m]	36	14.1	1.75

The schematic diagram of the Kühni and Oldshue-Rushton contactors used in the present study is depicted in Figure 3. The Kühni contactor consists of glass section, 700 mm in length and with an inside diameter of 113 mm, at 10 stages. Agitation at each stage is achieved with 50 mm diameter shrouded six-blade turbine agitator with an accurate speed control. The OldshueRushton column is built of a cylindrical glass section and is equipped with impellers

with accurate speed control, whereas the internal parts are constructed of stainless steel. The main section is made of Pyrex glass with 113 mm internal diameter and the height of the column with nine stages is 700 mm. Mixing is obtained by nine 6-blade impellers of 50 mm diameter located at the center of each stage and these impellers are driven by an electric motor via a variable gear box. In the two columns, the organic phase (dispersed phase) and water (continuous phase) were fed into the extraction column at the bottom and on the top respectively in countercurrent mode. The inlet and outlet of the extraction column were connected to four tanks, each of 85 L capacity.

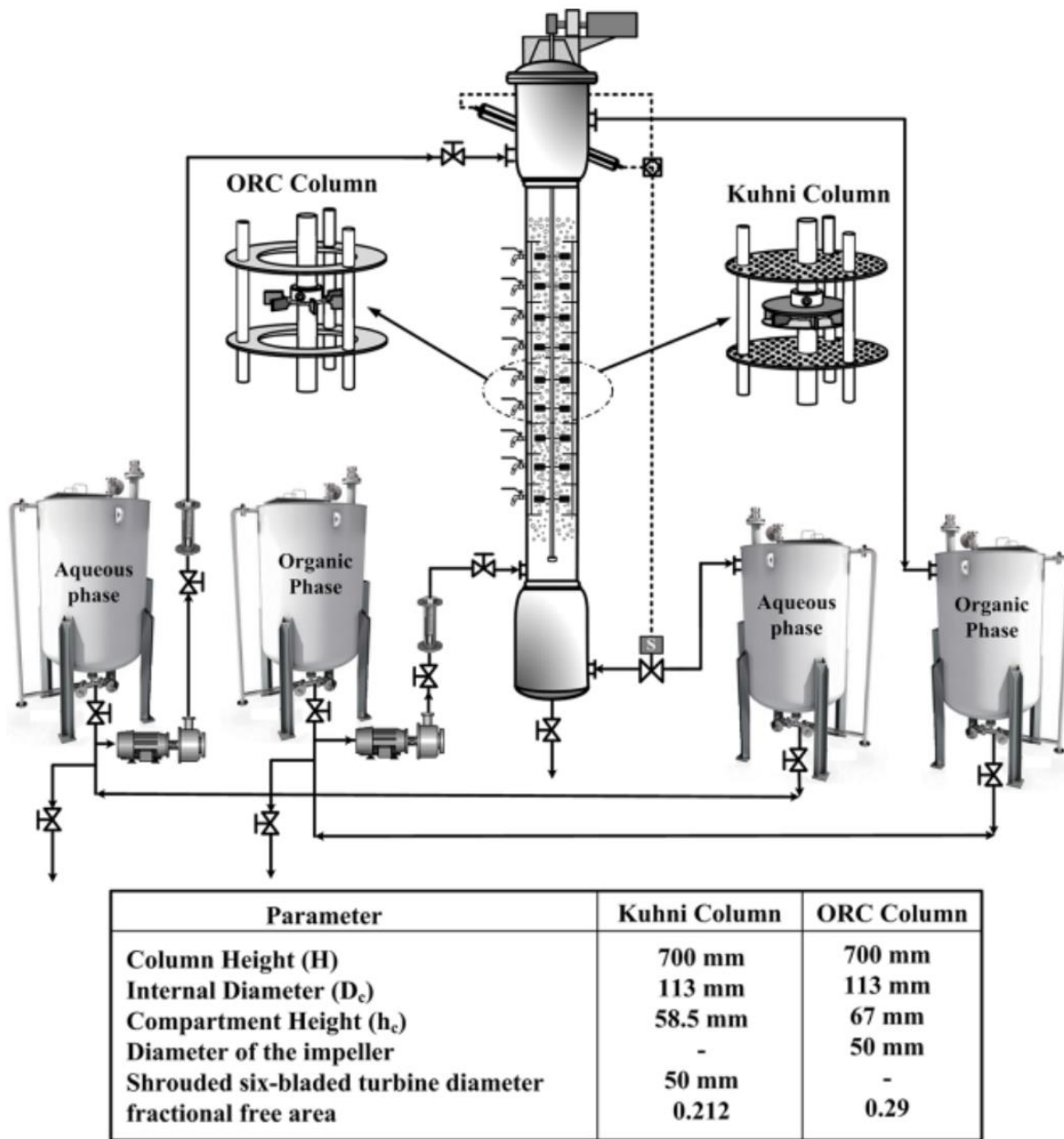


Figure 3. Schematic diagram of the Oldshue-Rushton and Kuhni column extractors.

### Drop Size Measurement

The drop size was measured by means of a very high-resolution Nikon D5000 digital camera used to take a digital photo of the extractor contents. Next, droplet dimensions were compared with the thickness of the stators as a reference. The four different heights of active column were selected to determine the size of the droplets. A minimum of 1000 drops was analyzed with the digital image analysis software for each experimental condition in order to guarantee the

statistical significance of the determined size distributions. The Sauter mean diameter was then calculated according to the following equation:

$$d_{32} = \frac{\sum_{i=1}^N n_i d_i^3}{\sum_{i=1}^N n_i d_i^2}$$

where  $n_i$  is the number of droplets of mean diameter  $d_i$  within a narrow size range  $i$ .

The effects of operating variables such as continuous and dispersed phase velocities, rotor speed and mass transfer direction on the Sauter mean drop diameter in the Oldshue-Rushton and Kühni columns are evaluated. The pictures of drop sizes in both columns are shown in Figure 4.

### **Effect of Rotor Speed on Sauter Mean Drop Size in Two Agitated Columns**

The experimental results for Sauter mean drop size in two columns with rotor speed are shown in Figure 4. It is observed that the agitation rate is increased, the average drop size significantly decreases. The rotor speed had a strong effect on the Sauter mean drop diameter. The explanation for this effect is related to the increment in the frequency of drop collisions against the internal parts of the column extractor in more turbulent fluid flow in their ascending path inside the equipment. An increase in the energy supplied via agitation to the dispersed phase overcomes the interfacial forces of the droplets and, therefore, the droplets break. From the results presented in Figure 5, 6 and 7 it was observed that smaller drops were generated from the low interfacial system (n-butanol-water) rather than medium or higher interfacial system (n-butyl acetate-water or toluene-water).

It is observed that the variations in the mean drop diameter with increasing continuous phase velocity are insignificant. Thus, the figure reveals that this effect has a negligible effect on the mean drop size.

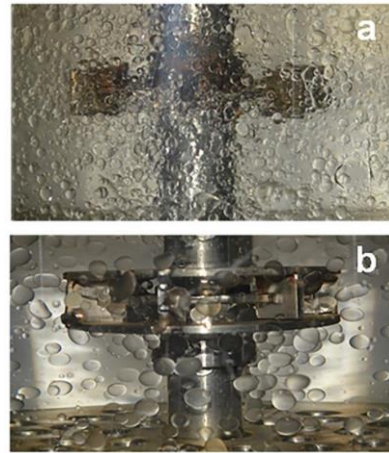


Figure 4. Variation of drop sizes in (a) Oldshue-Rushton column extractor and (b) Kühni column for toluene-water at  $N=135$  rpm,  $V_d=V_c=0.66$  mm/s.

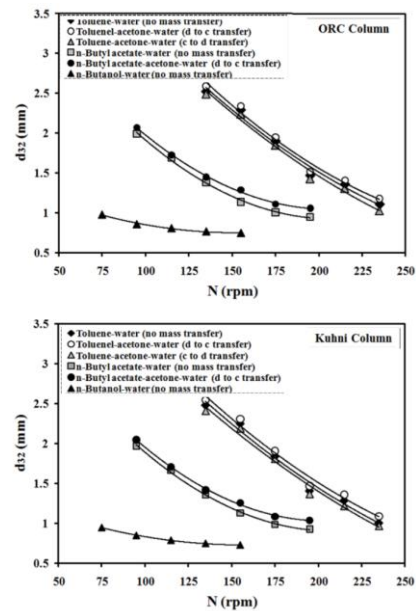


Figure 5. Effect of rotor speed on Sauter mean drop diameter in Oldshue-Rushton and Kühni columns ( $V_c=V_d=0.66$  mm/s).

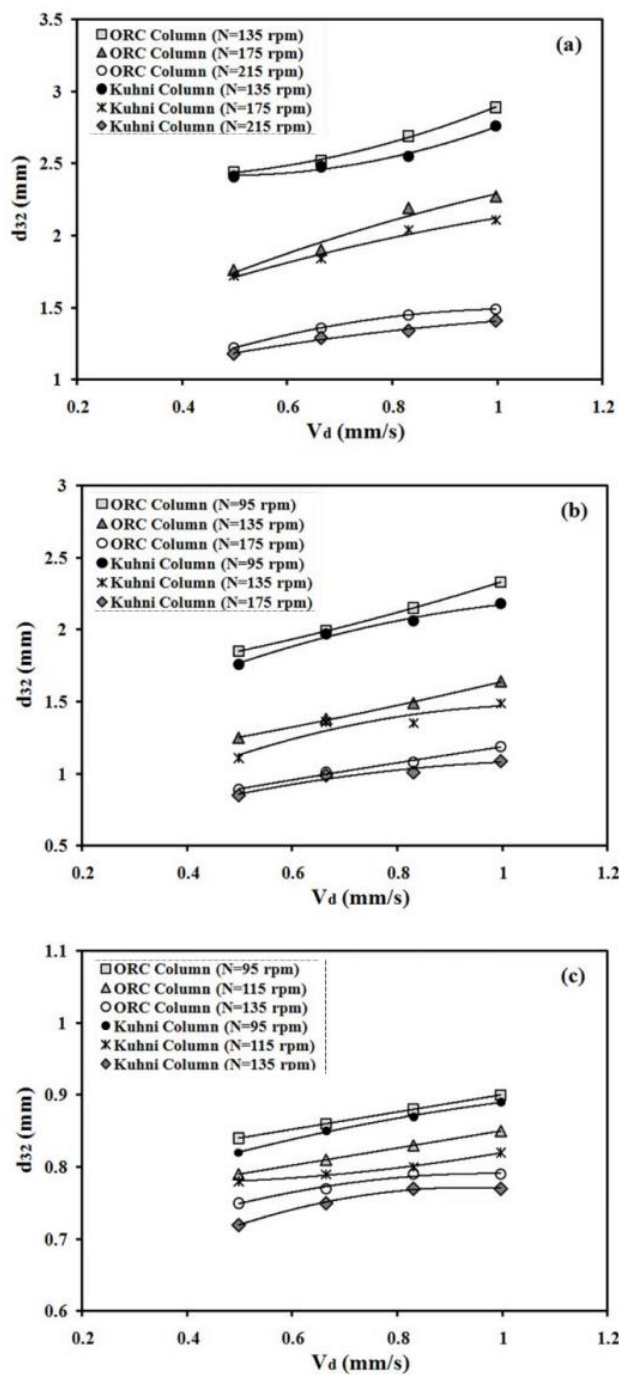


Figure 6. Effect of dispersed phase velocity on Sauter mean drop diameter in Oldshue-Rushton and Kühni columns for (a) toluene-water, (b) n-butyl acetate-water, (c) n-butanol-water ( $V_c=0.66$  mm/s)

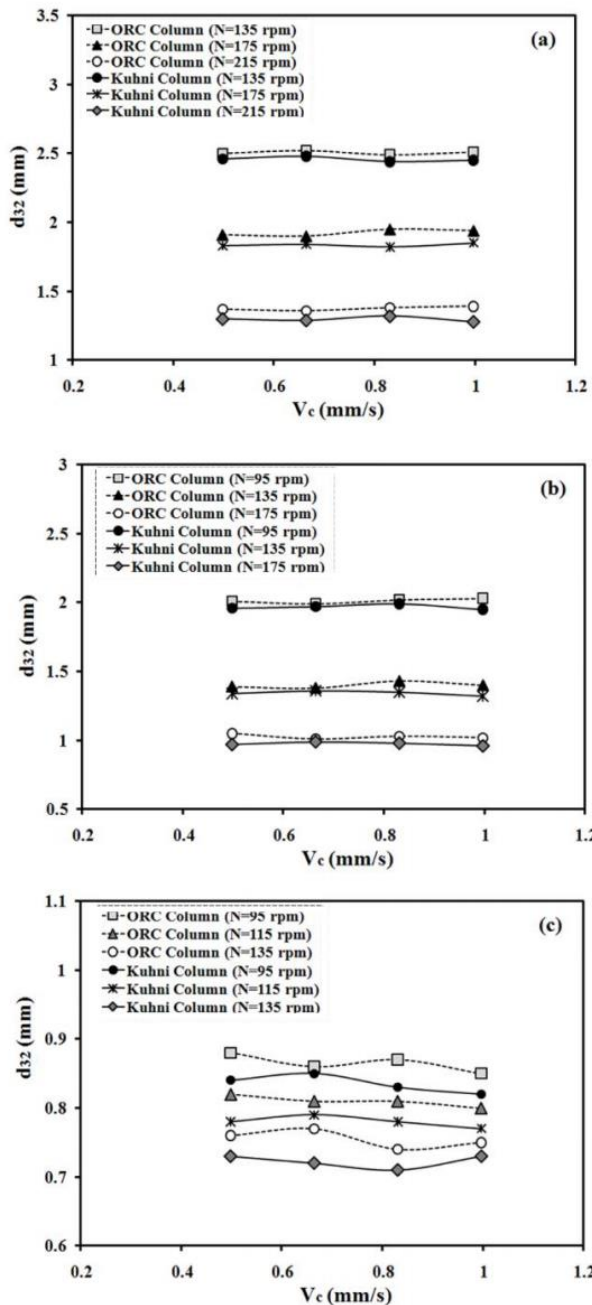


Figure 7. Effect of continuous phase velocity on Sauter mean drop diameter in Oldshue-Rushton and Kühni columns for (a) toluene-water, (b) n-butyl acetate-water, (c) n-butanol-water ( $V_d=0.66$  mm/s).

### Effect of Direction Mass Transfer on Sauter Mean Drop Size in Two Agitated Columns

The effect of mass transfer direction on mean drop sizes with phase velocities and rotor speed in OldshueRushton column is shown in Table 4.

The presence of a solute leads to lower interfacial tension between the two immiscible liquids.

The smaller drop sizes are observed due to the higher breakage rates for the mass transfer occurring from the continuous to the dispersed phase (c to d). For mass transfer in the opposite direction (d to c), the larger drops are created by the coalescence rate. When mass transfer occurs from the dispersed to continuous phase, the concentration in the liquid film between the drops is equilibrated rapidly with the drop concentration. The solute concentration in the draining film between the two approaching drops will be higher than in the surrounding continuous liquid. This phenomenon creates interfacial tension gradients which in turn causes interfacial flow. The enhanced mobility of the interface squeezes the continuous phase film between the drops rapidly and, therefore, the drop coalescence rate is increased.

TABLE 4. Effect of mass transfer direction on Sauter mean drop diameter in Oldshue-Rushton column for tolueneacetone-water system

	<b>V<sub>d</sub></b>	<b>V<sub>c</sub></b>	<b>rpm</b>	<b>c to d transfer</b>	<b>no mass transfer</b>	<b>d to c transfer</b>
Oldshue-Rushton column	0.6648	0.4986	155	2.21	2.27	2.32
	0.6648	0.6648	155	2.24	2.29	2.34
	0.6648	0.8309	155	2.22	2.25	2.31
	0.6648	0.9971	155	2.23	2.26	2.33
	0.6648	0.4986	195	1.42	1.49	1.55
	0.6648	0.6648	195	1.43	1.47	1.52
	0.6648	0.8309	195	1.40	1.48	1.53
	0.6648	0.9971	195	1.41	1.51	1.54
	0.4986	0.6648	155	2.11	2.16	2.19
	0.6648	0.6648	155	2.24	2.29	2.34
	0.8309	0.6648	155	2.33	2.36	2.41
	0.9971	0.6648	155	2.41	2.45	2.52
	0.4986	0.6648	195	1.36	1.40	1.46
	0.6648	0.6648	195	1.43	1.47	1.52
	0.8309	0.6648	195	1.47	1.53	1.58
	0.9971	0.6648	195	1.55	1.65	1.69
	0.6648	0.6648	135	2.49	2.52	2.59
	0.6648	0.6648	155	2.24	2.29	2.34
	0.6648	0.6648	175	1.85	1.9	1.95
	0.6648	0.6648	195	1.43	1.47	1.52
	0.6648	0.6648	215	1.31	1.36	1.41
	0.6648	0.6648	235	1.03	1.11	1.18
	<b>V<sub>d</sub></b>	<b>V<sub>c</sub></b>	<b>rpm</b>	<b>c to d transfer</b>	<b>no mass transfer</b>	<b>d to c transfer</b>
Kulni column	0.6648	0.4986	155	2.18	2.21	2.28
	0.6648	0.6648	155	2.19	2.25	2.31
	0.6648	0.8309	155	2.17	2.24	2.29
	0.6648	0.9971	155	2.16	2.23	2.30
	0.6648	0.4986	195	1.34	1.38	1.46
	0.6648	0.6648	195	1.37	1.41	1.47
	0.6648	0.8309	195	1.35	1.42	1.48
	0.6648	0.9971	195	1.34	1.39	1.49
	0.4986	0.6648	155	2.070	2.110	2.140
	0.6648	0.6648	155	2.190	2.250	2.310
	0.8309	0.6648	155	2.260	2.310	2.390
	0.9971	0.6648	155	2.340	2.370	2.440
	0.4986	0.6648	195	1.290	1.350	1.380
	0.6648	0.6648	195	1.370	1.410	1.470
	0.8309	0.6648	195	1.420	1.460	1.520
	0.9971	0.6648	195	1.490	1.550	1.590
	0.6648	0.6648	135	2.41	2.48	2.55
	0.6648	0.6648	155	2.19	2.25	2.31
	0.6648	0.6648	175	1.81	1.84	1.91
	0.6648	0.6648	195	1.37	1.41	1.47
	0.6648	0.6648	215	1.22	1.29	1.36
	0.6648	0.6648	235	0.97	1.01	1.09

## **Comparison of the Experimental Results with Previous Correlation**

The previous correlations in Table 2 were selected for comparison with the experimental data. The averaged absolute values of the relative error (AARE) of the calculated values of the Sauter mean drop diameter obtained by applying previous correlations to the experimental results are listed in Table 5. It is obvious from the results that the previous correlations could not accurately predict and fit the measured data.

## **Prediction of New Correlations**

As can be seen in Table 5, the amount of error is not acceptable for prediction of experimental data in Oldshue-Rushton and Kuhni columns. Therefore, a new correlation is proposed for prediction of the Sauter mean drop diameter in these columns. Also, the experimental data on the other rotary agitated columns is used to improve the accuracy of the correlation and generalized equation for these columns. All the independent variables may be rearranged in terms of dimensionless groups to give a general form. By using regression analysis, the following correlation was obtained from experimental data and other researchers.

$$d_{32} = C_1 \left( \frac{N^4 d_R^4 \rho_c}{g \sigma} \right)^{-0.19} \left( \frac{\mu_c^4 g}{\Delta \rho \sigma^3} \right)^{-0.05} \left( 1 + \frac{V_c}{V_d} \right)^{0.14} \left( \frac{V_d}{\left( \frac{\sigma \Delta \rho g}{\rho_c^2} \right)^{0.25}} \right)^{0.07} \left( \frac{\Delta \rho}{\rho_c} \right)^{0.98} \left( \frac{\mu_c}{\mu_d} \right)^{0.01}$$

The effect of mass transfer on Sauter mean drop diameter is shown by constant parameter ( $C_1$ ) in the above equation. The values of this parameter for mass transfer condition are presented in Table 6.

TABLE 5. The values of AARE in the predicted values of Sauter mean drop diameter obtained by previous correlations

Equation	Averaged absolute values of the relative error (AARE)	
	Oldshue-Rushton column	Kuhn column
Tsouris et al., 1990, Equation (1)	24.6%	23.2%
Moreira et al., 2005, Equation (2)	266.6%	261.0%
Al-Rahawi et al., 2008, Equation (3)	92.2%	92.3%%
Oliveira et al., 2008, Equation (4)	109.9%	107.5%
Kadam et al., 2009, Equation (5)	196.6%	189.6%
Yuan et al., 2012, Equation (6)	110.3%	109.7%
Yuan et al., 2012, Equation (7)	81.7%	89.3%
Hemmati et al., 2015, Equation (8)	65.3%	64.4%

TABLE 6. The constants and AARE values of Equations

Equation (10)	C <sub>1</sub>	AARE%
no mass transfer	5.7709	9.65
continuous to dispersed transfer (c→d)	7.1299	10.52
dispersed to continuous transfer (d→c)	6.7009	9.80
Equation (11)	C <sub>2</sub>	AARE%
no mass transfer	0.06475	10.41
continuous to dispersed transfer (c→d)	0.07083	10.95
dispersed to continuous transfer (d→c)	0.07104	9.45

The comparison of the obtained results via the experimental data reported by researchers in various rotary agitated columns and experimental work in two columns is shown in Figure 8. The correlation predicts the results with an average error of 9.99%. In the second correlation, the same variables are considered as for the first correlation and the column geometry term.

This correlation is derived based on the experimental results of the present work and the data taken from other researchers:

$$d_{32} = C_2 \left( \frac{N^4 d_R^4 \rho_c}{g \sigma} \right)^{-0.21} \left( \frac{\mu_c^4 g}{\Delta \rho \sigma^3} \right)^{-0.03} \left( 1 + \frac{V_c}{V_d} \right)^{-0.61} \left( \frac{V_d}{\left( \frac{\sigma \Delta \rho g}{\rho_c^2} \right)^{0.25}} \right)^{-0.37} \left( \frac{h_c d_R}{H D_c} \right)^{-0.44}$$

The effect of mass transfer in this equation is shown by constant parameter ( $C_2$ ) in the above equation. The values of this parameter for mass transfer condition and average absolute relative error are shown in Table 6. Comparison of the experimental results with the calculated values from the proposed correlation is shown in Figure 8 and 9.

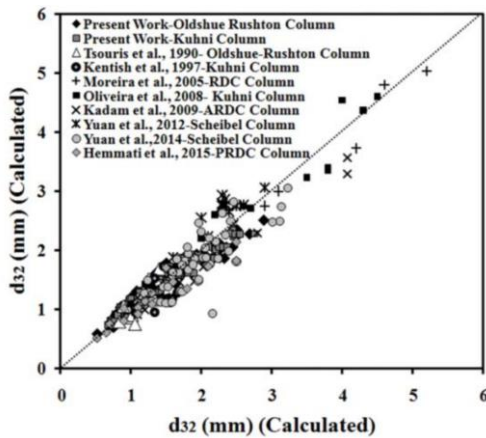


Figure 8. Comparison between experimental data and the estimated values using Equation for no mass transfer

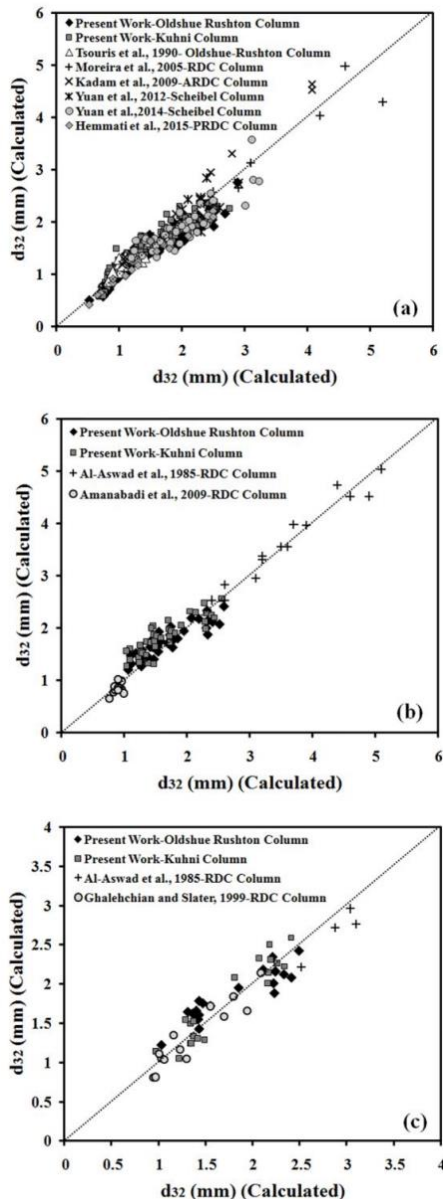


Figure 9. Comparison between experimental data and estimated values using Equation (11) for (a) no mass transfer, (b) d to c transfer and (c) c to d transfer.

The Sauter mean drop diameter predicted by the proposed correlations is in good agreement with the experimental results. The obtained results show that the proposed equation can be used for prediction of Sauter mean drop diameter of rotary agitated extraction columns (RDC, ARDC, Scheibel, Oldshue-Rushton and Kühni columns) for different physically equilibrated systems and can be extended to the cases with mass transfer.

**An experimental study of the mean drop size measurements in the two agitated columns (OldshueRushton and Kühnicolumns) was carried out. It was shown that the smaller drop size was produced by an increase in the agitation speed in two columns. The drop size could be increased with increasing dispersed phase velocity, but the continuous phase velocity does not have a significant effect. The Sauter mean drop diameter, required for estimation of the interfacial area of mass transfer is correlated with the knowledge of phase flow rates, physical properties, agitation speed, mass transfer conditions and also the column geometry of rotary agitated columns in the present work and the previous experimental works in the literature. The proposed equations pave the way for accurate predictions for the Sauter mean drop diameter in various rotary agitated columns with different physical properties. The present correlation is contrary to the previous studies in which the  $d_{32}$  was estimated for only one physical system such as toluene-water and for only one extraction column, but this correlation covers several physical systems for rotary agitated extractors. Therefore, this correlation can be incorporated in the design procedure for such contactors and this has been successfully extrapolated to the design of larger columns[2]**

## Population Balances for Extraction Column Simulations

### Population Balance Model

The general population balance equation (PBE) and its derivation based on Reynolds transport theory is given in Ramkrishna (2000)[4]. It is based on the deforming particle space continuum, which assumes that particles are embedded in this continuum at every point such that the distribution of particles is described by a continuous density function  $f(x, t)$ , and expressed by the following equation:

$$\frac{\partial f(x, t)}{\partial t} + \nabla_x \cdot (\dot{X}f) + \nabla_r \cdot (\dot{R}f) = S$$

Where  $R(x, t)$ ,  $X(x, t)$  are the velocities for internal and external coordinates respectively. Thus  $R(x, t)f(x, t)$  is the particle flux through internal coordinate space (concentration, droplet diameter, color, etc.) and  $X(x, t)f(x, t)$  is the particle flux through physical space.  $S$  is an integral expression source term, which depends on the specific processes by which particles appear and disappear from the system (particle breakage, aggregation, growth and nucleation) and is given in detail in Ramkrishna (2000)[4]. This model has been used widely for modeling and simulating in different chemical processes such crystallization, precipitation (protein precipitation), gas-liquid (bioreactors, evaporation) and gas-solid (fluidized bed reactors) processing and in polymerization.[5]

### Mathematical model

This general model has been adapted for LLECs to couple hydrodynamics and mass transfer in a one spatial domain by using the Multivariate Sectional Quadrature Method Of Moments (MSQMOM). The general spatially distributed population balance equation (SDPBE) can be presented by:

$$\frac{\partial f_{d,c_y}(\psi)}{\partial t} + \frac{\partial [u_y f_{d,c_y}(\psi)]}{\partial z} + \frac{\partial [\dot{c}_y f_{d,c_y}(\psi)]}{\partial c_y} = \frac{\partial}{\partial z} \left[ D_y \frac{\partial f_{d,c_y}(\psi)}{\partial z} \right] + \frac{Q_y^{in}}{A_c} f_y^{in}(d, c_y; t) \delta(z - z_y) + \Upsilon\{\psi\}$$

At the left hand side of the equation is the transient term, convection term and diffusion term, where the velocity along the concentration coordinates ( $c_y$ ) is ( $C_y$ ). The source terms are described on the right hand side of the equation. The first source term describes the droplet axial dispersion characterized by the dispersion coefficient  $D_y$ , which dependent on the energy dissipation, holdup and droplet rise velocity. The second one expresses droplet entering rate to LLEC with a volumetric flow rate that is perpendicular to column cross sectional area  $A_c$  at a location  $z_y$  with an inlet number density  $f_y$ . The third one ( $\Upsilon\{\psi\}$ ) represents the net number of droplets produced by breakage and coalescence per unit volume and unit time, which represents the four rates of droplet birth ( $B$ ) and death ( $D$ ) due to breakage ( $b$ ) and coalescence ( $c$ ) in a turbulent continuous phase:

$$\Upsilon\{\psi\} = B^b(d, c_y; t, z) - D^b(d, c_y; t, z) + B^c(d, c_y; t, z) - D^c(d, c_y; t, z)$$

In this equation the components of the vector  $\varphi = [d \ c_y \ z \ t]$  are those for the droplet internal bivariate coordinates: the droplet diameter ( $d$ ), solute concentration ( $c_y$ ) and the external coordinate: the location ( $z$ ) and time ( $t$ ) [5]

### Numerical methods

In technical geometries the population balance model (PBM) has no general analytical solution; therefore the only choice in most cases is a special numerical technique to solve the PBE.

Figure 10. Show numerical methods to solve the population balance equation.[6]

Several numerical approaches are proposed to solve the PBE which are classified into the following categories:

Classes method (CM), Monte Carlo method (MCM) and method of moments (MOM). The Classes method is known also as direct discretization method (DDM). In this method the internal

coordinate is discretized in the solution domain using a traditional discretization method such as finite difference method, finite element method or finite volume method directly. This method is straightforward; it gives the full particle size distribution with a good accuracy.

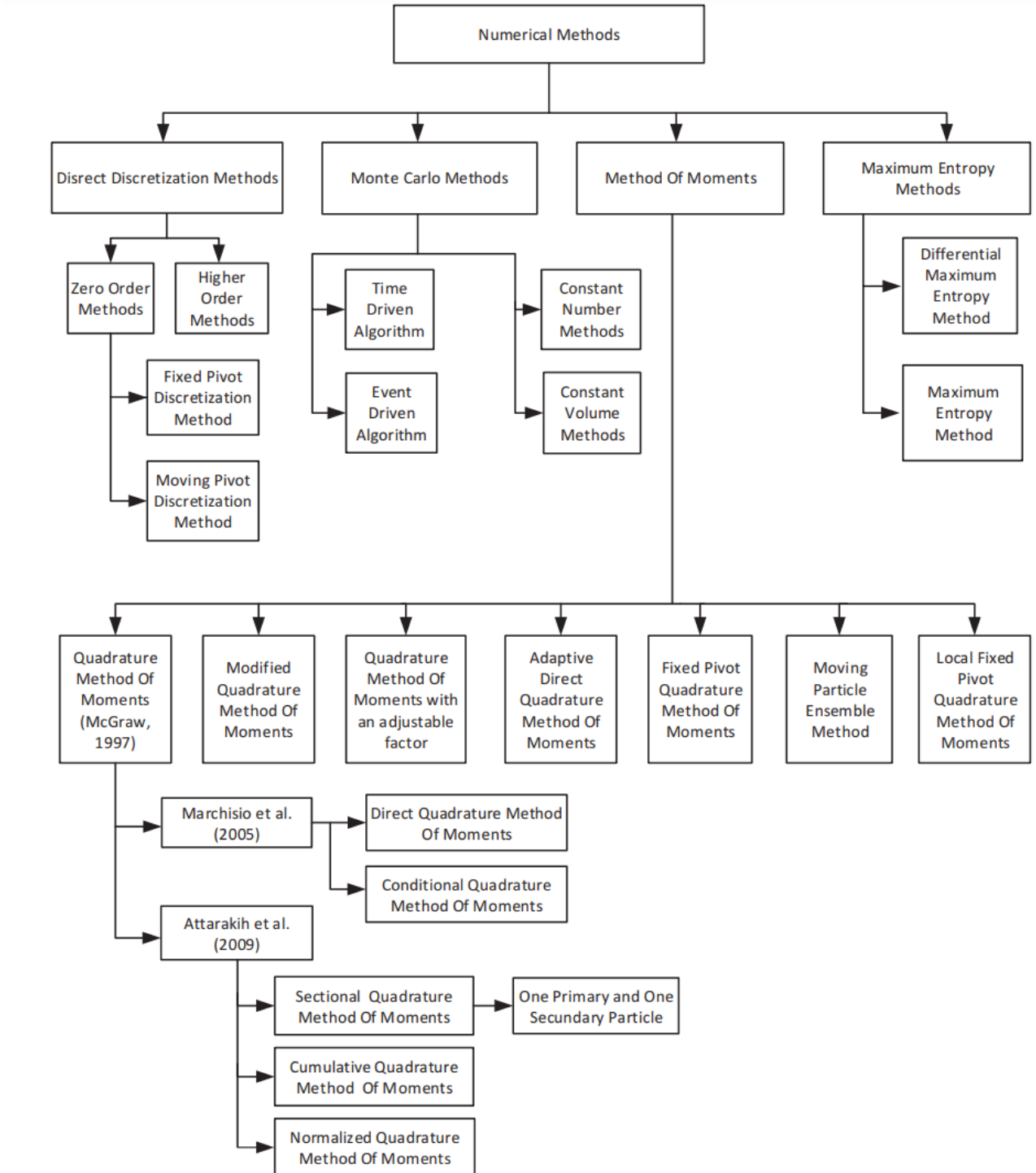


Figure 10. Numerical methods to solve the population balance equation[6]

In some cases to achieve a good accuracy a large number of classes has to be used, that will require large number of equations to be solved. This method is used in commercial CFD software (CFX, FLUENT), however, it needs a long computational time and it preserves only two integral properties of the distribution as Kumar and Ramkrishna proposed in the fixed pivot discretization method and the moving pivot technique [7]

On the other hand, the Monte Carlo method is a stochastic method that involves the construction of an artificial system to approximate the actual one based on the physical characteristics of the considered system. There are two classifications concerning this method. First, it can be divided into time and event driven algorithms according to the driven pattern of the discrete physical events. Second, it can be classified into constant volume and constant number methods according to the state of the particles in the artificial system. To decrease the statistical errors a very large number of particles are required and this will need a high computational time. The numerical results from this method usually contain ``noises'', for these reasons it is difficult to be coupled with a CFD code.

The method of moments has been widely used because of its efficiency and high accuracy also when it is coupled with CFD code FLUENT. In this method the particle size distribution is not tracked directly but through its moments, which are integrated over the internal coordinates. It needs a very low computational time. However this method does not give information on the shape of the distribution.

JunWei et al. (2009) has provided a brief literature review for different methods of MOM such as [8]:

Quadrature Method Of Moments (QMOM), Direct Quadrature Method Of Moments (DQMOM), Modified Quadrature Method Of Moments (M-QMOM), Adaptive Direct Quadrature Method Of Moments (ADQMOM), Fixed Pivot Quadrature Method Of Moments (FPQMOM), Local Fixed Pivot Quadrature Method Of Moments (LFPQMOM) and etc. In

2009, Attarakih has invented a new technique for the QMOM to solve of PBE using the Sectional Quadrature Method Of Moments (SQMOM), which combines the advantages of CM and MOM in one model with high accuracy, low computational time and without destroying the shape of the distribution. This model is based on primary and secondary particle concept which will be discussed in the next section. Then the SQMOM model was extended to the Bivariate Sectional Quadrature Method Of Moments (BVSQMOM) and the Multivariate Sectional Quadrature Method Of Moments (MSQMOM). Later this model has been extended to the Cumulative Quadrature Method Of Moments (CQMOM) and the Normalized Quadrature Method Of Moments (NQMOM).[5]

### **One Primary and One Secondary Particle Model (OPOSPM)**

The One Primary One Secondary Particle Method is the simplest discrete model case of the SQMOM that can approximate the continuous PBE. It provides a promising one group reduced PBM that reduces the computational time. This model is based on the primary and secondary particle concept, where the primary particles are responsible for reconstruction of the distribution and the secondary particle is to describe the particle interaction due to breakage and coalescence.

$$\frac{\partial N}{\partial t} + \frac{\partial(u_y N)}{\partial z} = \frac{1}{A_c} \frac{Q_y^{in}}{v_{in}} \delta(z - z_y) + S$$

$$\frac{\partial \alpha}{\partial t} + \frac{\partial(u_y \alpha)}{\partial z} = \frac{Q_y^{in}}{A_c} \delta(z - z_y)$$

This model is able to capture all the essential physical information contained in the PBM and is still tractable from computational point of view. The model conserves the total number (N) and volume ( $\alpha$ ) concentrations of the population by solving directly two transport equations for N and  $\alpha$ . The source term S represents the net number of the droplets and is expressed by :the following equation

$$S = (\vartheta(d_{30}) - 1)\Gamma(d_{30})N - \frac{1}{2}\omega(d_{30}, d_{30})N^2$$

The first term is the rate of droplet formation due to breakage, and is expressed in terms of the breakage frequency  $\Gamma$ .  $\vartheta$  is the mean number of daughter droplets that is determined by integrating the daughter droplet distribution function, in the simulation it is assumed equal to 3 (mother droplet breakup to form three daughter droplets). The second term represents the net rate of droplet death due to coalescence, and expressed as the coalescence frequency  $\omega$ . Both breakage and coalescence frequencies are function of droplet size, energy dissipation and system physical properties (density, viscosity and surface tension).  $d_{30}$  is the mean diameter and is given as the ratio between volume and number concentrations.

$$d_{30,i} = \sqrt[3]{\frac{6 \alpha_i}{\pi N_i}}$$

The OPOSPM model is used to simulate the droplet size distribution based on the model of Coulaloglou and Tavlarides (1977) for breakage and coalescence in the CFD simulation using the optimized parameters obtained from the solving inverse population balance problem.

### **Phenomena Affecting Droplet Size**

The droplet population balance model (DPBM) has to be used to predict the performance of liquid extraction columns that takes into account droplet transport and droplet interactions. Detailed description about these phenomena will be discussed in the next sections.

### **Droplet velocity**

In agitated columns there are two factors governing drop motion: first the drop motion due to buoyancy force and the second is random drop motion due to flow instability. Knowledge of the drop velocities necessary for the prediction of holdup, the residence time and mass transfer rates of both phases. This is based on determining the relative swarm velocity and the effective phase velocity. The droplet velocity and the axial dispersion are considered the key parameter

for calculating the drift term in the PBE. Semi-empirical correlations are used to determine the drop velocity for various sizes and physico-chemical that are dependent on the chemical test system. For the high interfacial liquid system: toluene- acetone-water (our studied system) Vignes' lawis proposed and is given by the following equation:

$$V_t = \frac{d}{4.2} \left( \frac{g\Delta\rho}{\rho_x} \right)^{2/3} \left( \frac{\rho_x}{\eta_x} \right)^{1/3}$$

On the other hand the characteristic velocity in stirred columns is controlled and modeled by the droplet size, geometry of the agitators and stators, and the energy input. This general description is used for the optimization algorithm to describe the dispersed phase hydrodynamics, and also has been used in the PPBLAB simulations.

### **Droplet interactions**

The droplet interactions occur at macro-scale (droplet breakage and coalescence) and micro-scale interphase mass transfer.

### **Drop breakage**

The deformation and breakup of fluid particles in turbulent dispersions is influenced by the continuous phase hydrodynamics and the interfacial surface tension. Also it is dependent on the droplet size, density, interfacial tension, viscosity of both phases, holdup, local flow and energy dissipation. Generally the breakage mechanism of the droplet can be classified into four main categories as are turbulent fluctuation and collision, viscous shear stress, shearing-off process and interfacial instability. In literature different mechanisms exist and they are strongly dependent on the geometry, especially in liquid extraction columns with different stirring devices. For example the droplet breakup in Kühni column while passing through the turbine outlet stream, but in RDC extraction columns it occurs only when the droplet touch the rotator disc. Several models exist in literature for droplet breakage, but here we will use the model of

Coulaloglou and Tavlarides (1977). This model was based on the turbulent nature of liquid-liquid dispersion, where the drop oscillates and deforms due to the local pressure fluctuation. The breakage frequency  $\Gamma(d)$  is defined by the following equation:

$$\Gamma(d) = \left( \frac{1}{\text{breakage time}} \right) \cdot \left( \frac{\text{fraction of drops breaking}}{} \right)$$

The breakage time is determined by isotropic turbulence theory by assuming that the motion of daughter droplets is the same as turbulent eddies. On the other hand the fraction of drops breakage is assumed proportional to the fraction of drops that have a turbulent kinetic energy greater than their surface tension. Coulaloglou and Tavlarides (1977) relationship is based on the fundamental model of mixer hydrodynamics with taking into account the influence of holdup:

$$\Gamma(d, \phi_d) = C_1 \frac{\varepsilon^{1/3}}{d^{2/3}(1+\phi_d)} \left[ \exp \left( -\frac{C_2 \sigma (1+\phi_d)^2}{\rho_x d^{5/3} \varepsilon^{2/3}} \right) \right]$$

The number of daughter droplets produced by a single breakage event is assumed to be three in order to simplify the computational problems of modeling, in which the  $\alpha(d_{30}) = 3$

### **Drop coalescence**

Droplet coalescence is considered more complex than breakage because of the droplet interaction with the surrounding liquid phase and with other droplets when they are brought together by external flow and body forces. For coalescence of droplets to occur in a turbulent flow field the droplet first collide then remain in contact for sufficient time so that the processes of film drainage, film rupture and coalescence to occur. The droplets may separate caused by a turbulent eddy or adsorption layers, which prevent the coalescence. Also the intensity of collision and the contacting time between the colliding droplets are the key parameters for

this phenomenon.

There are several models in literature for coalescence of fluid particles. The physical models calculate the coalescence frequency from the product of collision rate (frequency) ( $\omega$ ) and the coalescence efficiency ( $\lambda$ ) of two droplets from diameter  $d$  and  $d'$ [5].

Coualoglou and Tavlarides (1977) is one of the most used models because the derived model is based on the physical quantities of the chemical test system, therefore it is the one we choose for our optimization. This model was developed for stirred vessel, being based on the kinetic theory of gases and drainage film theory. It is given by the following equation:

$$\omega(d, d', \phi_d) = \left[ C_3 \frac{\epsilon^{1/3}}{1 + \phi_d} (d + d')^2 (d^{2/3} + d'^{2/3})^{1/2} \right] \times \left[ \exp\left(-\frac{C_4 \eta_x \rho_x \epsilon}{\sigma^2 (1 + \phi_d)^3}\right) \left( \frac{(dd')}{(d + d')} \right)^4 \right]$$

In this model the first term is the collision rate frequency of two droplets. It can be described in analogy to collision frequency between gas molecules of drop diameter  $d$  and  $d'$  for size intervals  $\Delta d$  and  $\Delta d'$ . In this term the influence of the holdup is considered as a damping effect on turbulent velocities. On the other hand the second term is the fraction of collisions between drops of size  $d$  and  $d'$  that result in a coalescence is known as coalescence efficiency. It accounts for the contact time between two droplets and the coalescence time. Unusually in this phenomenon the contact time must exceed the coalescence time, after collision. Furthermore, the coalescence efficiency for this model is classified for deformable particles with immobile interfaces and the initial and final film thickness are assumed to be constant.[5].

This EFPT detailed population balance numerical solver is used in a window-based software which include: – LLECMOD (Liquid-Liquid Extraction Column MODule) is a Fortran window-based program used to simulate pulsed and rotating columns based on the bivariate population balance modelling. The extended fixed pivot numerical technique[84] was adapted

from simple idealized test cases to simulate agitated batch and continuous vessels and the more complicated equipment including liquid-liquid extraction columns. – PPBLab® (Particulate Population Balance Laboratory) is the newest tool to model, simulate and design the hydrodynamics and mass transfer in LLECs using population balances (<http://population-balance-modeling.com/>). It is a MATLAB® graphical user interface and coupled with MATLAB CAPEOPEN Thermo Import from AmsterCHEM. Monte Carlo method (MC). It is a stochastic method and there are two classifications. Firstly, it can be divided into time- and event-driven algorithms according to the driven pattern of the discrete physical events. In time-driven simulations, a time step is specified and then the simulation implements all possible events within that step as shown in Liffmann. In event-driven algorithms, an event is implemented and then the time is advanced by an appropriate amount as shown in Garcia et al. Secondly, a further classification is into constant volume and constant number methods according to the state of the particles in the artificial system. For example, in the classical approach, the simulation tracks a constant reaction volume in which the number of particles varies depending on the mechanisms that transform the particle distribution. In coagulation, the number of particles decreases continuously while in fragmentation it increases. The drawback is the speed and accuracy and in order to decrease the statistical errors, a large number of particles are necessary and this will need a high computational time. In addition, numerical results using this method usually contain “noises”, for these reasons it is difficult to couple this method with a CFD code. On the other hand, Ramkrishna and Mahoney [4] stated the advantage of MC when the analytical solutions are unavailable. ReDrop (Representative Drops) software simulates the behaviour of individual droplets during their total life time in an LLEC using the MC method. Alternative approaches using the MC method are found. It is widely used because of its advantages, such as efficiency, high accuracy and low computational time even when coupled with CFD. The main idea behind these methods is to reduce the

detailed population balance equation into a set of Ordinary Differential Equations or Partial Differential Equations, and then the particle size distribution can be tracked through its moments. However, the main disadvantage of this method is that it does not provide information on the detailed shape of the distribution. The OPOSPM is able to capture all the essential physical information contained in the PBM and is still tractable from a computational point of view. This group model consists simply of two transport equations for the total number ( $N_y$ ) and volume ( $\phi_y$ ) concentrations of the dispersed phase, which are equal to the zeroth and third moment of the droplet population. The model conserves the  $N_y$  and  $\phi_y$  concentrations of the population by solving directly these two transport equations. OPOSPM is expressed by the following equations:

$$\frac{\partial N_y}{\partial t} + \frac{\partial(u_y N_y)}{\partial z} = \frac{u_y^{in}}{v_{in}} \delta(z - z_y) + S$$

$$\frac{\partial \phi_y}{\partial t} + \frac{\partial(u_y \phi_y)}{\partial z} = u_y^{in} \delta(z - z_y)$$

In Equation  $v_{in}$  is the feed mean droplet volume, while in Equation  $v_{in}= 1$  to conserve the droplet volume. The source term ( $S$ ) represents the net number of the droplets and is equal to zero in the volume balance equation. On the other hand, the source term ( $S$ ) from Equations, which preserves the number of droplets produced by breakage and coalescence per unit volume and unit time. It is expressed by the following equation:

$$S = (\vartheta(d_{30}) - 1)\Gamma(d_{30})N_y - \frac{1}{2}\omega(d_{30}, d_{30})N_y^2$$

The first term is the rate of droplet formation due to breakage and is expressed in terms of the breakage frequency ( $\Gamma$ ). ( $\vartheta$ ) is the mean number of daughter droplets produced by breakage that is determined by integrating the daughter droplet distribution function. The second term

represents the net rate of droplet death due to coalescence and expressed as the coalescence frequency ( $\omega$ ). Both breakage and coalescence frequencies are functions of droplet size, energy dissipation and system physical properties (density, viscosity and surface tension). The volume mean diameter ( $d_{30}$ ) is an adaptive Gauss-Christoffel quadrature node and is represented by the cubic root ratio of the third to the zeroth moment (as the ratio between volume and number concentrations) according to the equation below:

$$d_{30} = \sqrt[3]{\frac{m_3}{m_0}} = \sqrt[3]{\frac{6 \phi_y}{\pi N_y}}$$

For extremely fast simulations the modified OPOSPM model (MOPOSPM) is introduced to capture all the essential physical information as contained in the full detailed PBM (CM) and it is easily tractable from the computational point of view. The model conserves the population by solving directly the previous two transport equations for ( $N_y$ ) and ( $\phi_y$ ). For online prediction and modelbased forward control purposes, Attarakih proposed the idea of OPOSPM as a nonlinear autocorrelation PBM by introducing two learning parameters. Based on the idea, the source term has been modification by two parameters ( $K_b$  and  $K_c$ ) for the breakage and coalescence kernels, respectively, then implemented in the OPOSPMas:

$$S = K_b(\vartheta(d_{30}) - 1)\Gamma(d_{30})N_y - \frac{1}{2}K_c\omega(d_{30}, d_{30})N_y^2$$

The model parameters are derived in a learning process using offline or online experimental data, obtained from experimental setup developed for online measurement of a DSD as described elsewhere. The  $K_b$  and  $K_c$  can then be used effectively for online prediction and control of extraction columns without significant loss of information. In further works, the QMOM method is extended to the Cumulative QMOM (CQMOM) and to the Normalized QMOM (NQMOM). The QMOM and the other sub-methods (OPOSPM, SQMOM) have

proven their efficiency and accuracy, when they are implemented in commercial CFD codes like ANSYS Fluent®, OpenFOAM® or FPM®. Maximum Entropy Method (MaxEntM). It is a novel approach to solve the constrained nonlinear optimization problem, by maximizing the constrained Shannon entropy function. It is called the differential maximum entropy method (DMaxEntM). The usage of the MaxEntM has the advantage of reconstructing the distribution information that is lost by using the moment method.

### Case studies

Jildeh in her thesis [9] derived optimized droplet interaction parameters, which are independent of columns geometry (stirrer details, compartment height and diameter) and valid for three chemical systems. Here only the coalescence parameter sets are different and depend on the interfacial tension range (one for a low resp., one for a high one). Two different types, as a Kühni and an RDC column, were simulated. The simulations in the following are pure predictions without any adjustment of the model parameter when using OPOSPM for the simulations

Table 7. Final set of interaction model parameter for RDC extraction columns.

Test system/parameters	Slowing factor	Breakage	Coalescence
<b>Optimized model</b>	Modes <sup>[61]</sup>	Schmidt <sup>[63]</sup>	Coulaloglou & Tavlarides <sup>[184]</sup>
Toluene-water	$s_1 = -3.9838$	$b_1 = 2.13 \times 10^{-06}$	$c_1 = 1.52 \times 10^{-02}$
Toluene-acetone-water	$s_2 = 0.5231$	$b_2 = 2.740$	$c_2 = 1.33 \times 10^{11} \text{ m}^{-2}$
Butyl acetate-water	$s_3 = -1.3141$	$b_3 = 0.284$	
Butyl acetate-acetone-water	$s_4 = 0.2189$ $s_5 = 1.0339$ $s_6 = 0.7879$	$b_4 = 3.908$ $b_5 = 0.229$	$c_1 = 1.34 \times 10^{-02}$ $c_2 = 1.33 \times 10^{11} \text{ m}^{-2}$

RDC extraction column. The optimized parameters are summarized in Table 7. Here, two test cases under various operating conditions (flow rate, rotor speed) for each EFCE chemical test system toluene-acetone-water and butyl acetate-acetone-water are discussed. Direction of mass transfer is from continuous to dispersed phase with 5% acetone in the continuous phase. The inlet position for the dispersed phase is 0.85 m and 3.8 m for the continuous phase. These

parameters are used to simulate different column geometries and systems of Kühni type. To validate the estimated parameters, simulations of a Kühni extraction column with mass transfer were performed at different operating conditions (flow rate, rotor speed) for two ternary EFCE chemical test systems: toluene-acetone-water (see Figure 11) and butyl acetate-acetone-water (see Figure 12). Direction of mass transfer is from continuous to dispersed phase and with 5% acetone in water as solute was compared to experimental data taken from Garthe.

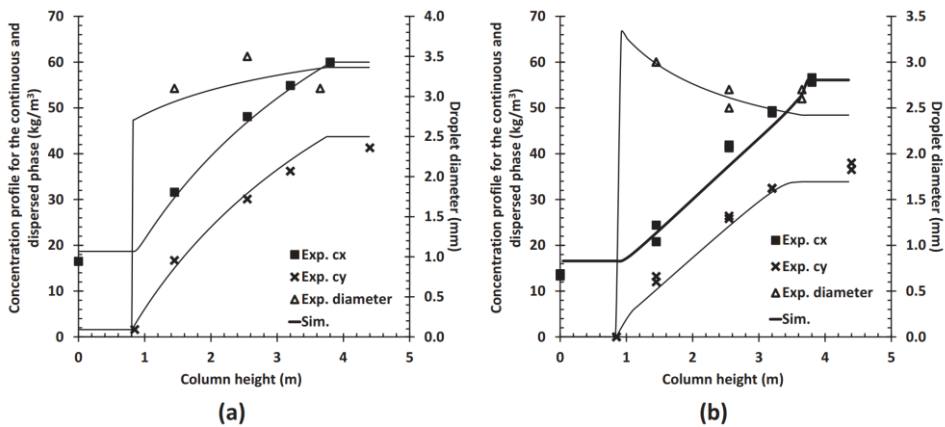


Figure 11. Droplet diameter and mass transfer profile: (a)  $Q_x = 82.6 \text{ L/h}$ ,  $Q_y = 99.6 \text{ L/h}$  at 200 rpm; (b)  $Q_x = 40 \text{ L/h}$ ,  $Q_y = 48 \text{ L/h}$  at 400 rpm (DN 80 RDC column; toluene-acetone-water).

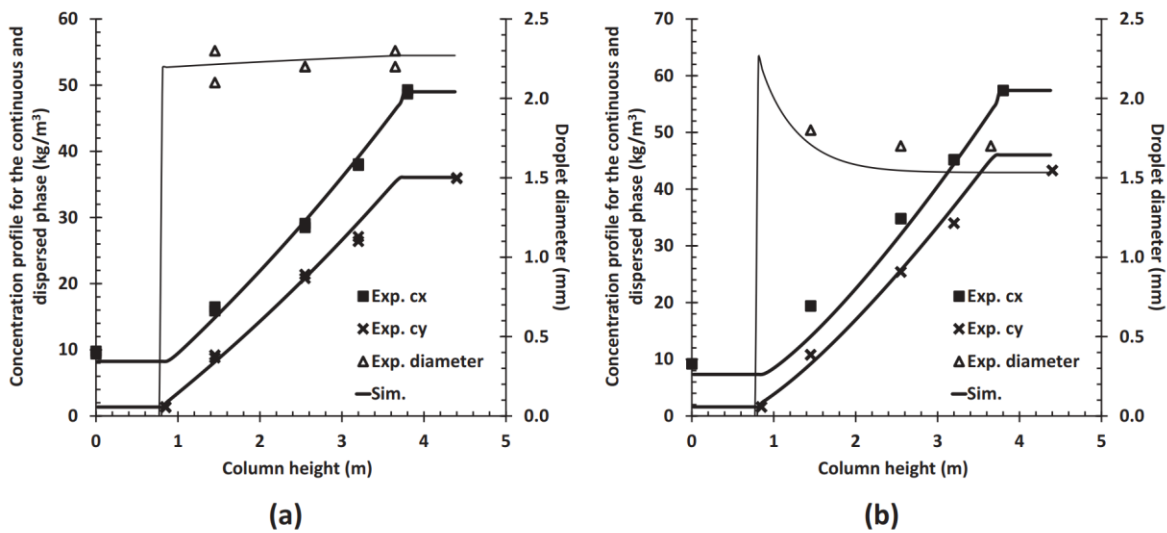


Figure 12. Droplet diameter and mass transfer profile: (a)  $Q_x = 40 \text{ L/h}$ ,  $Q_y = 48 \text{ L/h}$  at 200 rpm, (b)  $Q_x = 70 \text{ L/h}$ ,  $Q_y = 84 \text{ L/h}$  at 400 rpm (DN 80 RDC column; butyl acetate-acetone-water).

Table 8. Final set of interaction model parameter for Kühni extraction columns.

Test system/parameters	Slowing factor	Breakage	Coalescence
<b>Optimized model</b>	Garthe <sup>[174]</sup>	Schmidt <sup>[58]</sup>	Coualaglou & Taylarides <sup>[185]</sup>
Toluene-water	$s_1 = -1.9104$	$b_1 = 5.56 \times 10^{-02}$	$c_1 = 5.50 \times 10^{-02}$
Toluene-acetone-water	$s_2 = -2.621$	$b_2 = 1.719$	$c_2 = 1.33 \times 10^{11} \text{ m}^{-2}$
Butyl acetate-water	$s_3 = -58.55$	$b_3 = 0.68$	
Butyl acetate-acetone-water	$s_4 = 3.70 \times 10^{-03}$ $s_5 = -0.290$ $s_6 = 2.956$ $s_7 = 58.9154$ $s_8 = 4.20 \times 10^{-03}$	$b_4 = 0.739$ $b_5 = 4.00 \times 10^{-02}$	$c_1 = 3.20 \times 10^{-02}$ $c_2 = 1.33 \times 10^{11} \text{ m}^{-2}$

The inlet position for the dispersed phase is 0.85 m and 3.8 m for the continuous phase.

The predicted hydrodynamic and mass transfer profiles for both the continuous phase,  $c_x$ , and the dispersed phase,  $c_y$ , are in good agreement to the measured data of Garthe.<sup>[174]</sup> The interaction droplet parameters in Table 15 are used to predict the hydrodynamic and concentration profiles of Gomes et al. at different operating conditions. Results were compared to the experimental data at steady-state and transient state for toluene (d)-water with and without solute (acetone). A pilot DN 150 Kühni column with 2.25 m active height and 36 compartments was used. The effect of different rotational speeds and dispersed flow rates on dispersed phase holdup along the column stages at constant continuous phase flow rate 125 L/h was investigated. The steady-state simulation results (full lines) were compared to the experimental data and simulation profiles (dotted lines) of Gomes. Gomes<sup>[10]</sup> investigated two dynamic cases for toluene-acetone-water system. The resulting holdup profile for the first case is a negative step change in rotational speed from 170 to 140 rpm at constant flow rates ( $Q_x = 94 \text{ L/h}$ ,  $Q_y = 120 \text{ L/h}$ ). The second test case investigated the change in dispersed flow rate from 208 to 112 L/h (see Figure 16b) at a constant rotational speed of 140 rpm and continuous phase flow rate of 125 L/h. The simulation results are compared to experimental data points at different stage numbers. To refine this transient profile, the increment time ( $\Delta t$ ) set to 1 s for 1st case and 5 s for the 2nd case, thus the predicted profile corresponds to experimental data profile at steady state (before step change) and during step change response until it reaches

back to a steady-state trend.

The growing computational power enables the establishment of the population balance models to simulate the steady-state and dynamic behaviour of multiphase flow unit operations. Accordingly, the two-phase flow behaviour inside liquid-liquid extraction equipment is characterized by different factors. These factors include nonlinear interactions among droplets (breakage and coalescence), different time scales due to the dispersed phase droplet size movement, interfacial diffusional and reactive mass transfer processes. As a result, the bivariate population balance (solute concentration and droplet diameter) has no well-known analytical solution and therefore robust numerical solution methods with low computational cost are highly demanded. The paper gives an extended overview on the methods available, where moment-based numerical schemes prove to be very efficient and even allow a coupling with CFD methods to be used to optimize and analyze any apparatus/ compartment geometry in detail. A major part of the paper focuses on hydrodynamics and mass transfer with respect to the kernels of the population balance equation. This includes droplet rise and backmixing, droplet interactions like breakage and coalescence and an extended review on correlations for liquid-liquid extraction columns is given. Considering mass transfer, it includes also a reactive system, where the latter are based on zinc extraction with a liquid cation exchanger as recommended by the EFCE (European Federation of Chemical Engineering). Finally, case studies for RDC and Kühni columns are given and droplet interaction parameters are presented, which are valid for specified column type and differ only when a different chemical system (e.g. if one with high or low interfacial tension) is used. The correlations so far developed for physical extraction systems can be in principal used for the reactive ones. However, due to mass transfer physical properties may change drastically, which has then to be considered when evaluating axial concentration, holdup or droplet mean

**diameter profiles. The simulation of column behaviour with the given correlations is straightforward. However, there exists still now no predictive one for droplet coalescence. At high throughputs and energy dissipation, the droplets collide at high velocities, which makes droplet contact and drainage time difficult and coalescence is hindered. Otherwise, when solving the inverse population balance, the parameters can be evaluated from experimental data of a small scale or reduced height column so that minimal material is required. Concerning this matter, future work is needed to resolve this challenging topic.[11]**

# **Hanson mixer column for extraction liquid-liquid**

## **1-1) Hanson Mixer-Settler Extraction Column**

Hanson mixer-settler extractor is a rectangular mixer-settler with the horizontal arrangement of the mixer and the settler in each stage, i.e., each stage in the mixer settler extractor is piled up in a vertical direction. This column is designed to obtain efficient contacting of two phases and a high degree of phase inter-stage separation. In order to develop appropriate design procedures for Hanson mixer-settlers, the knowledge of average drop size and its distribution in terms of the operating variables and liquid physical properties is, thus, of some importance.[12]

### **1-1-1) Mean Drop Size and Drop Size Distribution in a Hanson Mixer-Settler Extraction Column**

The effects of agitation speed and dispersed phase and continuous phase flow rates have been investigated under a variety of operating conditions. Mean drop diameter axial profiles show a strong nonuniformity, while drop size distribution does not change significantly with the column height. Sauter mean diameter and drop size distribution are strongly affected by agitation speed and interfacial tension. Significant, but weaker are the effects of continuous phase and dispersed phase flow rates. An empirical correlation for mean drop size as a function of Weber number, dispersed phase holdup, and viscosities ratio is suggested. In a further correlation, the dispersed phase holdup is replaced by flow rates which will certainly be known in a practical case.

In the following text, results are reported on drop size determinations carried out in a pilot scale Hanson mixer-settler extraction column for two different liquid-liquid systems. The effects of agitation speed and continuous phase and dispersed phase flow rates have been investigated[12].

### **1-1-1) The toluene-acetone-water, n-butyl acetate-acetone-water systems**

The liquid-liquid systems studied were toluene-acetone-water (high interfacial tension) and n butyl acetate-acetone-water (medium interfacial tension). The schematic diagram of three stages is given in Fig. 13.

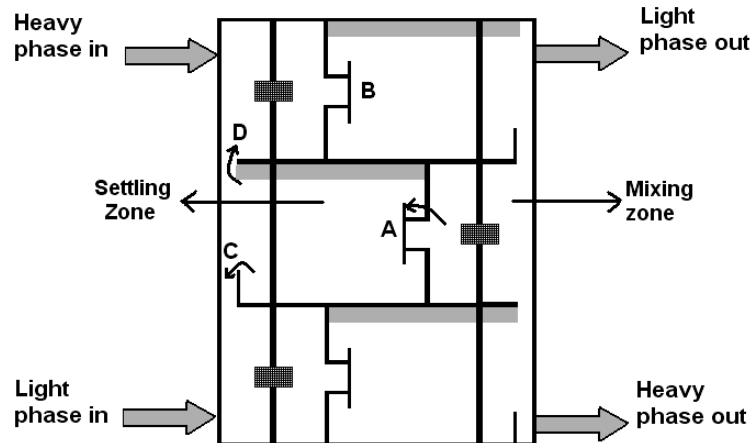


**Figure 13.** Schematic diagram of Hanson mixer-settler and flows of light and heavy phases

In each stage, the light and heavy phases were mixed in the mixing zone to provide initial contact. After that the unstable dispersion was transferred to a settler zone through the port .A. This port was located in the middle of a dividing wall and, in front of it, a vertical plate .B. was placed to decrease the effect of centrifugal rotation in the settler so that the drop coalescence was improved. In the settler zone, the phases were separated, so the heavy phase was led to the previous stage mixer through a weir .C. and the light phase was led to the next stage mixer through a port .D. The column geometry is listed in Table 9. [12]

**Table 9.** Geometrical characteristics of the column used

Column Components	Dimensions (cm)
Mixer dimensions (length × width)	13×13
Settler dimensions (length × width)	26×13
Stage height	12
Column height	172
No. of stages	7
Agitator diameter	6.5
Blade height	1.3

## Case study (Toluene-acetone-water (high interfacial tension) and n-butyl acetate-acetone-water systems)

The liquid-liquid systems studied were toluene-acetone-water (high interfacial tension) and n-butyl acetate-acetone-water (medium interfacial tension). These systems have been recommended by the European Federation of Chemical Engineering as official test systems for extraction investigations [12]. The content of acetone in dispersed or continuous phases was approximately 3.5 (w/w %). Distilled water was used as continuous phase and technical grade of toluene and n-butyl acetate were used as dispersed phase. The physical properties of the liquid-liquid systems used in these experiments are listed in Table 10. In the present work, the values of physical properties have been assumed to correspond to the mean values of acetone concentration in the continuous and dispersed phases. The mean value of acetone concentration was obtained by averaging the values obtained at the inlet and outlet of the column.

**Table 10.** Physical properties of liquid systems at 20°C [12]

Physical property	Toluene-acetone-water	n-Butyl acetate-acetone-water
$\rho_c$ (kg / m <sup>3</sup> )	994.4–995.7	994.3-995.8
$\rho_d$ (kg / m <sup>3</sup> )	864.4– 865.2	879.6-881.4
$\mu_c$ (mPas)	1.059-1.075	1.075-1.088
$\mu_d$ (mPas)	0.574-0.584	0.723-0.738
$\sigma$ (mN / m)	27.5-30.1	12.4-13.2

Before the experiments, both phases were mutually saturated by circulation through the column. After filling the column with the continuous phase, the rate of agitation and continuous phase flow

rate were set on desired values and the dispersed phase gradually admitted to enter into the column up to the selected volumetric flow rate. The interface position was then maintained at the desired height by using the optical sensor, and the system was allowed to reach steady state, which necessitated 2-3 changes of column volume. A photographic technique was used to measure the drop diameter, since it proved to be more accurate and reliable than other techniques. When the conditions became steady, photographs were taken at different positions along the column. The drops were photographed using a Sony DSC-F828 digital camera. Drop dimensions were then determined using AutoCAD software. Drop sizes were converted to absolute dimensions by comparing measured value with packing size. In the case of non-spherical droplets, the major and minor axes,  $d_1$  and  $d_2$ , were measured and the equivalent diameter,  $d_e$ , calculated from Eq. (1).

$$d_e = (d_1^2 d_2)^{1/3}$$

The Sauter mean diameter was then calculated from Eq. (2).

$$d_{32} = \frac{\sum_{i=0}^n n_i d_i^3}{\sum_{i=0}^n n_i d_i^2}$$

where  $n_i$  is the number of droplets of mean diameter  $d_i$  within a narrow size range  $i$ . For each case, at least 400 drops were analyzed to ensure good statistical accuracy. In order to fulfill the overall experimental objective, more than eighty runs were carried out. The holdup of dispersed phase was measured by rapid withdrawal of a 100 ml sample from the mixers.

The effect of agitation speed on the drop size distribution is shown in Fig. 14. In each Figure, distributions corresponding to the different column heights have been included. It can be seen that the shape of the drop size distribution histograms does not change significantly along the column height. Drop size distributions are, on the other hand, found to be dependent on the agitation rate and interfacial tension. As can be seen in this Figure, higher agitation speed leads to a narrower and more symmetric distribution around the mean value. Moreover, drop size distributions are

found to be narrower and more evenly distributed about the mean size for the system of lower interfacial tension (Note that the scales in the following Figures are different).

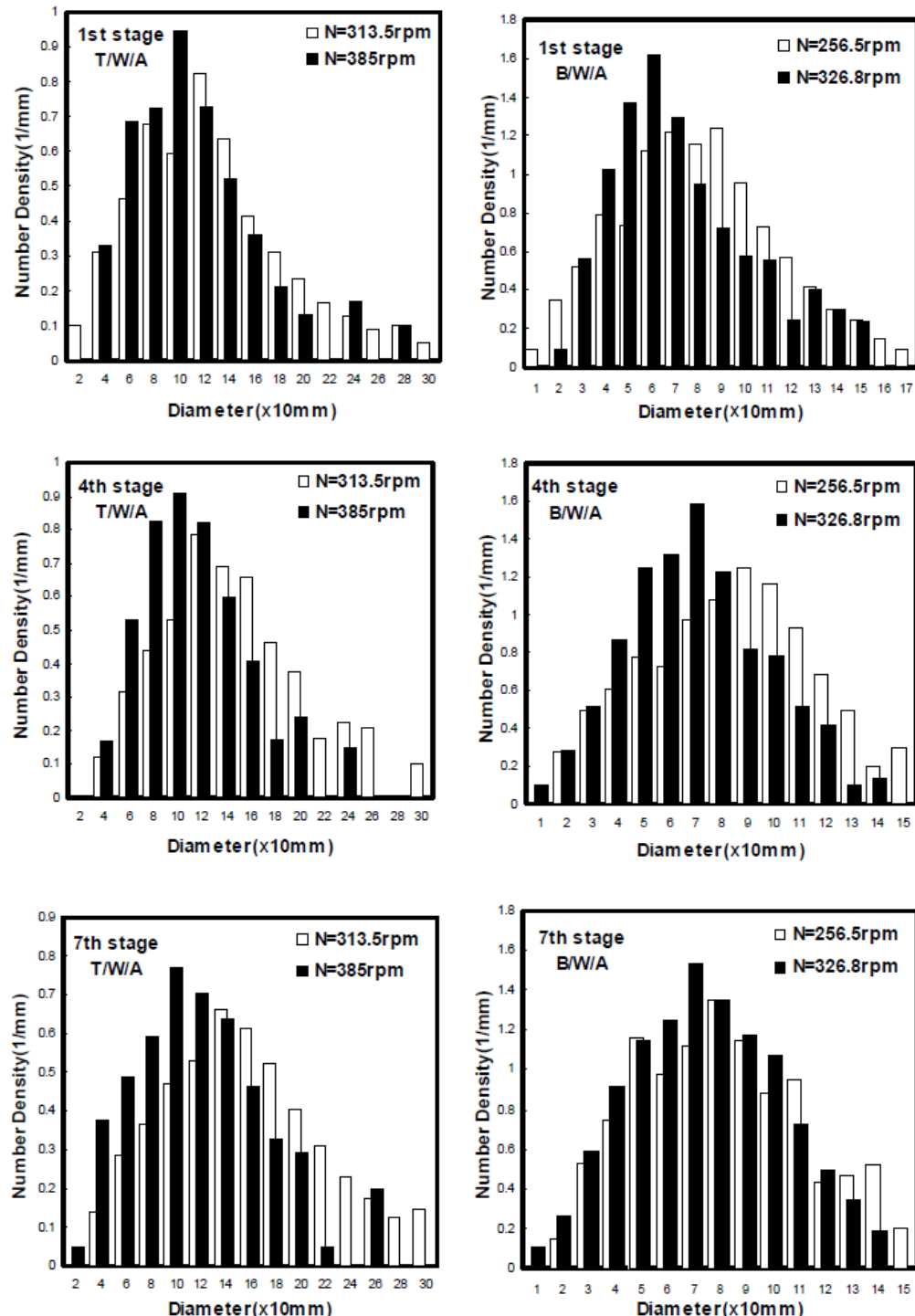


**Figure 14.** Effects of stage numbers on drop size distributions

The effect of continuous phase and dispersed phase flow rates are shown in Fig. 15. As can be seen in this figure, continuous phase and dispersed phase flow rates do not have a significant effect on the shape of drop size distribution. Changes in these variables, however, affect drop sizes by shifting the distribution towards larger drops. These results are in agreement with the observations of Rincon-Rubio *et al.* [13] and Takahashi *et al.* [14]; their experiments show a similar trend in other types of mixer-settler extraction columns.

Typical variations in the mean drop size with the column height are given in Fig. 16. Three different curves, corresponding to three different rates of agitation, are given for each mass transfer direction. For  $c \rightarrow d$  direction, the large drops formed at distributor disappeared rapidly. This rapid decrease of the Sauter mean diameter along the column is due to the predominance of the drop breakage mechanism. On the contrary, for  $d \rightarrow c$  direction, the profiles show that the drops are still growing in the first part of the column and the mean size of drop population remains nearly constant after the second or third stages, due to the competition of coalescence and breakage. This result exhibits the influence of coalescence in a case where it becomes predominant. It is also observed that the mean drop size does not change significantly above the middle of the extractor. This observation indicates that, at a certain height inside the column, the rate of coalescence becomes equally important with drop breakage for both mass transfer directions. Fig. 5 shows the effect of agitation speed on mean drop size for both systems and both mass transfer directions. As can be seen in this figure, agitation has a strong effect on the Sauter mean diameter. For both systems, it was found that as the agitation speed is increased, the mean drop size strongly decreases. The rise of agitation rate carries to higher shear stress and to intense drop breaking and consequently the Sauter mean diameter will decrease. However, at high agitation speed, the fall in the values of Sauter mean diameter is gradual and it can be conjectured that further breakup of dispersed phase drops into smaller ones is limited.

Possibly drop stabilization occurs due to the high turbulence in the continuous phase. The results confirmed that the drop size in this column changes with the direction of mass transfer. This fact

has been well known for other types of the extraction columns. When the mass transfer occurs from the continuous to the dispersed phase, the concentration of the solute in the draining film between two approaching drops will be lower than the surrounding continuous liquid. For mass transfer in the opposite direction, the concentration will be correspondingly higher.

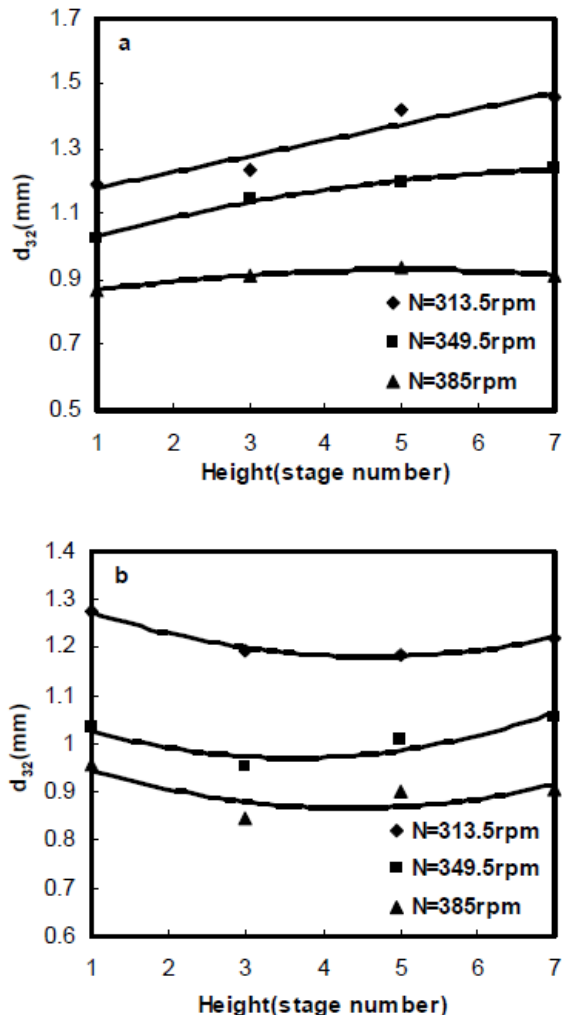


**Figure 15.** Variations in mean drop size with column height (a)  $d \rightarrow c$  direction (b)  $c \rightarrow d$  direction  
(Toluene-Acetone-Water System)

The resulting gradients of interfacial tension will retard drainage and inhibit coalescence in the former case and accelerate drainage and coalescence in the latter case. Therefore, this figure shows that  $c \rightarrow d$  transfer tends to produce smaller drops than the opposite direction. For all runs, the mean drop diameters are strongly affected by system properties. Smaller drops are generated from the medium interfacial tension system (nbutyl acetate-acetone-water) than are produced from the higher interfacial tension system (toluene-acetone-water).

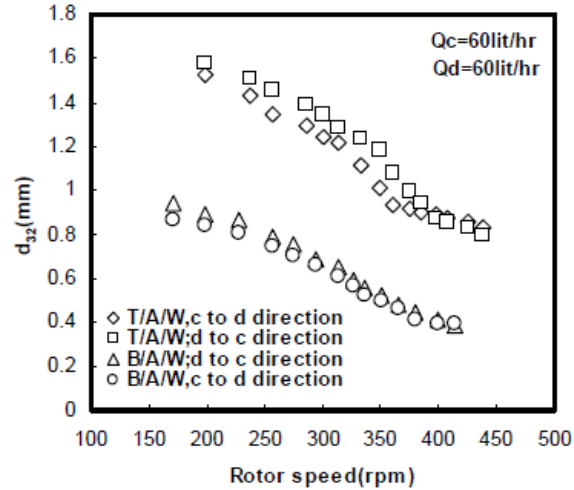


**Figure 16.** Effect of agitation speed on mean drop diameter

Fig. 17 illustrates the effect of dispersed phase flow rate on the average drop size. Increasing the flow rate of dispersed phase tends to increase the average drop size. As can be seen in Fig. 7, the effect of  $Q_d$  is weaker than the effect of agitation speed. For a 100% increase of  $Q_d$ , only a 10% increase in  $d_{32}$  was found. The increase in droplet size may be attributed to an increase in the coalescence rate due to the larger holdup values that are observed as  $Q_d$  increases. As shown in Fig. 18, the flow rate of the continuous phase has a comparable influence on the mean drop diameter. Increasing the continuous phase flow rate was found to increase the Sauter mean diameter. This increase in the mean drop size may be attributed to a decrease in residence time accompanying the decrease in the holdup. Comparing Figs. 17 and 18, it can be seen that the effect of dispersed phase flow rate on  $d_{32}$  is larger than that of continuous phase flow rate. It should be noted that the dotted lines in Figs. 17 and 18 are only a guide tool for better vision.

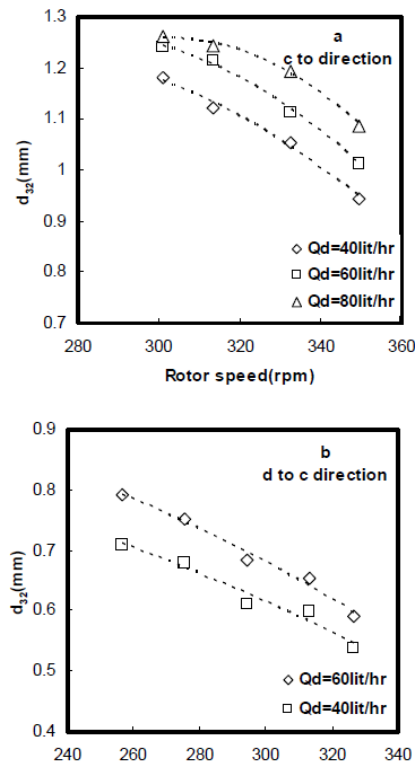


**Figure 17.** Effect of dispersed phase flow rate on Sauter mean diameter (a)-Toluene-Acetone-Water  
(b)-Butyl acetate-Acetone-Water

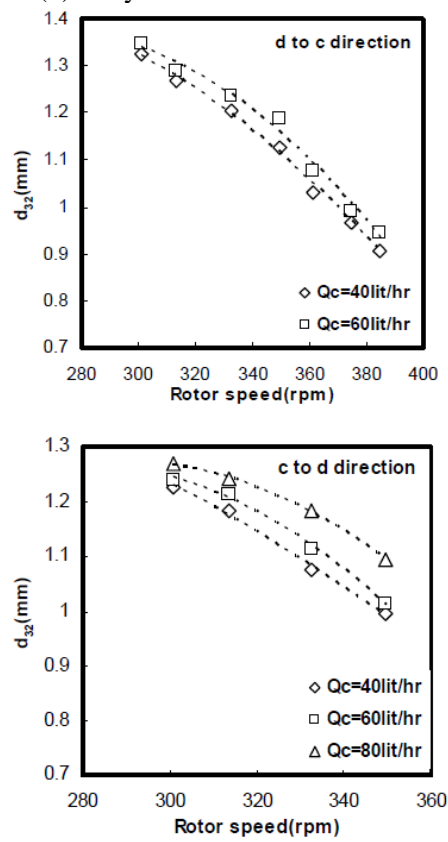


**Figure 18.** Effect of continuous phase flow rate on Sauter mean diameter (Toluene-Acetone-Water System)

### 3.1. Modeling of mean drop size

One of the main objectives in this study is to generate a reliable correlation to represent the mean drop diameter in Hanson mixer-settler columns. Currently the basic theoretical concept of Hinze [13] is commonly applied to calculate the Sauter mean diameter in stirred liquid-liquid dispersion. The maximum stable drop diameter  $d_{max}$  is calculated under the assumption that the turbulent kinetic energy of drop  $E_{kin}$  equals the interfacial energy  $E\tilde{a}$ . The Weber number  $We$  describes the ratio between  $E_{kin}$  and  $E\tilde{a}$ . This value marks a critical state where the drop is still stable:

$$We_{d_{max}} = \frac{E_{kin}}{E_\gamma} = \frac{\rho \overline{w'^2} d_{max}}{\sigma}$$

Under the condition that the energy dissipation rates in the stirred tank are spatially uniform, Eq. (3) results in an equation for the maximum drop diameter:

$$\frac{d_{max}}{D_i} = C_1 \cdot \left( \frac{N^2 D_i^3 \rho}{\sigma} \right)^{-0.6} = C_1 \cdot We^{-0.6}$$

According to several authors the maximum drop diameter correlates linearly with the Sauter mean drop diameter:

$$\frac{d_{32}}{D_i} = C_2 \cdot We^{-0.6}$$

Following the findings of previous investigations on drop size distribution in agitated vessels and extraction columns, the effect of coalescence drop size can be expressed in terms of dispersed phase holdup as:

$$d_{32} = C_4 (1 + C_3 \phi) We^{-0.6}$$

Therefore, the exponent -0.6 of the Weber number in relation to  $d_{32}$  is of great importance for scale up. On this basis, the following correlations for each mass transfer direction are derived in terms of Weber number, dispersed phase holdup, and viscosity ratio for two different systems

(Toluene-Acetone-Water and Butyl acetate-Acetone-Water) by using the least squares method:

$$\frac{d_{32}}{D_i} = 0.197(1+3.04\phi)We^{-0.6} \left( \frac{\mu_d}{\mu_c} \right)^{-1.27}$$

(d→c direction)

$$\frac{d_{32}}{D_i} = 0.23(1+2.24\phi)We^{-0.6} \left( \frac{\mu_d}{\mu_c} \right)^{-1.14}$$

(c→d direction)

which are based on 95 data points. The average relative deviation in predicted values of  $d_{32}$  from experimental points is 7.78%. The comparison of experimental results with those calculated by Eqs is shown in Fig. 19.

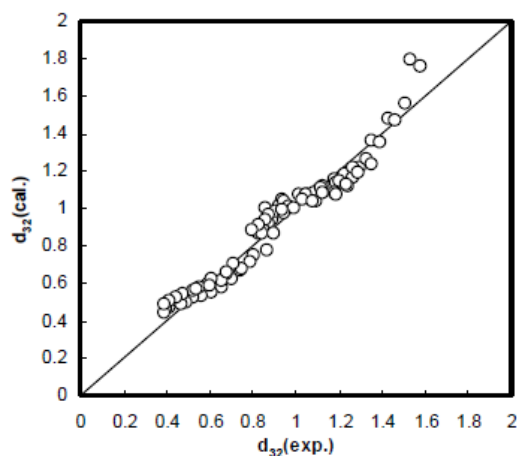


**Figure 8.** Comparison of experimental  $d_{32}$  with those calculated from Eqs.

In practice, the dispersed phase holdup is not known and should be calculated from another correlation. If predicted values of the holdup are used in Eqs. (7) and (8) to calculate mean drop size, an additional error will be introduced. An alternative drop size correlation in terms of  $N$ ,  $\phi$  and continuous and dispersed phase superficial velocities is therefore developed. The results are:

$$d_{32} = 0.187 N^{-0.83} \sigma^{0.89} V_d^{0.05} V_c^{0.15}$$

(d→c direction)

$$d_{32} = 0.31 N^{-0.51} \sigma^{0.81} V_d^{0.02} V_c^{0.13}$$

(c→d direction)

which reproduce the experimental data with an average relative deviation of 7.09%. These equations show that agitation speed and interfacial tension of liquid-liquid systems are the variables having the largest effect on  $d_{32}$ . The effect of both continuous and dispersed phase superficial velocities is small and positive, that is, increasing either results in higher drop size.

Fig. 20 shows the agreement between experimental and predicted data, using correlations. Figs. (19) and (20) indicate that the suggested correlations can predict Sauter-mean drop diameter with high accuracy and both methods can be used for prediction of  $d_{32}$ , although equations do not need any experimental values.

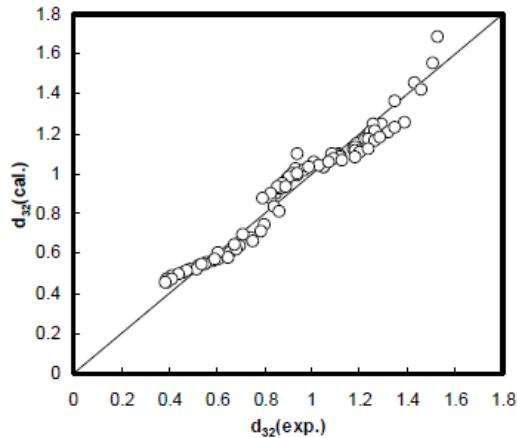


**Figure 20.** Comparison of experimental  $d_{32}$  with those calculated from Eqs. (9) and (10)

The effects of agitation speed, dispersed phase and continuous phase flow rates, interfacial tension, mass transfer direction, and the height of column on drop sizes were studied experimentally in a pilot scale

Hanson mixer-settler. The results showed that mean drop size and its distribution are drastically affected by agitation speed as well as interfacial tension, while they are only slightly dependent on phase flow rates. Drop size distribution shape varied little along the column height. The experiments revealed that mass transfer direction had a significant effect on drop behavior along the column height, although at a certain height above the middle of the column mean drop size became constant for both mass transfer directions. Additionally, in the present work, two empirical correlations are derived to predict the Sauter mean drop diameter from the measurement of more than 30000 drops. The predictive correlations can reproduce the experimental data with very high accuracy. The present work is useful to those that apply Hanson mixer-settler column and the results of this study can reduce the experimental work associated with the design of this type of extractor.[12]

## Kühni column system for extraction liquid-liquid

### **Introduction**

Liquid-Liquid Extraction is a mass transfer operation in which a liquid solution (the feed) is contacted with an immiscible or nearly immiscible liquid (solvent) that exhibits preferential affinity or selectivity towards one or more of the components in the feed. The construction of the tie –line on the binodal curve to determine the number of theoretical stages, has to be made graphically using the relevant correlations. This requires experimental determination of the mutual solubility and tie-line data. Treybal even before Hand and other workers introduced a method of construction without using tie-lines data of binodal curves to determine the number of theoretical stages. This method is investigated and proved to be correct, rapid and does not require experimental determination of tie-line data. Treybal method is used in the present work and proved to be accurate and easy to apply. The number of stages is determined using this method and all other design parameters of a sieve tray extraction column are obtained. Complete design by hand calculation procedure is realized and Outlined. The number of theoretical stages is calculated using ASPEN PLUS SOFTWARE. [14]

### **Drop Size in a Kuhni Extraction Column**

The hydrodynamic behaviour of a Kuhni extraction column has been investigated experimentally. The experiments were carried out in the absence of mass transfer for two different standard chemical systems. In the experiments operating variables including agitation speed, the flow rate of both liquid phases and interfacial tension have been studied. Sauter-mean drop diameter, flooding velocity and holdup at flooding have been measured in the Kuhni column. The results showed that Sauter-mean diameter is strongly affected by agitation speed and interfacial tension whereas the effects of continuous phase and dispersed phase flow rates are negligible. Two rigorous empirical correlations are proposed for predicting flooding

velocities and Sauter-mean drop diameter with a mean deviation of 5.7% and 7.2%, respectively. The mean drop size correlation is a function of column geometry, operating conditions and physical properties of liquid systems. Good agreement between predictions and experiments is found for all operating conditions investigated. [15]

In this work, the hydrodynamic behaviour of a Kühni column was investigated by measuring the Sauter-mean drop diameter and flood point characteristics using two different liquid systems. The effects of operating variables on mean drop size and flood point are examined. Also, experiential correlations for mean drop size and flooding velocities as a function of operating conditions, physical properties of the liquid systems and column geometry were proposed.

### **Description of Experimental Setup**

A pilot-scale Kühni extraction column with ten stages that made of 2 mm perforated stainless steel sheet was used in the experiments. The active part of the column consisted of a 0.75 m long glass tube with 0.117 m internal diameter. Two settlers with 0.1775 m diameter were employed at both ends of the column to separate the two liquid phases. There are two pumps, one for the dispersed phase and one for the continuous phase. The interface level was controlled automatically by an optical sensor. A solenoid valve was provided at the outlet stream of the heavy phase. This valve received electronic signals from the sensor. When the interface location was going to change, the optical sensor sent a signal to the solenoid valve and the aqueous phase was allowed to leave the column by opening the diaphragm of the solenoid valve. The organic phase was allowed to leave the column via the overflow. Other geometrical characteristics of the column are presented in Table 11. The schematic diagram of Kuhni extraction column is shown in Figure 21.

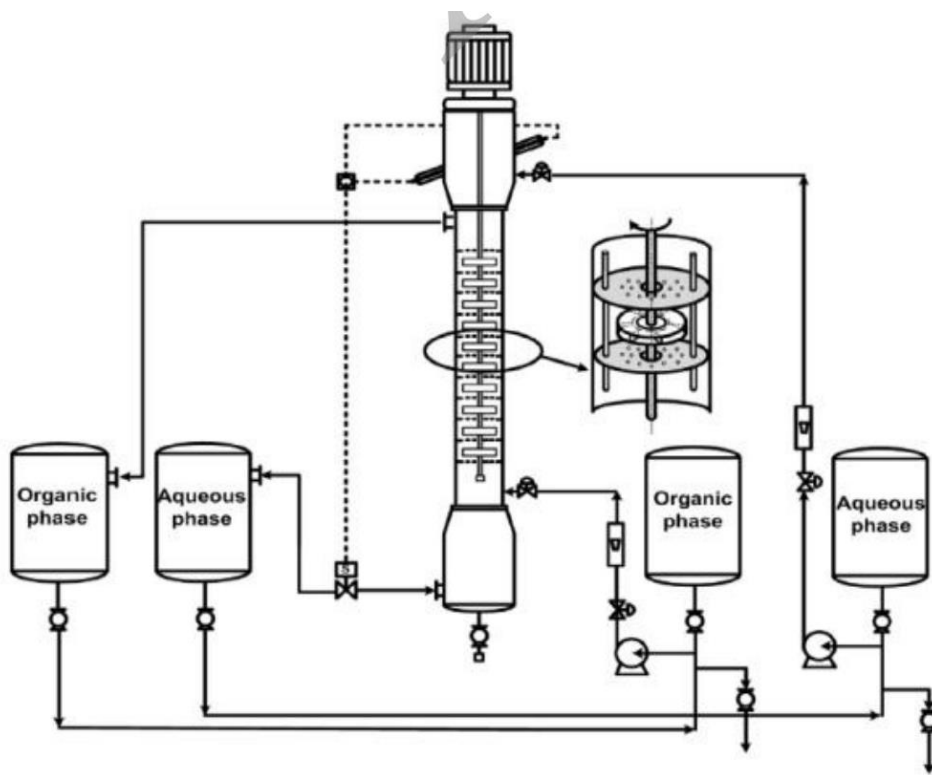


Figure 21. A schematic diagram of the Kuhni column

### Liquid–Liquid Systems

Two liquid-liquid system to cover a wide range of interfacial tension values were chosen according to the recommendations of the European Federation of Chemical Engineering [12]. The liquid-liquid systems that studied were toluene–water (high interfacial tension), n-butyl acetate–water (medium interfacial tension). The technical grade, solvents at least 99.5 wt % purity were used as the dispersed phase. All experiments were carried out at the  $20\pm2$  C. The physical properties of the liquid-liquid systems used in the experiments are shown in Table 13.

**TABLE 12.** Technical parameters of Kuhni extraction column

Parameter	Value	Parameter	Value
Column diameter (m)	0.117	Settler diameter(m)	0.1775
Tray number	10	Active volume of the column( $m^3$ )	0.0075
Number of holes	27	Impeller diameter (m)	0.05
Tray perforation diameter (m)	0.0075	Plate thickness(m)	0.002
Column height(m)	0.7	Compartment height(m)	0.055

**TABLE 13.** Physical properties of liquid systems

Physical property	Toluene-water	n-Butyl acetate-water
$\rho_a$ (kg/m <sup>3</sup> )	998.2	997.6
$\rho_b$ (kg/m <sup>3</sup> )	865.2	880.9
$\mu_a$ (m Pas)	0.963	1.027
$\mu_b$ (m Pas)	0.584	0.734
$\sigma$ (mNm <sup>-1</sup> )	36.0	14.1

### Droplet size measurements

According to the importance of droplet size, many researchers studied the effect of column operating variables on drop size and developed correlations for predicting the mean drop size. Drop size affects almost all the parameters that influence hydrodynamics and mass transfer in an extraction column. The drop size developed for different extractors is presented in Table 4. It shows that drop size depends on column geometry, phases properties and flow rates and agitation speed. In this work, to measure the drop diameter a photographic technique was used. By taking a digital photo of the column by a Nikon D3100 digital camera and comparing the drop dimensions with the known size of the column as a reference droplet size were obtained. For this comparison two characteristic lengths of the internals were used, being the tray thickness and spacing. The recorded photos were analyzed with image processing software to determine the size of the drops. At least 300 drops were analyzed for each experimental condition. For elliptical drops, both the minor and major axes,  $d_1$  and  $d_2$ , were measured and the equivalent diameter,  $d_e$ , calculated from the following equation:

$$d_e = (d_1 d_2)^{1/3}$$

After the determination of the drop sizes, the Sautermean drop diameter,  $d_{32}$ , was calculated at experimental conditions used as follows:

$$d_{32} = \frac{\sum_{i=1}^n n_i d_i^3}{\sum_{i=1}^n n_i d_i^2}$$

where  $n_i$  is the number of droplets of mean diameter  $n_i$  within a narrow size range  $i$ .

## Numerical methods

Numerical solutions including Genetic Algorithms (GA) and Particle Swarm Optimization (PSO) were used to obtain optimum values of flooding velocities and drop size correlations parameters. GA is a search method to find an approximate solution optimization problem using the concepts of biology such as inheritance and mutations. In this algorithm based on Darwin's theory of evolution, the problem variables by using appropriate binary strings are coded. Then, by simulation of a struggle for survival rules, regularly more appropriate disciplines (that in fact, represents the improved solutions) are obtained. Like other optimization techniques, GA is an optimization method based on probabilities, namely to ensure obtaining the general optimal solution, in any given optimization problem this algorithm is run several times and compare the results. Also, the probability of finding a global optimum solution by GA is very high. To solve the minimization problems before applying GA should be converting the problem to a maximization problem.

The most common way is to define a fitness function, the contrast is a linear combination of the cost function. For example, if the goal of the optimization is to find the minimum of the function,  $f(x)$  and this function will return the value of all slopes greater than -1 then it can be used to define the fitness function.

$$F(x) = \frac{1}{1 + f(x)}$$

PSO is a population-based stochastic optimization technique, inspired by the social behaviour of bird flocking or fish schooling. PSO shares many similarities with evolutionary computation techniques such as GA. The system is initialized with a population of random solutions and searches for optima by updating generations. However, unlike GA, PSO has no evolution operators such as crossover and mutation. In PSO, the potential solutions, called particles, fly through the problem space by following the current optimum particles.

Each particle keeps track of its coordinates in the problem space which is associated with the best solution (fitness) it has achieved so far (The fitness value is also stored). This value is called pbest. Another "best" value that is tracked by the particle swarm optimizer is the best value, obtained so far by any particle in the neighbors of the particle. This location is called lbest. When a particle takes all the population as its topological neighbors, the best value is a global best and is called gbest

The PSO concept consists of, at each time step, changing the velocity of each particle toward its pbest and lbest locations. Acceleration is weighted by a random term, with separate random numbers being generated for acceleration toward pbest and lbest locations.

### **Sauter-Mean Drop Diameter**

Agitation speed and phase flow rates are the most important parameters that have an effect on droplet size. The effect of agitation speed on Sauter-mean drop diameter is shown in Figure 22. It shows that smaller drops are observed at higher rotor speeds, that is a result of increased droplet breakup. Although the decrease in Sauter-mean diameter at a higher rotor speeds is smooth. Coalescence of droplets at high rotor speeds is increased by increasing the probability of droplet collision. So, at the high rotor speeds, the increased rate of coalescence dominance the increased sentiment for droplet breakage and the drop size stabilized. Figure 22 also shows that an increase in the interfacial tension results in an increase in drop diameter. The effect of dispersed phase velocity on the mean drop size is shown in Figures 23 and 24. As shown in Figure 23, increasing the dispersed phase flow rate tends to increase the mean drop size. Increasing in dispersed phase velocity cause to a larger drop formation diameter and a higher coalescence frequency. Figures 25 and 26 also show that the effect of dispersed phase velocity grows in importance as the interfacial tension of the system increases.

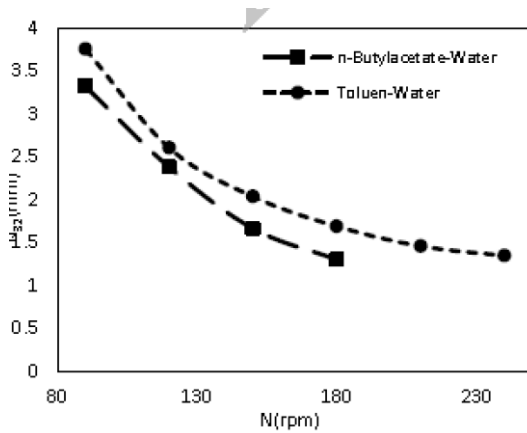


**Figure 22.** Effect of rotor speed on mean drop size  $Q_d=QC=24$  lit/hr

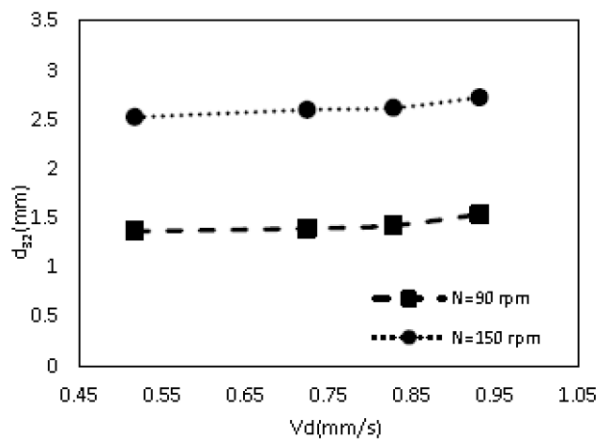


**Figure 23.** Effect of dispersed phase velocity on mean drop size  $QC= 24$  lit/hr, n-butyl acetate-water

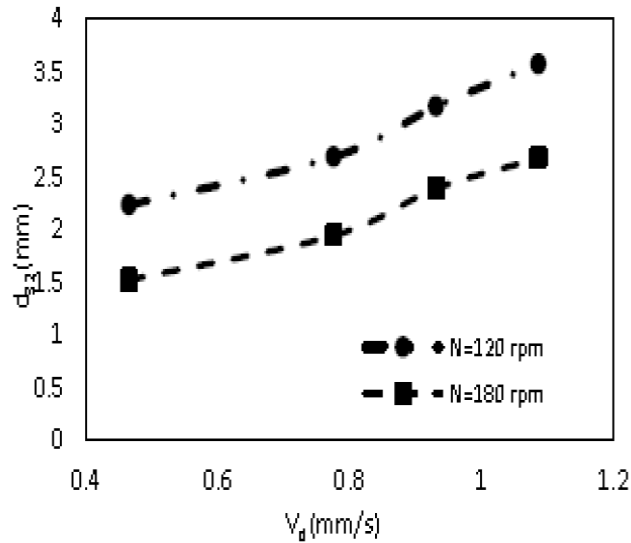


**Figure 24.** Effect of dispersed phase velocity on mean drop size  $QC= 24$  lit/hr, Toluene-water

### Prediction of Sauter-mean Drop Diameter

One of the main objectives of this study is to propose a new correlation for the prediction of mean drop size. Since a correlation for the mean drop size,  $d_{32}$ , in Kuhni column is not available, Kumar and Hartland Used the following Equation to predict the Sauter-mean drop diameter. This correlation is proposed for predicting mean drop size in Kuhni column. This equation reproduces the experimental results with an average relative deviation (ARE) of 26.8%.

$$d_{32} = C_\psi \sqrt{\left[ \frac{1}{[C_\Omega (\frac{\gamma}{\Delta \rho g})^{0.5}]^2} + \frac{1}{[C_\Pi \epsilon^{-0.4} (\frac{\gamma}{\rho_c})^{0.6}]^2} \right]^{1/2}}$$

To obtain the sound correlation for predicting the mean drop size, dimensional analysis with considering influencing parameters such as the geometry of column, operating conditions and physical properties of liquid systems was used. The following equation for the mean drop size was obtained using the Buckingham theorem. In order to consider the column geometry effect on Sauter-mean drop diameter and also to increase the total number of data points, the experimental results are taken from Oliveira et al for water-Exxsol D-80 system.

$$d_{32} = n_1 \left( \frac{V_c}{V_d} \right)^{n_2} \left( \frac{\mu_d N}{V_d^2 \Delta \rho} \right)^{n_3} \left( \frac{V_d \Delta \rho D_{cu}}{\mu_d} \right)^{n_4} \left( \frac{V_d \Delta \rho D_{im}}{\mu_d} \right)^{n_5} \\ \left( \frac{\mu_c}{\mu_d} \right)^{n_6} \left( \frac{\rho_c}{\Delta \rho} \right)^{n_7} \left( \frac{\sigma}{\mu_d V_d} \right)^{n_8} \left( \frac{\mu_d \varepsilon \bar{\epsilon}}{V_d^3 \Delta \rho} \right)^{n_9} \left( \frac{\mu_d}{\Delta \rho V_d} \right)$$

To fit the experimental data and to obtain the parameters and minimize the relative absolute error, the following objective function was minimized.

$$ARD\% = 100 \times \frac{|(d_{32}^{exp} - d_{32}^{cal})|}{d_{32}^{exp}}$$

Numerical solutions including GA and PSO were used to obtain optimum values of Equation (5) parameters.

In this work, an experimental study of mean drop size and flooding velocity in a Kühni extraction column was presented. The effects of agitation speed, dispersed phase and continuous phase flow rates, on drop sizes and flooding velocity, were introduced. The results showed that Sauter-mean drop diameter is strongly affected by agitation speed as well as interfacial tension whereas volumetric flow rates of the dispersed and continuous phase have almost no significant effect. Sauter-mean drop diameter decreases with both increases in rotor speed and a decrease in interfacial tension. Two rigorous empirical correlations for predictions of flooding velocity and drop size diameter in Kühni columns were presented. The correlations are functions of operating variables, the physical properties of liquid systems and column geometry. The results showed that the maximum throughput decreases with the increase in agitation speed and flow ratio, while it increases with the increase in interfacial tension. The predictive correlations can be used for prediction of maximum capacity of existing Kühni columns and final sizing of the column diameter. [15]

## A STUDY OF THE DROP SIZE DISTRIBUTIONS AND HOLD-UP IN SHORT KÜHNI COLUMNS

The hydrodynamic behaviour of a short Kühni column was investigated under no mass transfer conditions using the binary system water (continuous phase) and Exxsol D-80 (dispersed phase). The countercurrent flow pattern of the liquid phases was characterised regarding the Sauter mean drop diameter, drop size distribution and hold-up; a photographic method was used to assess drop sizes. The following operating variables were studied: rotor speed, flow rate of both liquid phases and column stage. The log-normal probability density function was found to be adequate to fit the experimental drop size distributions along the column. As expected, smaller drops and more uniform drop size distributions were obtained with the

increase of rotor speed and column stage number, thus indicating the predominance of drop breakage phenomena in short columns. The total hold-up was influenced mainly by rotor speed and flow rate of the dispersed phase. Recommended correlations available in the literature were found to be inadequate for predicting experimental drop sizes and hold-up, so alternative expressions, valid only for short Kühni columns, were proposed. [16]

As a general trend, the Sauter mean diameter decreases everywhere in the extraction column with agitation, while the drop size distribution becomes narrower. On the other hand, an increase in the flow rates results in larger drops, an effect which is more significant for the dispersed phase flow rate in comparison with the continuous one (Tsouris et al., 1990). In the absence of turbulence or for low agitation levels ( $ReR = 10,000$ ), the average size of drops is controlled by the balance between buoyancy and interfacial tensions and is given by the following equation (Bailes et al., 1986):

$$d_{32} = C_1 \left( \frac{\gamma}{\Delta \rho g} \right)^{0.5}$$

where  $C_1$  is an empirical parameter depending on the column geometry, mass transfer direction, temperature and physical properties. For a rotating disc contactor, similar values for  $C_1$  have been found by Chang-Kakoti et al. (1985) and Moreira et al. (2005) for drops of n-butyl alcohol ( $C_1 = 1.3$ ) and n-heptane ( $C_1 = 1.4 \pm 0.2$ ) in water, respectively. More turbulent conditions ( $ReR > 10,000$ ) will result in smaller drops that can be conveniently predicted by empirical or semiempirical correlations such as those proposed by Fischer (1973) and Kumar and Hartland (1996) for the Kühni column. Experimental investigations carried out in a rotating disc contactor have shown that mean drop sizes are strongly influenced by rotor speed, column height and dispersed phase flow rate when  $ReR > 10,000$  (Yamaguchi et al., 2002; Moreira et al., 2005). Concerning drop size distributions, experimental studies with agitated columns have shown that distributions of rising organic drops dispersed in a continuous aqueous phase are

broad in the first stages, becoming narrower and shifting toward smaller drop sizes along the column until a steady-state distribution is achieved (Tsouris et al., 1990; Moreira et al., 2005). On the other hand, a contrary behaviour, resulting in relatively larger drops, has been observed in the upper stages of the column due to the continuous phase feed effect, thus indicating that drop breakage dominates in the base of the column, whereas coalescence and breakage rates reach equilibrium in the upper stages (Tsouris et al., 1990). Consequently, a variation in drop size distribution produces a hold-up profile exhibiting a maximum value along the column depending on the operating conditions, which can be used to determine the column flooding. A unified correlation for the prediction of the total hold-up of the dispersed phase in columns has been proposed by Kumar and Hartland (1995) for engineering calculations. This correlation predicted the experimental hold-up obtained by Kentish (1996) in a Kühni column (72mm diameter, 25 stages) to within a deviation of 17.7% for the system acetic acid-water-MIBK (methyl isobutyl ketone). Despite the obvious importance of knowledge of drop size for the theoretical description of extraction operation in columns, Grimaum (2006) points out that this is a far more problematic variable than holdup. In some practical situations, drops are quite difficult to observe and sometimes just impossible to be measured as no dispersion is identified. Moreover, when dispersion is observed, drops are not spherical at all but form big bulges or lumps. In the case of agitated columns, however, drops are practically spherical for a broad range of operational conditions, so CFD or drop-population balances can describe their behaviour with satisfactory accuracy. Therefore, at the current stage of knowledge, piloting and modelling contributions are both important (and also complementary) for improving the design procedure for extraction columns. In the present work, experimental drop size distributions and hold-up have been measured in a short Kühni column (150 mm diameter and 5 stages) using the binary system water (continuous phase) and kerosene Exxsol D-80 (dispersed phase) at room temperature in order to investigate the hydrodynamic behaviour of

ascending drops in short columns under normal operating conditions in the range of 7225 ReR 21675. According to Fan et al. (1987), the main difficulties to be recognised in a short column are the end effects and inlet drops being of uncharacteristic size for a given geometry and degree of agitation, so this work aims to gain a better understanding of drop behaviour in short columns to provide basic data required for column design at a reduced cost.

### **Kühni Pilot Scale Unit**

The current experimental work was carried out in a short Kühni column of 5 stages and 150 mm diameter which was built in a cylindrical precision bore glass section. Each stage was equipped with a six-blade turbine agitator (rotor diameter = 85 mm and rotor height = 10 mm) with accurate speed control, and stator plate (fractional free cross-sectional area = 30 %) spacing of 70 mm. All the internal parts of the column were constructed in AISI 316 stainless steel. Teflon annular gaskets were fixed on the stators to prevent any liquid from passing between the stators and the column wall. The dispersed phase was introduced into the column using a conical distributor of 92 mm diameter made of AISI 316 stainless steel centrally located in the base of the column. In the distributor, a total of 170 holes of 1 mm diameter each are distributed into five concentrical circles. The diameter of the smaller circle of holes is 37 mm and the distance between each circle of holes is 9 mm; in each circle, the distance between holes is around 6-7 mm. In the unit, all piping was constructed of resistant plastic and pumps were helicoidal provided with a PID system for precise flow rate control. Tanks were made of polypropylene. A scheme of the experimental pilot-scale unit used in this work is shown in Figure 25. Reagents Runs were carried out in the absence of mass transfer using water as the continuous phase and commercial kerosene Exxsol D-80 (Exxon Mobil, predominantly aliphatic, aromatic max. of 0.5%wt.) as the dispersed phase, at room temperature. Distilled water and Exxsol D-80 were mutually saturated before being fed into the column to prevent miscibility effects from interfering with drop size measurements. The physicochemical

properties of saturated liquids at 25°C are given in Table 14. After each run, the column was cleaned using a solution of non-surface-active detergent, then thoroughly rinsed with tap water and finally cleaned with distilled water. All joints and pipes were washed to ensure thorough removal of the detergent. Experimental and Image Analysis Procedures. The same experimental methodology and image analysis procedure proposed by Moreira et al. (2005) for the photographic determination of drop size distributions in a rotating disc contactor has been adopted in this study. The following operating variables and range levels were investigated in this work: rotor speed (60, 90, 120, 150 and 180 rpm), the flow rate of the continuous phase (1.24 and 2.00 L/min), the flow rate of the dispersed phase (1.24 and 2.00 L/min) and stage number from the bottom of the column (0 or distributor, 1, 3 and 5). These variables and levels have been chosen based on a previous study (Mansur et al., 2003). Under this range of operating variables, the short Kühni column described in Section 2.1 operates at 7225 ReR 21675 conditions. Firstly, the column was filled with the continuous aqueous phase until it reached a previously set level (1- 2 mm above the top stage); this was done carefully to avoid the formation of small bubbles below the plates. The rotor motor was started and agitation speed adjusted. Then both phases were fed to the column at a specified throughput and allowed to circulate in the unit for 30 minutes according to Figure 1 (closed system) to assure that the hydrodynamic steady-state condition has been reached. A digital camera (Nikon® Coolpix 990) was suitably placed 200 mm from the column wall to provide photographs of the two-phase mixture at a given operating condition for drop size measurements. A graduated scale was fixed by the side of the column as a size reference. In the photographs obtained from runs at 150 and 180 rpm, drops of stages 3 and 5 were photographed using the zoom mode of the camera to obtain clearer pictures of the fine drops. The photographs were analysed with the aid of the software Quantikov Image Analyser (version 5.1 for Windows®) for drop size determination. All drops were assumed to be spherical because they did not exhibit very

significant deviations from the spherical shape for the operating conditions evaluated in this work. Drops were measured in the vertical position only according to Moreira et al. (2005) and measured drop values were multiplied by a factor of 0.8 to correct the parallax deformation of drops photographed inside the column. A minimum of 400 drops was analysed for each experimental condition to guarantee the statistical significance of the determined size distributions (Colella et al., 1999). The total hold-up of the dispersed phase was assessed using the shut-down method (Gayler et al., 1951). Measurements were done in triplicate to verify experimental reproducibility.

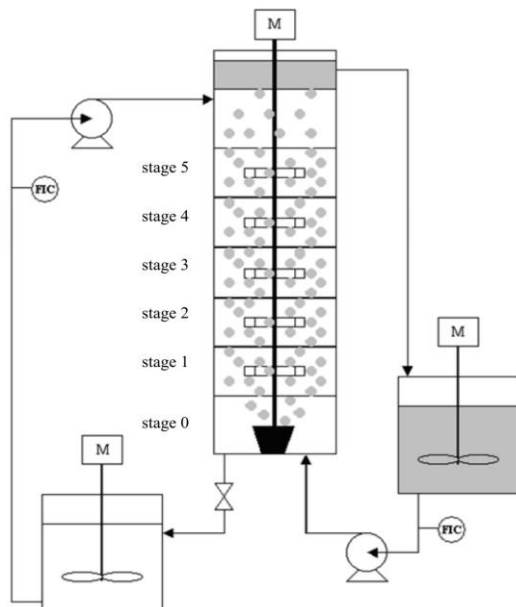


**Figure 25:** Experimental arrangement of the pilot unit.

Table 14: Physicochemical properties of saturated liquid phases (25°C).

	Water	Exxsol D-80
Density (kg/m <sup>3</sup> )	996	801
Viscosity (kg/m.s)	0.0011	0.0016
Interfacial tension (N/m)		0.017

Drop Size Distributions in a Short Kühni Column The drop diameters determined in the analysis of the photographs of the two-phase mixture were used to establish the corresponding drop size distributions considering 18 equally spaced size classes in the range 0.0 d (mm) 9.0

for all analyzed operating conditions. The effect of rotor speed on the experimental drop size distributions at different positions along the short Kühni column (stages 0, 1, 3 and 5) is shown in Figure 26 at constant flow rates of both phases ( $Q_c = 1.24 \text{ L/min}$  and  $Q_d = 2.00 \text{ L/min}$ ). It was observed that drop size distributions shifted to the left with the increase of agitation, thus evidencing that smaller drops and more homogeneous distributions are obtained in more turbulent conditions, as verified also for other types of liquid-liquid columns (Tsouris et al., 1990; Moreira et al., 2005). It was also observed that, for a given stage, the distribution became narrower as the rotor speed increased (this is rather evident in Figure 26 for stage 5). Furthermore, for a given rotor speed, the drop size distribution was broader at the bottom of the column than at the top. Such behaviour was attributed to an increase in the frequency of drop collisions with the internals of the column due to the increase in the shear force produced by the rotors to break the dispersed phase into smaller drops. The effect of rotors in order to enhance drop breakage was not significant at stage 0, which contains no rotor, and the small shift to the left observed in the drop size distribution at 180 rpm could be attributed to the turbulence effect from stage 1.

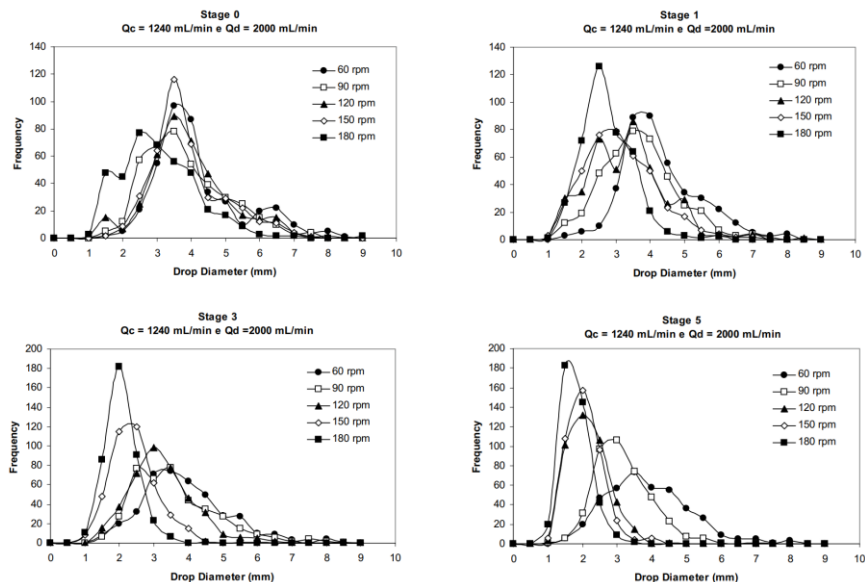


Figure 26: Effect of rotor speed on the drop size distributions at stages 0, 1, 3 and 5 in the short Kühni column ( $Q_c = 1.24 \text{ L/min}$  and  $Q_d = 2.00 \text{ L/min}$ ).

Figure 27 shows the influence of the stage number on the experimental drop size distributions measured in a short Kühni column at changing rotor speeds and fixed flow rates of both phases. The measured drop sizes ranged from 0.5 to 8.5 mm for the operational conditions investigated. Broader distributions were found at lower rotor speeds and at stages near to the bottom of the column, thus evidencing how inaccurate the use of a representative mean drop size is for these populations. According to Figure 3, drop size distributions did not change significantly at stages 0, 1 and 3 if rotor speeds were lower than (or equal to) 120 rpm. Actually, for these slow rotor speeds, the breakage frequency was too small to bring about significant changes in the size distribution for the small differences in column stages 0, 1 and 3. The same behaviour was verified for the other flow rate levels investigated as well. The effect of flow rates of the continuous and dispersed phases on the experimental drop size distributions at changing rotor speeds and at stages 3 and 5 of the short Kühni column is shown in Figure 28. No significant effect was observed for the flow rate of the dispersed phase for the operational conditions investigated. On the contrary, the flow rate of the continuous phase affected significantly the drop size distributions at higher levels of agitation, e.g., 150 and 180 rpm. Again, for rotor speeds lower than 120 rpm, a small breakage frequency might explain the lack of an effect of the flow rate of the continuous phase on the drop size distributions. In fact, the increase of the flow rate of the continuous phase led to an increase in the drag force, which then resulted in a reduction in the ascending velocity of the drop and thus to an increase in the drop residence time in the column. Consequently, the frequency of drop collisions with the internals of the column is increased, so smaller drops were then obtained. In addition, no significant effect was identified on the drop size distributions measured at stages 0 and 1 for the flow rate levels studied. Apart from the qualitative analysis of the effects of the considered operating variables upon the drop size distributions, an attempt was made to enable some quantitative

representation of these effects. In this study, the log-normal probability density function was chosen for representing the experimental drop size distributions:

$$p_{lg}(d) = \frac{1}{\sqrt{2\pi}d\sigma} \exp\left[-\left(\frac{\ln d - \mu}{\sqrt{2}\sigma}\right)^2\right]$$

in which  $d$  is the drop diameter and  $P$  and  $V$  are parameters to be fitted. It should be emphasised that the log-normal function was already found to be adequate for describing drop size distributions in extraction columns (Giles et al., 1971; Tsouris et al., 1990; Moreira et al., 2005). For a given diameter  $d_i$ , the corresponding cumulative frequency  $F_i$  is expressed as follows:

$$F_i = \int_0^{d_i} p(x)dx$$

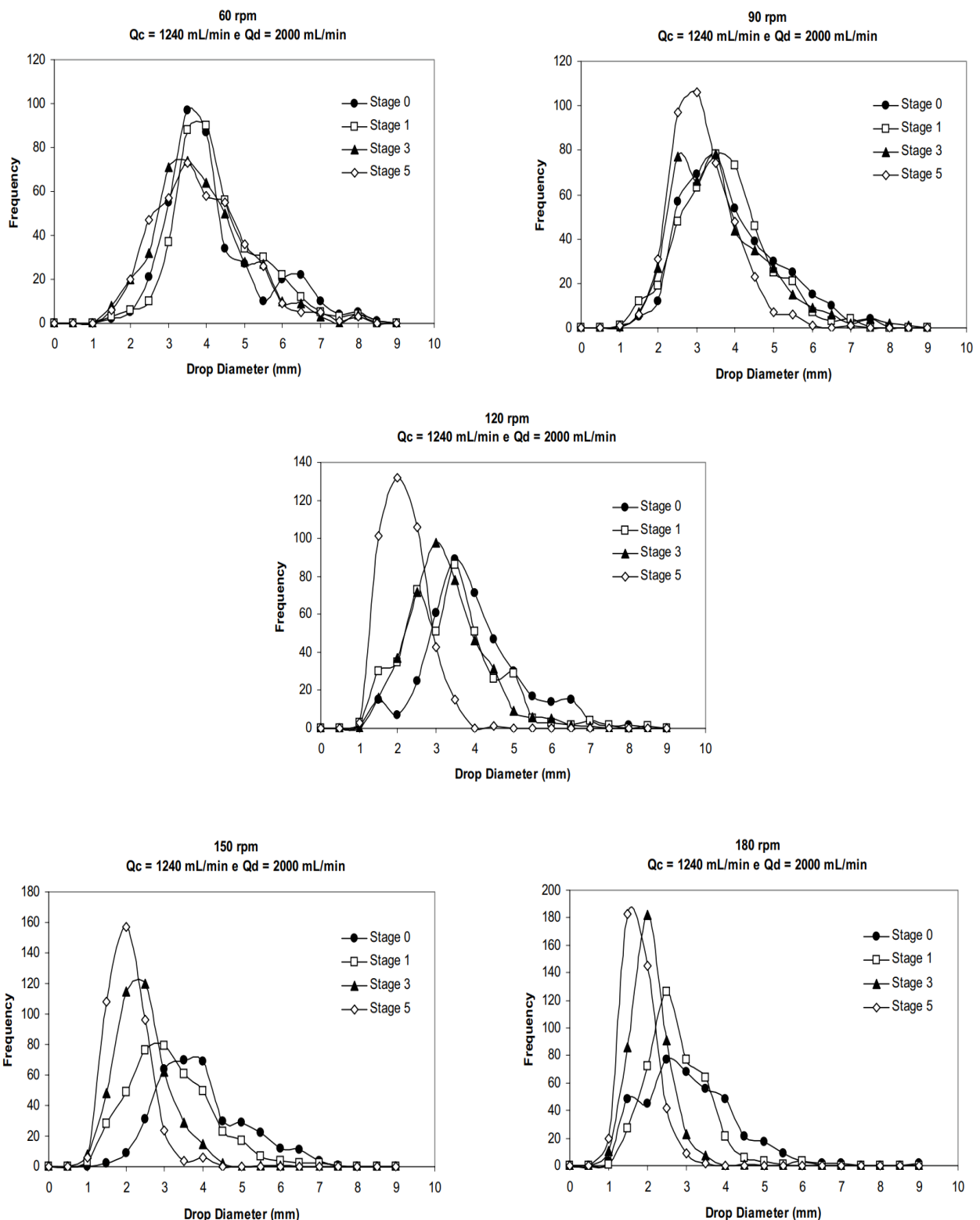


Figure 27: Effect of the number of the stage on the drop size distributions at changing rotor speeds in the short Kühni column ( $Q_c = 1.24 \text{ L/min}$  and  $Q_d = 2.00 \text{ L/min}$ ).

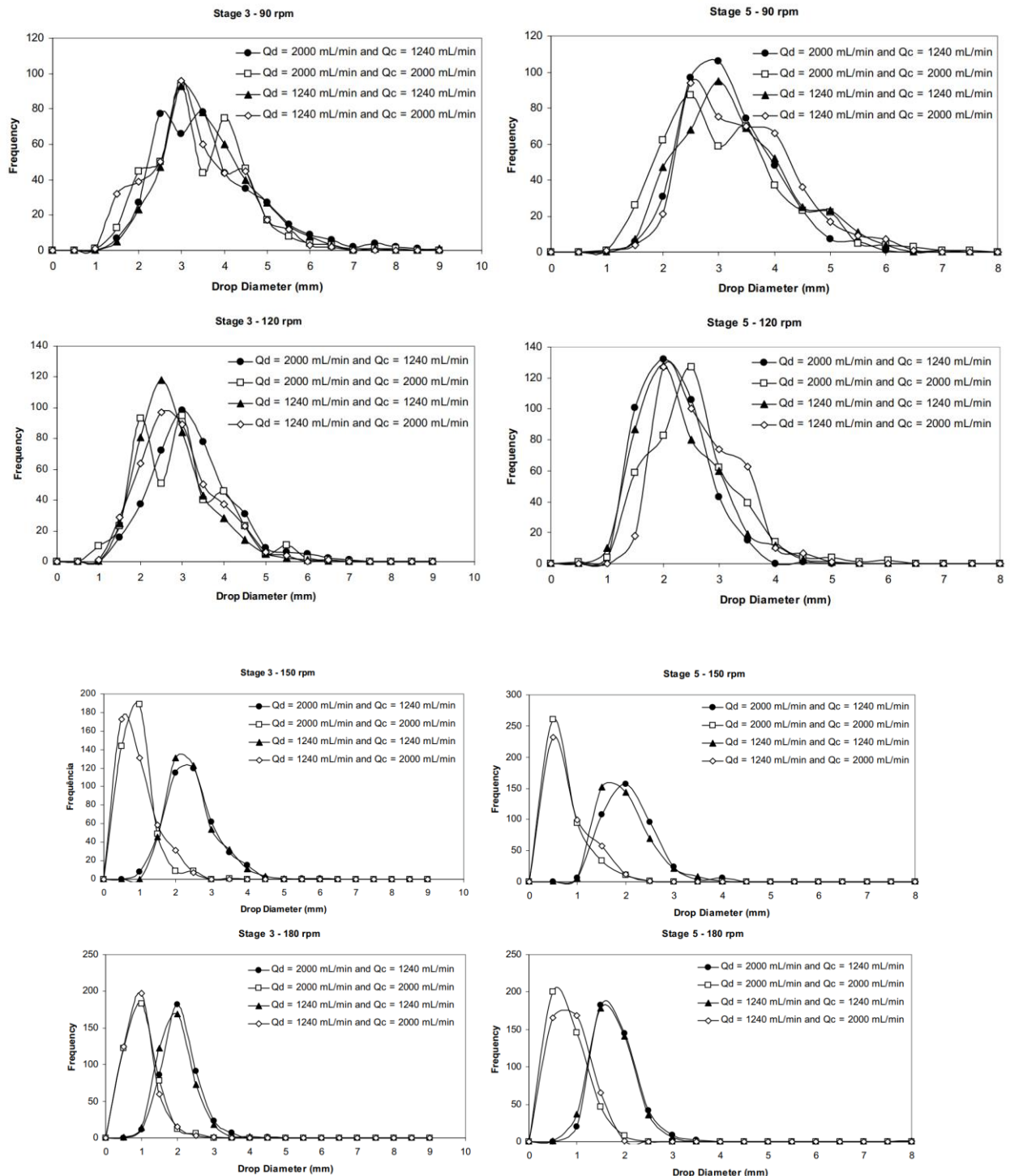


Figure 28: Effect of flow rates of the continuous and dispersed phases on the drop size distributions at changing rotor speeds in the short Kühni column (stage numbers 3 and 5).

For each diameter  $d_i$ , the experimental cumulative frequency was estimated as the number of drops with a diameter equal to or smaller than  $d_i$  divided by the total number of analysed drops plus two. The values of  $d_i$  as a function of  $F_i$  were used in the fitting of the inverse cumulative

log-normal distribution to the data set with the aid of the software Statistica®, thereby determining the parameters P and V for each set of studied operating conditions. As far as the fitting determination coefficient ( $R^2$ ) is concerned, the log-normal function represented the data well within the investigated range of operating parameters, as most of the fittings exhibited values of  $R^2$  greater than 0.970, the minimum value being equal to 0.927. No significant correlation between P and V was found (p-level < 0.05), whose values were thus chosen to represent the drop size distributions in the short Kühni column. The parameters P and V were fitted in order to obtain empirical correlations that related these parameters to the corresponding values of flow rates of the continuous and dispersed phases, rotor speed and stage number. After a series of trial-and-error tests, the following functions, whose linear coefficients were adjusted by multiple linear regression, were found to be adequate to estimate the parameters of the log-normal drop size distribution in the short Kühni column for 7225 ReR 21675 including 95% confidence interval (p-value < 0.05;  $R^2$  equal to 0.96 and 0.67, respectively) for the operational conditions investigated in this work:

$$\mu = (2.08 \pm 0.45) - (0.34 \pm 0.27)Q_c - (0.08 \pm 0.07)E - (0.52 \pm 0.17)N_R + (0.05 \pm 0.04)Q_c E + (0.21 \pm 0.11)Q_c N_R - (0.03 \pm 0.01)Q_c EN_R$$

$$\sigma = (0.62 \pm 0.19) - (0.15 \pm 0.10)Q_d - (0.16 \pm 0.12)Q_c - (0.04 \pm 0.02)N_R + (0.09 \pm 0.06)Q_d Q_c + (0.02 \pm 0.01)Q_c N_R$$

in which  $Q_d$  and  $Q_c$  are given in L/min and  $N_R$  in rps. The increase of the operating variables rotor speed, stage number and flow rate of the continuous phase results in smaller drops, as verified experimentally. The effect of variable rotor speed was found to be statistically more significant for the conditions investigated. The effect of the flow rate of the dispersed phase was found to be nonsignificant from the statistical point of view. Comparative plots shown in

Figure 29 indicated that Eq. suitably reproduced the parameter P with a deviation lower than 15% while Eq. (5) reproduced the parameter V with 20% deviation. However, the use of Eqs. (4) and (5) is restricted to the operational conditions (1.24 d Qc d 2.00 L/min; 1.24 d Qd d 2.00 L/min; 60 d NR d 180 rpm), chemical system and column characteristics (short Kühni column, 150 mm diameter and 5 stages) investigated in this work. It is important to emphasise that, for both fitted functions, the analysis of residuals did not show any evidence against the adequacy of the least squares method employed in the regression (Montgomery, 1991).

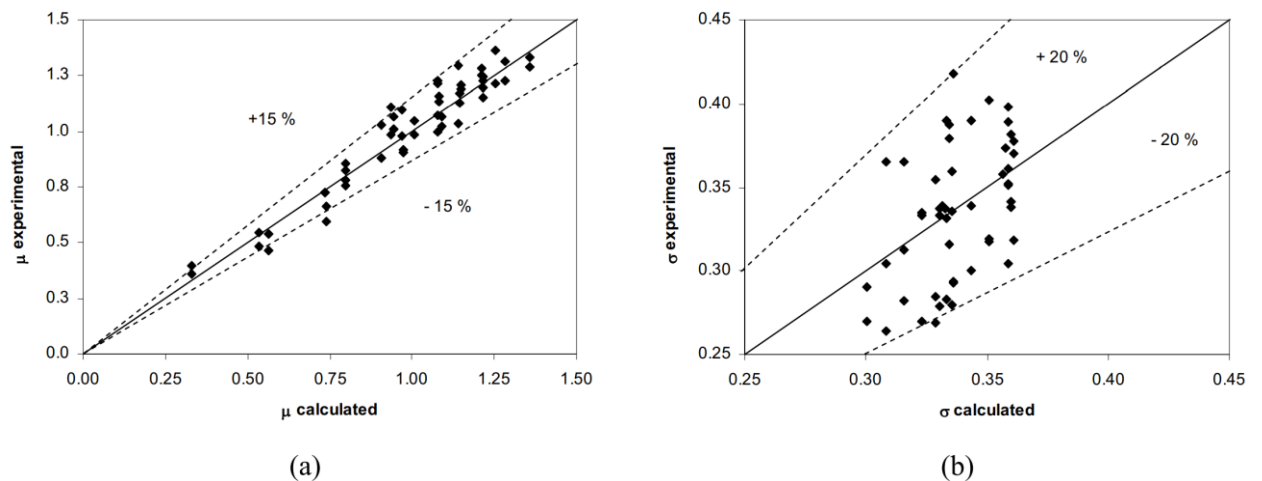


Figure 29: Comparison between the predictions of Eqs. and the parameters of the fitted log-normal distribution using experimental data: (a) parameter P; (b) parameter V.

Sauter Mean Drop Diameter in a Short Kühni Column The effect of the operating variables rotor speed and stage number on the Sauter mean drop diameter in a short Kühni column is shown in Figure 30. As expected, smaller drops were found at higher rotor speeds and along the column height. The explanation for both effects is related to the increase in the frequency of drop collisions against the internal parts of the column in more turbulent environments during their ascending path inside the equipment. But the significance of the combined effect of these variables changed considerably depending on the column stage. At stages 0 and 1, for instance, drops sizes were found to be practically unchanged, independent of rotor speed. This occurred because there is no rotor in stage 0 and also because drops still did not reach a stable

size at stage 1. However, at stages 3 and 5, drops became smaller and smaller with the increase of agitation and this effect was found to be more significant when rotor speed changed from 120 to 150 rpm, as shown in Figures 27(a) and 30(b). The effect was less pronounced when the flow rate of the continuous phase was diminished, as can be seen from Figures 30(b) and 30(c). Actually, the effect of flow rates of the continuous and dispersed phases on the Sauter mean drop diameter were less significant for the operational range studied in comparison to the variables rotor speed and stage number. In the case of the flow rate of the dispersed phase, no significant change in drop size was verified for the operating range investigated. As shown in Figure 30, the Sauter mean drop diameter is practically constant at 60 rpm ( $Re_R = 7225$ ), independent of the operating variables number of the stage and flow rates of both liquid phases, so all experimental drop sizes measured at 60 rpm (16 points) were fit to Eq. (1), resulting in  $C_1 = 1.5 \pm 0.1$  (error 7.1%), a value similar to previous results obtained by Chang-Kakoti et al. (1985) and Moreira et al. (2005) in a rotating disc contactor. In the case of drops measured at stage 0, the average drop size was found to be  $d_{32} = (4.6 \pm 0.4)$  mm (13 points, error 8.7%); this value could be predicted by using Eq. (1), e.g.,  $d_{32} = 4.5$  mm. The correlations proposed by Fischer (1973) and Kumar and Hartland (1996) underpredicted the experimental Sauter mean drop diameters with 66% and 75% error, so these correlations seem to be inadequate for describing drop sizes in a short Kühni column. So, the following empirical correlation was derived, which is valid for  $1.24 \leq Q_c \leq 2.00$  L/min,  $1.24 \leq Q_d \leq 2.00$  L/min and  $60 \leq NR \leq 180$  rpm conditions (p-level < 0.05 including 95% of confidence level,  $R^2 = 0.92$ ):

$$d_{32} = (5.43 \pm 0.35) - (1.38 \pm 0.22)N_R + [(0.57 \pm 0.15) - (0.10 \pm 0.02)E]Q_c N_R$$

in which  $d_{32}$  is given in mm,  $Q_c$  in L/min and  $NR$  in rps. According to Eq. (6), the Sauter mean drop size diminishes with the increase of the operating variables rotor speed and stage number,

thus corroborating the experimental observation (Figure 31). No significant statistical effect was found for the flow rate of the dispersed phase. As shown in Figure 31, the experimental data was suitably predicted by Eq. (6) with a relative deviation within 10% on average.

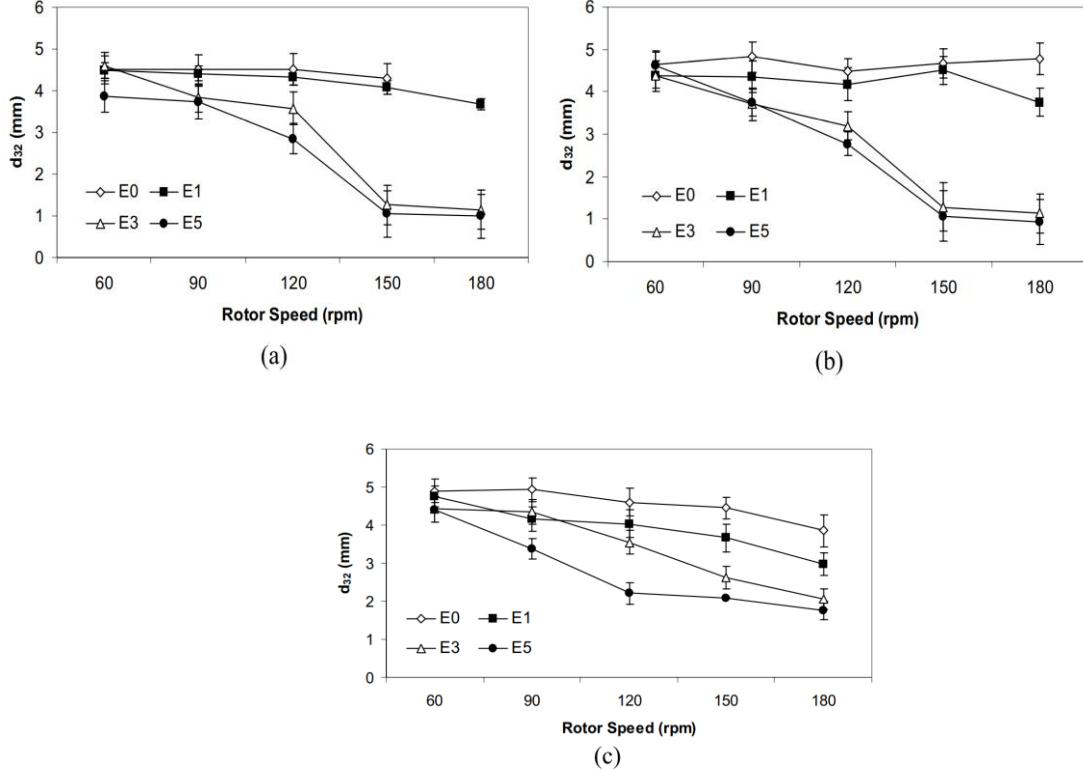


Figure 30: Experimental Sauter mean drop diameter in a short Kühni column: (a)  $Q_c = Q_d = 2.00 \text{ L/min}$ ; (b)  $Q_c = 2.00 \text{ L/min}$  and  $Q_d = 1.24 \text{ L/min}$ ; (c)  $Q_c = 1.24 \text{ L/min}$  and  $Q_d = 2.00 \text{ L/min}$ .

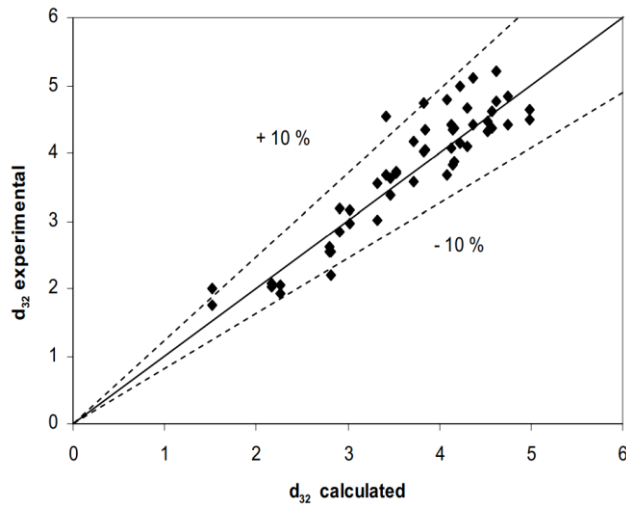


Figure 31: Comparison between experimental Sauter mean drop diameters and the predictions of Eq. (6).

The use of short columns to obtain design data for extraction columns is an alternative way to reduce costs in piloting investigations. As verified in this work, short columns exhibit similar hydrodynamic behaviour concerning drop size, drop size distribution and total hold-up as those found in longer columns. However, empirical correlations valid for longer columns should be adapted; expressions were proposed in this work valid for a short Kühni column (150 mm diameter, 5 stages) with operational conditions ranging from 7225 ReR 21675, e.g., 60 NR 180 rpm, 1.24 Qc 2.00 L/min, 1.24 Qd 2.00 L/min. It was also verified that the effect of drop breakage dominates in the whole short Kühni column for the range of operating conditions investigated, similarly to what is commonly verified in the bottom section of long extraction columns. Further investigations using short columns, including mass transfer effects to hydrodynamics, are suggested.[16]

## **Population balance model in Kuhni extraction column**

Weinstein et al. applied a differential model to Kuhni column with toluene-acetone-water system and 40% chaos in input sporadic phase (Weinstein et al. 1998). Their numerical solution included a general balance equation in the sporadic phase, which was considered as dynamic effects. [17]

Hasseine et al. studied the application of population balance model for the prediction of the dispersed phase and droplet diameter in Kuhni extraction columns and the rotating disk (2005).

They evaluated the mean droplet size and the amount of dispersed phase through the two columns of water and toluene experimentally and using the modeling and population balance equations. Gomes et al. modeled an industrial Kuhni column using population balance equations (Gomes et al., 2006). They found that increasing column height raised the amount of dispersed phase in the column due to an increase in shear forces. Oliveira et al. evaluated the effect of operating parameters consisting of mixing speed, dispersed and continuous phases of the droplet size distribution debit, and dispersed phase supply along a Kuhni extraction column for water and Exxsol D-80 system (Oliveira et al., 2008). They found out that with increasing mixing speed the reduction of droplet size was witnessed, and, in conclusion, droplet size distribution became more symmetric and narrower, and it was shifted toward the left side of the diagram; they also found out that due to the shear forces resulting by blade rotation and the inner components of the column, droplet size distribution at the top of the column is narrower and more symmetric than the one at the bottom of the column. Rodea et al. investigated the undesirable phenomenon of outburst in Kuhni columns (Rodea et al., 2013). Attarakiha et al. used the OPOSPM method using droplet population balance and studied it in a small Kuhni column (Attarakiha et al., 2013). The results of their modelling were very close to experimental data. Artur and Marcelo achieved results coherent to the laboratory results with dynamic

modelling of Kuhni extraction column and mixing it with the droplet population balance equation (Attarakiha et al., 2013). According to the conducted studies in this work, a non-equilibrium dynamic model based on rate-based model was developed for modelling extraction process in a Kuhni column. Population balance equations were used for the hydrodynamic modelling of Kuhni column considering breakage effects and droplet coalescence for two chemical systems, including n-butyl acetate-water-acetone with medium surface tension and toluene-water-acetone with high surface tension simultaneously. The population A. H. Tahershamsi et al. / Modeling and Simulation of Kuhni Extraction balance method is recommended due to its accuracy, its low cost, and its extent of equations for determining various behaviours of chemical processes. The model results were evaluated using a bench scale Kuhni experimental data[18]

### **Population balance model in Kuhni extraction column**

Researchers in different sciences evaluate molecules, particles, and cells with regards to existing rules in their science to achieve a certain distribution of material proportions and its variation with time and location. The distribution must be explainable for all materials regarding the general laws specific to a certain science, and this general law, which is included in a general mutual concept, is called population balance equation (Attarakih and Bart, 2014). In the liquid-liquid extraction process, the population balance model is used to explain hydrodynamic interactions and mass transmissions which are explainable based on the macroscopic nature of the dispersed and continuous phases. Droplet population balance is a powerful method to forecast extraction column behaviour which has been used in many works during recent years. When this method is solved, a great number of differential equations are acquired, and droplet size distribution is obtained by solving these equations. For hydrodynamic simulation, the column is divided into elements with a certain height and droplet classification, and a certain diameter is created due to mass displacement, breakage, and droplet

coalition. In this model, the basic variable, droplet size distribution, is shown by  $p(z,d,t)$ , and location fatigue can be obtained by Equation 1 (Casamatta and Vogelpohl, 1985). [17]

$$\phi(z,t) = \int_0^{d_{\max}} P(t,z,d) \partial d \quad (1)$$

The basic population balance in a dynamic mode is explained by Equation 2 (Modes et al., 1999).

$$\frac{\partial P(z,d)}{\partial t} = - \frac{\dot{P}(z,d)V_d(z,d)}{z} + \frac{\dot{\xi}}{z} E_d \frac{\partial P(z,d)}{\partial z} + P(z,d) \quad (2)$$

In Equation 2,  $p(z,d)$  is production and consumption statement at the same time, which includes breakage effects, coalition, nucleation, and droplet growth. Equation 2 demonstrates the  $p(z,d)$  phrase.

$$P(z,d) = PB^+(z,d) - PB^-(z,d) + PC^+(z,d) - PC^-(z,d) \quad (3)$$

In which  $PB^+(z,d)$  and  $PB^-(z,d)$  respectively show the increase and decrease in droplet numbers due to droplet breakage; also, the phrase  $PC^+(z,d)$  and  $PC^-(z,d)$  respectively shows the increase and decrease in droplet number due to droplet coalition (Godfrey and Slater, 1994).

$$PC^-(z,d) = P(z,d) \int_0^{\sqrt[3]{d_{\max} - d^3}} h(d_1, d_2) \frac{P(z,d_1)}{v(d_1)} \partial d_1 \quad (4)$$

$$PC^+(z,d) = \frac{1}{2} v(d) \int_0^d h(d_1, d_2) \frac{P(z,d_1)P(z,d_2)}{v(d_1)v(d_2)} \left(\frac{d}{d_2}\right)^2 \partial d_1 \quad (5)$$

Equation 5 is multiplied by 0.5 because particle collision with (d1,d2) size is not different from particle collision with (d1,d2) size. Considering the fact that  $p(d)$  is a breakage possibility,  $r(z,d)$  is called collision frequency obtained by an equation achieved by the provided case. Breakage frequency is also dependent on droplet existence time.  $P(d)$  is breakage possibility of a droplet with diameter  $d$ , and  $r(z,d)$  is breakage frequency obtained by Equation 7 (Steiner et al., 1988).

$$\frac{p(d)}{1-p(d)} = 0.2148 We_m^{0.7796} \quad (6)$$

$$r(z,d) = \frac{p(d)v_d(z,d)}{H_C} \quad (7)$$

$$We_m = \frac{\rho_c^{0.8} \mu_c^{0.2} d D_R^{1.6} (\varpi^{1.8} - \varpi_{crit}^{1.8})}{\sigma} \quad (8)$$

$$\varpi_{crit} = 2\pi \cdot 0.65 \frac{\rho_c D_R^{3/2}}{\sigma} \left( \frac{d}{D_R} \right)^{-0.72} \quad (9)$$

The coalition rate has been obtained using Equation 10 (Wang et al., 2003).

$$h(d_1, d_2) = 1.247 \epsilon^{1/3} (d_1 + d_2)^{7/3} \quad (10)$$

To calculate child droplet size distribution, beta equation is usually used although beta equation is very complex in practice. The following equation is based on the hypothesis that if any droplet breakage does not occur, the impact energy will be absorbed in the droplet as much as possible. Then, this energy turns into surface energy in order to make the best interface area possible. This means that the creation possibility of interface area is more suitable for the child droplets with a bigger droplet size distribution. Daughter droplet size distribution is acquired by beta distribution based on the mother droplet diameter,  $d_0$  (Schmidt, 2006).

$$\beta(d_0, d) = 3x_m(x_m - 1)(1 - \frac{d^3}{d_0^3})^{(x_m - 2)} \frac{d^3}{d_0^6} \quad (11)$$

Here, the mean of daughter droplet is calculated using the following equation.

$$x_m = 2 + 0.838 \frac{\frac{d_0}{d_{crit}}^{1.309}}{1 - \frac{d_0}{d_{crit}}} \quad (12)$$

Critical diameter for every drop beginning to break out is obtained using the following equation.

$$d_{crit} = 0.65 D_R We_R^{-0.72} \quad (13)$$

Also, Modes et al. presented these two parameters, i.e. term destruction and failure of the process as follows (Modes et al., 1999):

$$PB^-(z,d) = r(z,d)P(z,d) \quad (14)$$

$$PB^+(z,d) = \int_{d_0}^{d_{max}} r(z,d_0)P(z,d_0)\beta(d_0,d) \frac{d}{d_0} \quad (15)$$

In order to describe the hydrodynamic problem, the population balance model considering the failure of the coalition drops were used simultaneously. Also, the effect of axial mixing in the dispersed phase was discarded. In conclusion, the main population balance equation will change as follows:

$$\beta(d_0, d) = 3x_m(x_m - 1)(1 - \frac{d^3}{d_0^3})^{(x_m - 2)} \frac{d^3}{d_0^6} \quad (11)$$

Here, the mean of daughter droplet is calculated using the following equation.

$$x_m = 2 + 0.838 \frac{\frac{d_0}{d_{crit}}^{\frac{1}{2}} - 1}{\frac{d_0}{d_{crit}}^{\frac{1}{2}}} \frac{d^{0.309}}{d_0} \quad (12)$$

Critical diameter for every drop beginning to break out is obtained using the following equation.

$$d_{crit} = 0.65D_R We_R^{0.72} \quad (13)$$

Also, Modes et al. presented these two parameters, i.e. term destruction and failure of the process as follows (Modes et al., 1999):

$$PB^-(z, d) = r(z, d)P(z, d) \quad (14)$$

$$PB^+(z, d) = \int_{d_{crit}}^{d_{max}} r(z, d_0)P(z, d_0)\beta(d_0, d) \frac{d}{d_0} \quad (15)$$

In order to describe the hydrodynamic problem, the population balance model considering the failure of the coalition drops were used simultaneously. Also, the effect of axial mixing in the dispersed phase was discarded. In conclusion, the main population balance equation will change as follows:

$$\frac{\partial P(z,d)}{\partial t} = \frac{[V_d * P(z,d)]_{i+1} - [V_d * P(z,d)]_i}{\Delta z} + PB^+(z,d) - PB^-(z,d) + PC^+(z,d) - PC^-(z,d) \quad (16)$$

The final form of the developed model can be obtained by substitution of Equations 4, 5, 14, and 15 in Equation 16 as follows:

$$\begin{aligned} \frac{\partial P(z,d)V_d(z,d)}{\partial z} &= r(z,d_0)P(z,d_0)\beta(d_0,d)\frac{\partial d_0}{\partial d} \\ &+ \frac{1}{2}V(d)\sum_{d_1=0}^d h(d_1,d_2)\frac{P(z,d_1)P(z,d_2)}{V(d_1)V(d_2)}\left(\frac{d}{d_2}\right)^2\frac{\partial d_1}{\partial d} \\ &- r(z,d)P(z,d) - P(z,d)\sum_{d_1=0}^{\sqrt[3]{d_{max}-d^3}} h(d_1,d_2)\frac{P(z,d_1)}{V(d_1)}\frac{\partial d_1}{\partial d} \end{aligned} \quad (17)$$

Number of the droplets in volume unit is as defined by:

$$N(z,d) = \frac{P(z,d)}{V(d)} \quad (18)$$

in which,  $V(d)$  is droplet volume. To solve Equation 17, it is important for the equation to be independent of the droplet diameter. Hence, droplet diameter range was classified into 9 classes with equal difference:

$$d_{min} = d_0 < d_1 < \dots < d_9 = d_{max} \quad (19)$$

Now we can rewrite  $p(z,d,t)$  as given by:

$$\begin{aligned} P(t,z,d) &= \sum_{k=1}^9 P_k(t,z)b_k(d) \\ b_k(d) &= \begin{cases} 1 & \text{if } d \in [d_{k-1}, d_k] \\ 0 & \text{if } d \notin [d_{k-1}, d_k] \end{cases} \end{aligned} \quad (20)$$

After the independence of the equation of the droplet diameter, discretization is performed on the premises of location. By discretization on the premises of location, a series of partial differential equations appear, which will be solved. Boundary conditions at the bottom of the tower are obtained by the Log-Normal distribution function (Oliveira et al., 2008).

$$p(d) = \frac{1}{\sqrt{2\pi}\sigma} \exp\left[-\left(\frac{(d)-\mu}{\sqrt{2\sigma}}\right)^2\right] \quad (21)$$

According to Equation 21, the amounts of  $\sigma$  and  $\mu$  were corrected by using experimental data by minimizing sum of squared errors for this extraction column:

$$\mu = 3.06894 + 0.0642988 Q_c - 0.00789922 Q_d - 0.743064 N_R - 0.0203485 Q_c N_R \quad (22)$$

$$\sigma = 0.457495 + 0.0215919 Q_c - 0.0139703 Q_d - 0.0888132 N_R - 0.00955705 Q_c N_R + 0.00558636 Q_d N_R \quad (23)$$

The population balance equations were solved simultaneously using the algorithm shown in Figure 1.

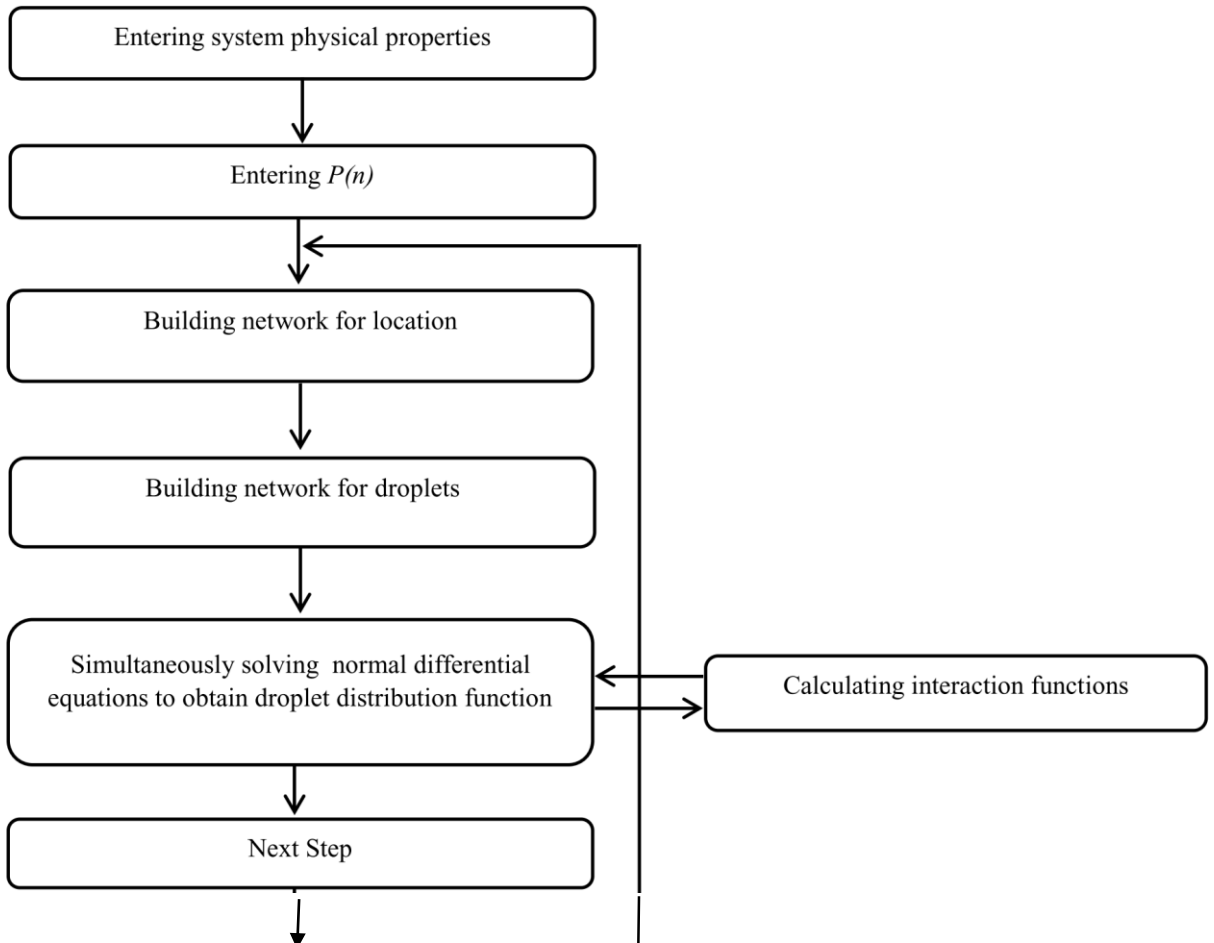


Figure 32 Population balance equation solution algorithm.

### Kuhni column and phases properties

Kuhni extraction column used in this study is a contactor on the semi-industrial scale, and the active part of the column is made of glass to be resistant against corrosion. Kuhni column has one axis rotated by an electromotor. The geometric properties of the column and physical properties of the liquid-liquid systems are presented in Tables 15 and 16.

Table 15 Geometric properties of the column.

Column component	Unit	Dimension
<b>Column height</b>	m	0.700
<b>Column diameter</b>	m	0.117
<b>Height of each stage</b>	m	0.055
<b>Number of stages</b>	-	10
<b>Number of holes per tray</b>	-	27
<b>Hole angle comparing to others</b>	-	40 degrees
<b>Plate thickness</b>	m	0.002
<b>Active volume of the column</b>	$\text{m}^2$	0.00752

Table 16 Physical properties of liquid-liquid systems.

Physical properties	Unit	Toluene-water	n-Butyl acetate-water
<b>Continuous phase density</b>	$\text{Kg m}^{-3}$	998.2	998.2
<b>Dispersed phase density</b>	$\text{Kg m}^{-3}$	865.2	880.9
<b>Continuous phase viscosity</b>	$\text{mPa.s}$	0.9630	1.0274
<b>Dispersed phase viscosity</b>	$\text{mPa.s}$	0.584	0.734
<b>Interfacial tension</b>	$\text{mN s}^{-1}$	36.0	14.1

The model equations including mass balance, momentum balance, and population balance equations were solved simultaneously using numerical techniques. In the following, the hydrodynamic and mass transfer results are indicated. In Figure 33, the range of mean diameter as a function of rotor speed is demonstrated for n-butyl acetate-water and toluene-water systems. Considering that the operating condition is constant, the mean droplet diameter size is bigger in toluene-water than the one in n-butyl acetate-water. The main reason for this occurrence is related to surface tension between the phases. Since the interfacial tension in toluene-water is almost twice as large as interfacial tension between n- butyl acetate-water, this causes an increase in drag force and resistance to the motion of the dispersed phase. The effect of mixing speed on the mean droplet size in the toluene-water system (system with a high interface tension) is more than that in n-butyl acetate-water system because droplet breakage in system with a medium interface tension is limited. Moreover, the diagram has a logical theme and the mean size of droplets decreases with an increase in rotor speed.

Weinstein et al. considered only average diameter to solve equations by solving their differential model, and they solved the equations using this diameter. But in this work, the population balance equations were employed. The droplets were classified in 9 classes according to the assumptions. The modeling results were consistent with the experimental results and the changes in physical properties of the system are fixed because the column length is low. In Table 17, mean droplet diameter and their deviation with experimental data for the two chemical systems are presented. The results show that with an increase in the phase flow rate, the mean droplet diameter rises. It shows that increasing the flow rate of both phases enhances the coalescences of drops. Additionally, the results indicate that raising rotor speed drops mean droplet diameter. Flow rate rise in integrated phase has poor effects on the increase of droplet mean size, and it could lead to an increase in retention time and droplet collisions. Moreover, it could result in a decrease in the relative velocity of the droplets.

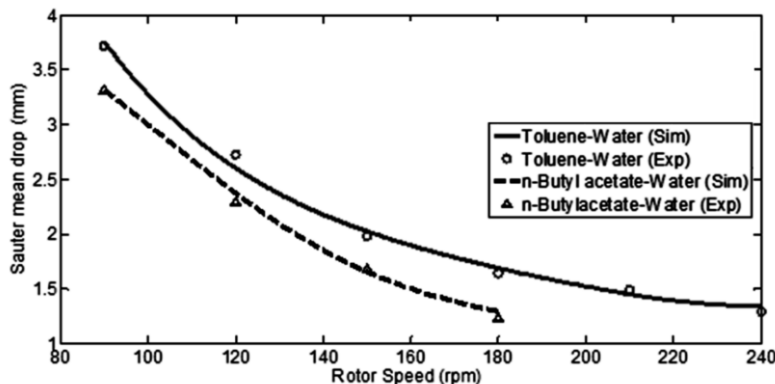


Figure 33 Mean diameter versus rotor speed for n-butyl acetate-water and toluene-water systems. It is observed that along with the column height, droplet breakage overcomes their coalition (Figure 34); the reduced surface tension causes droplet breakage and reducing the size of the larger droplets. On the other hand, in the dispersed phase, the amount of circular and rotational currents leads to more stability, increasing the time of coalition, thereby reducing the amount of droplet coalition. Thus, the peak of the diagram leans toward the left, which shows higher breakage of droplets and shrinkage of the droplet mean diameter. Furthermore, according to

the fact that the interface tension of the toluene- water system is more than that of n-butyl acetate-water system, higher power is needed to break the droplets in this system to achieve a class of droplets with a smaller diameter.

Table 17 Experimental and simulation results of the droplet mean diameter

n-Butyl acetate-water					
Error	Simulation $d_{32}$ (mm)	Experimental $d_{32}$ (mm)	$Q_d$ (lit/hr.)	$Q_c$ (lit/hr.)	$N$ (rpm)
0.7784	1.5017	1.4901	24	20	150
2.2920	1.6468	1.6099	24	28	
1.9769	1.6214	1.6541	24	32	
0.4503	1.7020	1.7097	24	36	
0.7784	1.5017	1.4901	20	24	150
2.2920	1.6468	1.6099	28	24	
1.9769	1.6214	1.6541	32	24	
0.4503	1.7020	1.7097	36	24	
Toluene-water					
1.8052	1.6580	1.6286	24	18	180
1.0413	1.7950	1.7765	24	30	
1.5932	1.8300	1.8013	24	36	
0.4127	1.9950	1.9868	24	42	
1.2693	1.5012	1.5205	18	24	180
1.2154	1.9180	1.9416	30	24	
1.5079	2.3514	2.3874	36	24	
1.1696	2.6448	2.6761	42	24	

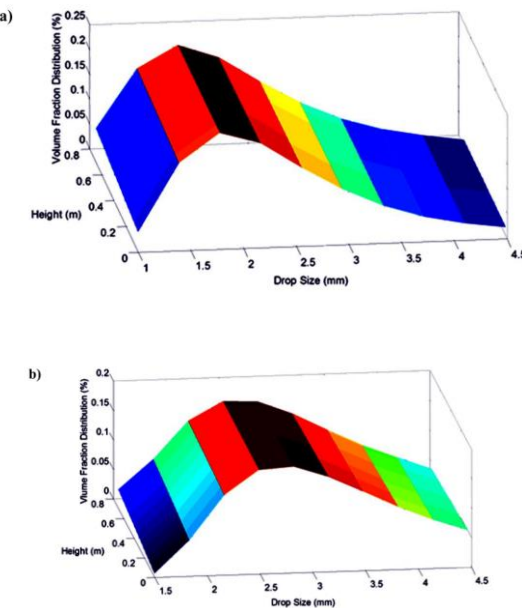


Figure34 Volume distribution of droplets versus the droplet diameter and the length of the column: a) n-butyl acetate- water-system water-system and b) toluene-water system.

Oliveira et al. found that by increasing the speed of mixing, a reduction in droplet size was seen, and droplet size distribution became narrower and more symmetrical and passed to the left of the graph. As indicated in the graph, by increasing the speed of mixing, the droplet size lessens and shifts to the left. Because of the small diameter of the column, the changes in the radial average speed and concentration can be ignored.

Figure 35 presents the influence of rotor speed on the interface tension of the two existing phases. By increasing the rotor speed, and thus increasing the shear forces, mother droplets break into child droplets and droplet coalition becomes minimum. Reducing the droplet size raises the amount of the dispersed phase in the extraction column. Moreover, due to a rise in interfacial tension, droplet coalition is enhanced and consequently results in bigger droplets. In addition, relative phase velocity increases, which could lead to a reduction in the amount of the dispersed phase. Furthermore, it can be seen that higher rotor speeds influence the dispersed phase in the toluene-water system (with a higher interfacial tension) because droplet breakage in this system is more effective, thereby leading to an increase in the hold up of dispersed phase.

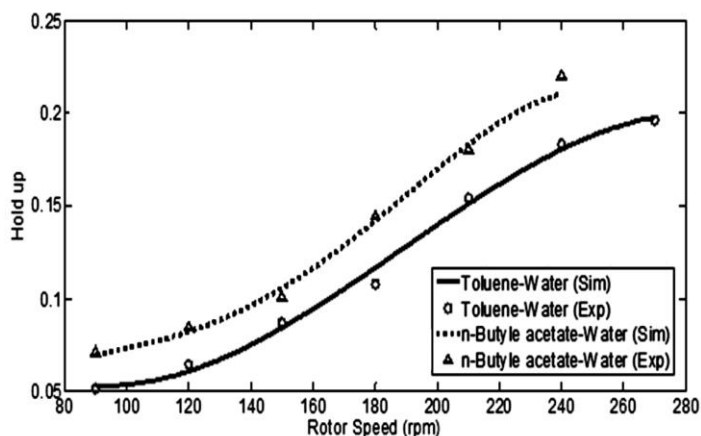


Figure 35 Effect of two rotor speeds on the amount of hold up for n-butyl acetate-water and toluene-water systems.

Comparison of the presented model results with the previous model results is presented in Table 18; it is obvious that the presented model is more rigorous than previous models.[18]

Table 18 Comparison of the presented model results with other models.

Model	Deviation percentage average	Column type	Reference
Morales et al.	8.0	Structure packing	(2007)
Lorena et al.	20.0	fixed-bed extractor	(2012)
Schmidt et al.	15.0	RDC extractor	(2006)
This work	4.0	Kuhni extractor	

**In this study, the droplet breakage and the coalition and its impact on the number of droplets in the Kuhni extraction column were modelled and simulated by considering the balance equation. The most important parameters affecting the droplet breakage are rotor speed, interface tension and dispersed and continuous phase flow rates. An increase in rotor speed causes stronger shear forces and thus results in the breakage of droplets; therefore, dispersed phase holdup increases. The holdup of the dispersed phase decreased by increasing the surface tension and droplet diameter. Increased surface tension and droplet diameter raise speed but reduce the relative phases of the dispersed phase. The results showed that droplet coalition plays a major role in population balance equation, and it was increased by increasing the flow rates of the dispersed and continues phases. The comparison of droplet means diameter changes and the dispersed phase holdup shows that the effect of rotor speed in the n-butyl acetate-water-acetone system (with a low interface tension) is less than that in the toluene- water-acetone system (with a high interface tension). The results indicate that the simulation results of the process are in good agreement with the experimental data; therefore, using the presented model is recommended for modelling industrial Kuhni column. Furthermore, this model is suggested for modelling other types of extraction columns, especially RDC and structure**

columns. Finally, an investigation on droplet mean diameter and mass transfer coefficients based on non-spherical droplets is proposed[17]

## **Asymmetric rotating disc column (ARDC) for extraction liquid-liquid**

On comparing the performance characteristics of the different extractors, rotating columns are found highly efficient and exhibit low costs in respect of stage numbers, solvent inventory, settler area, site area and maintenance. The asymmetric rotating disc column extractor (ARDC) is a rotary agitated column developed with emphasis on balanced throughput and separation performance and on reduction of axial mixing effects. It has been in industrial use since 1965. The ARDC column is used for processing liquid systems within a broad range of physical properties. Typical industrial applications are found in the different fields such as organic and petrochemical, inorganic and metallurgical and miscellaneous. The asymmetric rotating disc column extractors are currently in operation in more than 100 processes [19]

Agitation speed influences the droplet size of the dispersed phase, the throughput capacity and the separation effect of the contactor. The ordered helical flow pattern of both phases is prerequisite for high throughput and low axial mixing effects, a characteristic feature of the ARDC column. The forces acting on the dispersed phase in the extraction section give rise to the disperse droplet population. Elementary processes of stochastic character, such as droplet breakup, random movements, and coalescence, take place along the path of droplets. [20]

### **1-1) Drop Size and drop Distribution in a Liquid-Liquid Extraction ARDC Column**

Among the liquid dispersion properties affecting the ARDC column behaviour, the drop size distribution is one of the important parameters. Its control could positively contribute to optimizing the column performance. The experimental works were carried out in a pilot plant ARDC column with three different systems. The effect of operating parameters on the Sauter mean drop diameters and drop size distributions were investigated. The drop size distribution

is largely dependent on the agitation conditions in the column, but, the effect of phase flow rates is not significant. The empirical drop size distributions in the ARDC column are compared with the five common theoretical distribution functions (normal, log-normal, Gamma, Inverse Gaussian, Weibull). The constant parameters in these functions were correlated with operating conditions and physical properties of three systems. The Weibull is found to perform adequately and accurately in fitting the drop size distributions. Except for these findings, an empirical correlation is proposed for estimation of the Sauter mean drop diameter in terms of operating variables, column geometry and physical properties.[19]

The droplet size distribution in the column is usually represented as the average volume to surface area, known as the Sauter mean drop diameter. It is a key variable in the extraction column design. It influences on both throughput and specific interfacial area available for mass transfer, dispersed phase holdup, flooding conditions. At present little information has appeared in the literature regarding the droplet sizes of the ARDC column. Misek and Marek (1970) have shown that the maximum droplet diameter under mild agitation is independent of rotor speed and is given by:

$$d_{\max} = 2.03 \left( \frac{\sigma}{\Delta \rho g} \right)^{1/2}$$

For intensive agitation, the expression was proposed for  $d_{\max}$  in terms of column variables and physical properties, the transition rotor speed and the droplet size distribution. Kumar and Hartland (1996) reported that the equations for drop size proposed by Misek and Marek (1970) gave an average deviation of 54% in the case of rotating disc contactors. The mean drop size correlations for various rotating columns were illustrated in Table 1. However, the available correlations for the prediction of mean drop sizes are either approximate or scarcely applicable.

**Table 1.** Unified correlations for prediction of the drop size in mechanically agitated

columns.

Equation	Column	Reference
(2) For $Re \leq 50000$	Rotating column	disc (Kumar et al., 1986)
$\frac{d_{32}}{D_e} = 0.18 \left( \frac{ND_e^2 \rho_e}{\mu} \right)^{-0.12} \left( \frac{\mu_e}{\sqrt{\sigma \rho_e D_e}} \right)^{-0.38} \left( \frac{\Delta \sigma}{\rho_e} \right)^{-0.24} \left( \frac{D_e^2 \rho_e g}{\sigma} \right)^{-0.05} \left( \frac{h}{d_s} \right)^{0.42}$		
$\frac{d_{32}}{H} = \frac{C_p e^n}{\frac{1}{C_n \left( \frac{\sigma}{\Delta \sigma H^2} \right)^{1/2}} + \frac{1}{C_p \left[ \left( \frac{\sigma}{g} \right) \left( \frac{\rho_e}{g \sigma} \right)^{1/4} \right]^{n_1} \left[ H \left( \frac{\rho_e g}{\sigma} \right)^{1/2} \right]^{n_2}}}$	(3) Rotating column Asymmetric rotating column Kühni Column Wirtz Column Pulsed column Karr Column	disc (Kumar and Hartland, 1996)
$d_{32} = 0.705 \left( \frac{\sigma}{g \Delta \sigma} \right)^{0.5} \frac{d_R^{0.8}}{N^{0.185}} \frac{\left( \frac{Q_c}{Q_d} \right)^{0.15}}{(Q_c + Q_d)^{0.1}}$	(4) Rotating column	disc (Al-Rahawi, 2007)
$d_{32} = 0.194 \left( \frac{P}{V} \right)^{-0.45} \sigma^{0.766} (\rho_e \mu_e)^{-0.3} \left( \frac{\mu_d}{\mu_e} \right)^{0.07}$	(5) ARDC column	(Kadam et al., 2009)
$d_{32} = 10 \left( \frac{N^4 d_R^4 \sigma_e}{\sigma g} \right)^{-0.294} \left( \frac{\mu_e^4 g}{\Delta \sigma \sigma^3} \right)^{-0.087} \left( 1 + \frac{V_e}{V_d} \right)^{-0.402}$	(6) Perforated rotating Column	disc (Hemmati et al., 2015)

The knowledge of average drop size in terms of the liquid physical properties, column geometry and operating variables is thus of the paramount importance. The drop size distribution in ARDC column has been studied by changing the operating parameters, such as dispersed and continuous phase flow rates and agitation speed. The results were compared with predictions obtained using the probability density functions. In the process of making comparisons, estimates will be made of the parameters in these functions as a function of

effective variables. Furthermore, empirical correlations were derived for the determination of Sauter mean drop diameter.

## **1-2) The extraction of n-butanol–water, toluene–water, n-butyl acetate–water systems in an ARDC pilot plant column**

The drop behaviour in the pilot plant ARDC column was investigated for three systems (toluene-water, n-butyl acetate-water and n-butanol-water) in the absence of mass transfer. Statistical analysis revealed the main effect of the rotor speed on the drop size diameter. The drop size could be increased with increasing dispersed phase flow rate, but the continuous phase flow rate does not have a significant effect. Drop size distributions measured by image analysis were suitably fitted to the Weibull probability distribution function. The empirical expressions were derived to predict the parameters of the distribution curve as a function of operating variables and physical properties for different probability density functions. Also, empirical correlation for the Sauter mean diameter was proposed with the experimental data in ARDC column. [19]

A pilot scale asymmetric rotating disc column was used in the present work. A scheme of the ARDC pilot-scale unit used in the present study is shown in Fig. 1 and the specific column geometries studied are summarized in Table 2.

**Table 2.** Dimensions of the pilot plant ARDC

Column diameter (m)	0.113
Rotor diameter (m)	0.042
Column working height (m)	1.43
Compartment height (m)	0.033
No. of compartments (-)	36

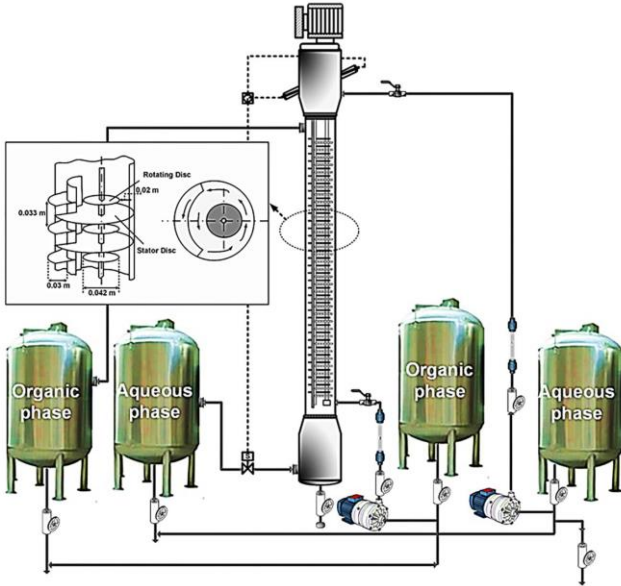


**Fig.1.** Schematic flow diagram of ARDC pilot plant column

The contactor consists of a cylindrical shell, a baffled stator, and a multistage agitator. The shell houses an extraction section and two settling zones. The extraction section consisted of a 1430 mm long glass tube of 113 mm internal diameter, enclosing a stock of 36 discs mounted on a vertical shaft and driven by an electronic motor via a variable speed gear box.

The extraction section is divided by an asymmetrically positioned vertical stator baffle into a contact zone and a transport zone. Both of these are subdivided by horizontal baffles into a series of staggered chambers that communicate with each other through openings on both sides of the vertical baffle. Disc impellers mounted on the agitator shaft and centered in each contact chamber provide mechanical agitation.

All internal parts of the column and the blade impellers were made of AISI 316 stainless steel. A settler of 168 mm diameter at each end of the column permitted the liquids to coalesce and decant separately. Four stainless steel tanks with 85 L capacity were used to store the liquid feeds, and to collect the extract, and raffinate streams. The interface is maintained at the required level by using an optical sensor as previously work[21].

## 1-2-1) Case study (n-butanol–water, toluene–water, n-butyl acetate–water were)

Three various systems with different interfacial tensions consisting of n-butanol–water, toluene–water, n-butyl acetate–water were used in these experiments. The European Federation of Chemical Engineering (E.F.C.E) has adopted these systems as Recommended Systems [22]. The physical properties for the three systems are listed in Table 3. The purity of organic phase solvents is more than 99.5% and all solvents are used without purification.

**Table 3.** Physical properties of systems studied a 20°C [22]

Physical property	Toluene-Water	n-Butyl acetate-Water	n-Butanol-Water
$\rho_c$ [kg/m <sup>3</sup> ]	998.2	997.6	985.6
$\rho_d$ [kg/m <sup>3</sup> ]	865.2	880.9	846.0
$\mu_c$ [mPa.s]	0.963	1.027	1.426
$\mu_d$ [mPa.s]	0.854	0.734	3.364
$\sigma$ [mN/m]	36	14.1	1.75

## 1-2-2) Determination of drop size

Droplet size was measured by Nikon D5000 digital camera used to take a digital photo of extractor contents. The photographs were analyzed with the software CAD for drop size determination. The real drop sizes were measured by comparing the size of the drops with size-defined articles which were the thickness of stators in this work. It is found that the curved surface of the glass extraction column and significant differences between air and the glass refractive indices leads to a parallax deformation of the objects photographed in the extraction column. In order to omit this phenomenon, a container which filled with water was attached to the extraction column and the photographic approach was used to calculate the size of stator thickness served as the reference for drop size measurements. Consequently, ten photos were taken for every experimental condition and the diameters of nearly 500 drops were measured for one photo and the Sauter mean droplet size was calculated from the following equation

$$d_{32} = \frac{\sum_{i=1}^N n_i d_i^3}{\sum_{i=1}^N n_i d_i^2}$$

where  $n_i$  denotes the number of drops of diameter  $d_i$ .

The total holdup of the dispersed phase was assessed using the shutdown method.

Measurements were made in triplicate to verify experimental reproducibility.

The drop size distribution and mean drop size of the dispersed phase could be affected by operation conditions and physical properties of the liquid-liquid system. A series of experiments were designed to ascertain the influence of factors such as  $N$ ,  $V_d$ ,  $V_c$ ,  $\Delta\rho$ ,  $\rho_d$ ,  $\mu_d$ ,  $\mu_c$ , and  $\sigma$  on the drop size distribution and Sauter mean drop. The pictures of drop sizes for the three systems are shown in Fig 2.

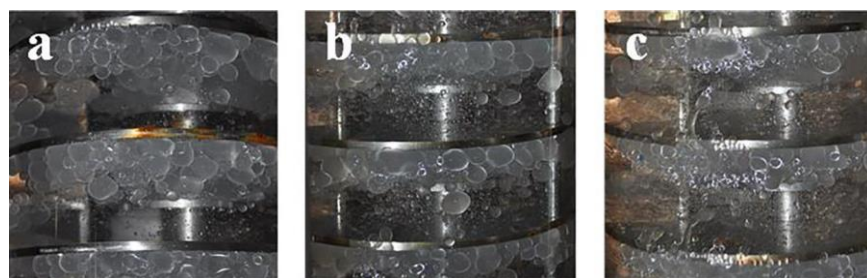


**Fig.2.** The photo of drops for three systems (a) toluene –water, (b) n-butyl acetate-water, (c) n-butanol-water

### 1-2-3) Drop size distribution investigation

The drop size distribution is a very important parameter in liquid-liquid extraction columns.

Three vital operating parameters including aqueous and organic phase velocities and agitation speeds were chosen for the investigation of drop size distribution and Sauter mean drop diameter in the ARDC columns.

#### 1-2-3-1) Effect of agitation speed on the drop size distribution

To investigate the influence of agitation speed on drop size distribution, the rotor speed was varied for different levels of agitation. The amount of drop size distribution for three different

systems for different rotor speeds is portrayed in Fig. 3. In the case of constant values of  $V_d$  and  $V_c$ , the size distribution clearly shifts towards the left upon an increase in the rotor speed, evidencing drop breakup. The energy grows with the rotor speed and the drop breakup frequency increases along the column. So, the size distribution is shifted towards smaller diameter and therefore leading to higher interfacial tension area values. In addition, the drop size distributions are also found to be narrower and more evenly distributed about the mean value for n-butanol-water (lower interfacial tension). The observation in this column is in good agreement with the results reported by (Moreira et al., 2007) in the RDC column.

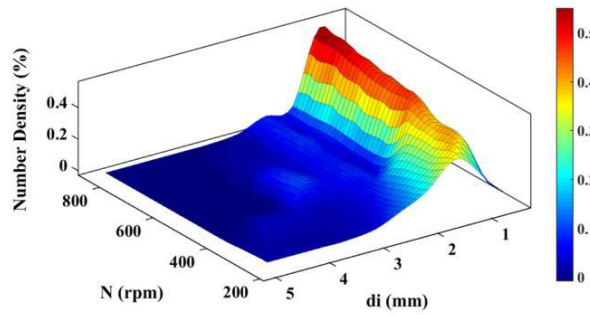


**Fig.3a.** Effect of agitation speed on the drop size distribution for toluene-water ( $V_d=V_c=1.44$  mm/s)

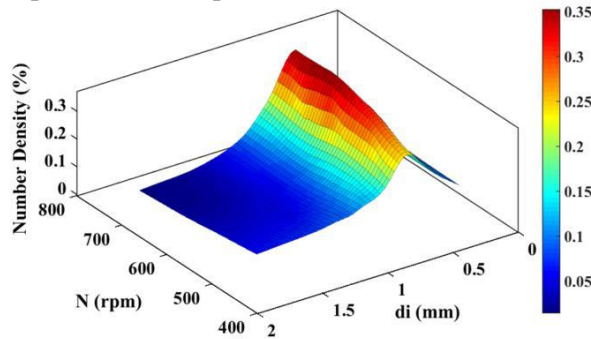


**Fig.3b.** Effect of agitation speed on the drop size distribution for n-butyl acetate-water ( $V_d=V_c=1.44$  mm/s)

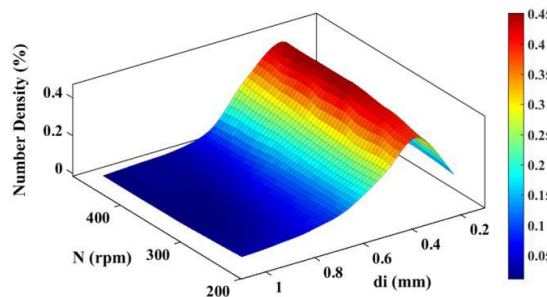


**Fig.3c.** Effect of agitation speed on the drop size distribution for n-butanol-water ( $V_d=V_c=1.44$  mm/s)

### 1-2-3-2) Effect of aqueous and organic phase flow rates on the drop size distribution

The effect of the continuous and dispersed phase flow rates on the drop size distribution in the column is discussed as follows. The size distributions for three different systems with the changing dispersed phase velocity are shown in Figs.4a, 4b and 4c.

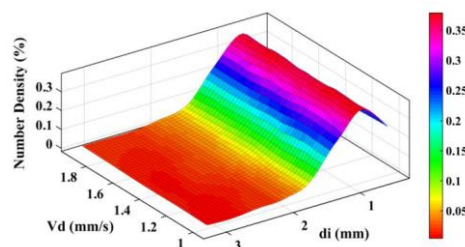


**Fig.4a.** Effect of dispersed phase velocity on the drop size distribution for toluene-water ( $V_c=1.44$  mm/s,  $N=670$  rpm)

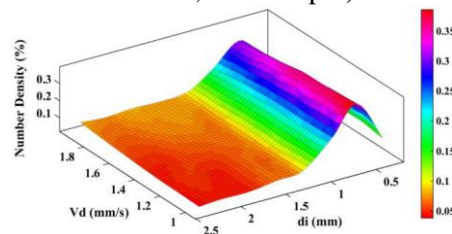


**Fig.4b.** Effect of dispersed phase velocity on the drop size distribution for n-butyl acetatewater ( $V_c=1.44$  mm/s,  $N=400$  rpm)

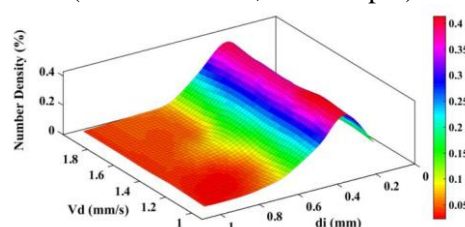


**Fig.4c.** Effect of dispersed phase velocity on the drop size distribution for n-butanol-water ( $V_c=1.44$  mm/s,  $N=220$  rpm)

The dispersed phase velocity does not have any considerable effect on drop size distribution, hence it can be neglected. Also, no significant effects were observed from Figs.5a, 5b and 5c for the flow rate of the continuous phase velocity in the operating conditions. Thus, the drop size distribution is independent of both phase velocities in the ARDC column.

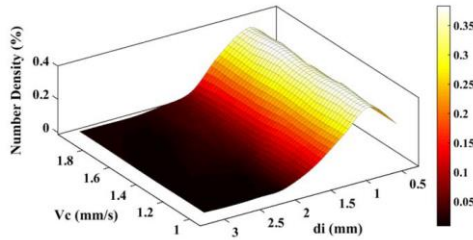


**Fig.5a.** Effect of continuous phase velocity on the drop size distribution for toluene-water  
( $V_d=1.44$  mm/s,  $N=670$  rpm)

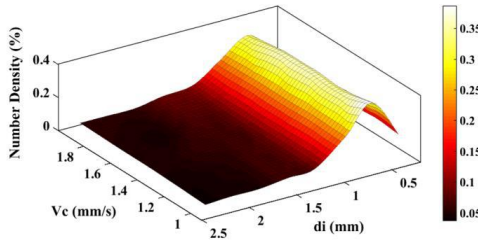


**Fig.5b.** Effect of continuous phase velocity on the drop size distribution for n-butyl acetate water  
( $V_d=1.44$  mm/s,  $N=400$  rpm)

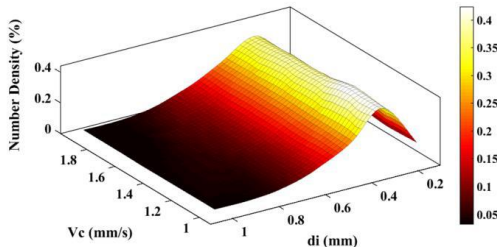


**Fig.5c.** Effect of continuous phase velocity on the drop size distribution for n-butanol-water ( $V_c=1.44$  mm/s,  $N=220$  rpm)

#### 1-2-4) Mean drop size

The effect of agitation speed, dispersed and continuous phase velocities on  $d_{32}$  is illustrated in Figs.7 to 9. As shown, the mean drop size is strongly affected by the rotor speed (Fig.7). The reason for this is that the energy input by the rotor blades increases with increasing agitation speed, so the dispersed phase is dispersed more easily. An increase in the energy supplied via agitation to the dispersed phase overcomes the interfacial forces of the droplets and, therefore, the droplets break. The different liquid-liquid systems show different values of  $d_{32}$ , indicating that the physical properties of the liquid-liquid system affect the Sauter mean drop diameter.

The mean drop size of the system with higher interfacial tension is bigger because the drops coalesce more easily under the same operating conditions.

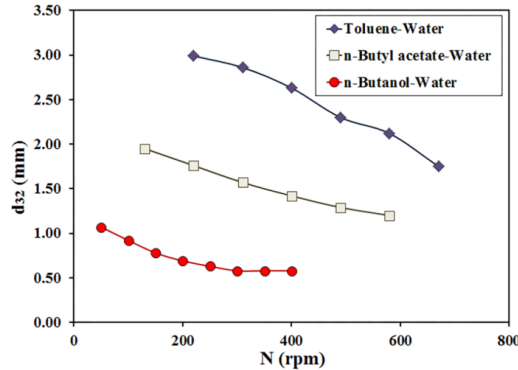


**Fig.7.** Effect of agitation speed on the Sauter mean drop diameter ( $V_c=V_d=1.44 \text{ mm/s}$ )

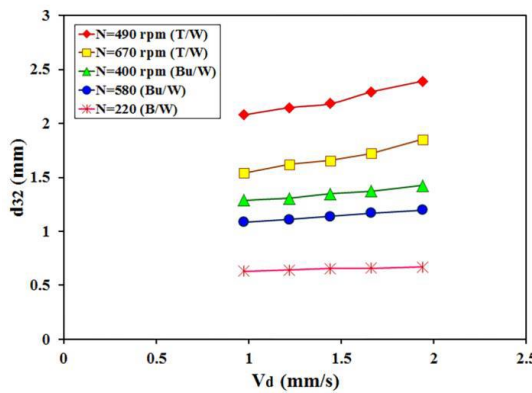


**Fig.8.** Effect of dispersed phase velocity on the Sauter mean drop diameter (toluenewater (T/W), n-butyl acetate-water (Bu/W), n-Butanol-water (B/W)) ( $V_c=1.44 \text{ mm/s}$ )

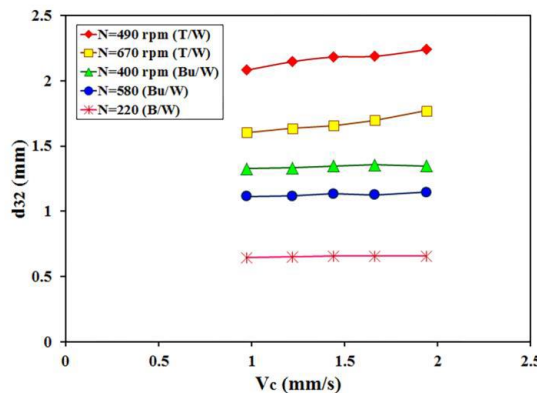


**Fig.9.** Effect of continuous phase velocity on the Sauter mean drop diameter (toluene-water (T/W), n-butyl acetate-water (Bu/W), n-Butanol-water (B/W)) ( $V_d=1.44 \text{ mm/s}$ )

The Sauter mean drop size diameter is shown as a function of continuous and organic phase velocities in Figs. 8 and 9. An increase in dispersed phase velocity leads to an increase in the

mean drop size. However, it is changed slightly at low interfacial tension. This observation could be attributed to the energy impressed on per unit dispersed phase by the rotor blades. When the dispersed phase velocity increases, this energy decreases along the column and the dispersed phase is harder to disperse. Fig. 9 shows that the continuous phase velocity has a negligible effect on the mean drop size. Therefore, the continuous phase velocity is not the main factor affecting the dispersed phase mean drop sizes.

### New correlelation for mean drop size

The previously correlations to estimate drop size lead to the large errors when applied to the experimental data in this column. Therefore, the new correlation for prediction of Sauter mean drop diameter is considered in this work. According to the experimental results, the main factors affecting the Sauter mean drop diameters are rotor diameter, agitation speed, dispersed phase flow velocity and physical properties of the three systems. Therefore, the following correlation can be suggested:

$$d_{32} = f(d_R, N, V_d, V_c, \rho_d, \Delta\rho, \mu_d, \mu_c, \sigma)$$

According to the dimensional analysis method, all the drop sizes obtained from this study have been correlated by the following equation:

$$d_{32} = 0.089 \left( \frac{N^4 d_R^4 \rho_c}{g \sigma} \right)^{-0.015} \left( \frac{\mu_c^4 g}{\Delta\rho \sigma^3} \right)^{-0.10} \left( 1 + \frac{V_c}{V_d} \right)^{0.10} \left( \frac{V_d}{\left( \frac{\sigma \Delta\rho g}{\rho_c^2} \right)^{0.25}} \right)^{-0.07} \left( \frac{h_c d_R}{D_c H} \right)^{-0.26}$$

In the above equation, the geometric parameter was defined by the last dimensionless number. The experimental data by (Moreira et al., 2007) (RDC column), Kadam et al. (Kadam et al., 2009) (ARDC column) and (Hemmati et al., 2015) (PRDC column) were used for prediction of Sauter mean drop diameter.

The results obtained are shown in Fig.11 where it was found the absolute average error was 9.78% with the experimental results. This figure indicates that the suggested correlation can make highly accurate estimate for the Sauter mean drop diameter with the experimental data and the experimental works by other researchers (Hemmati et al., 2015; Kadam et al., 2009; Moreira et al., 2007). [23][19]

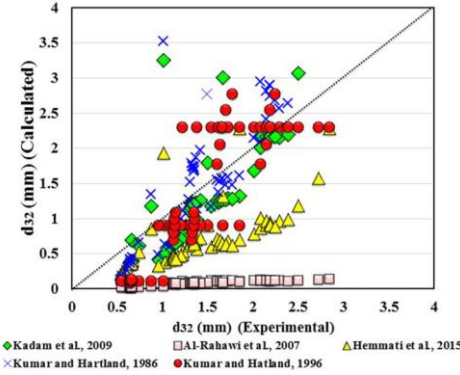


**Fig.10.** Comparison of experimental values of Sauter mean drop diameter with previous correlation in Table 1.

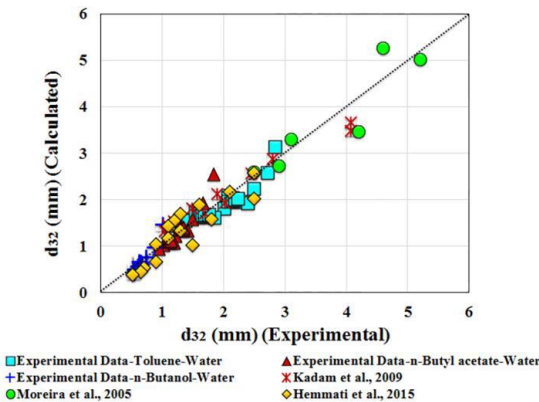


**Fig.11.** Comparison between experimental data and the estimated values using Eq. 12

**The drop behavior in the pilot plant ARDC column was investigated for three systems (toluene-water, n-butyl acetate-water and n-butanol-water) in the absence of mass transfer. Statistical analysis revealed the main effect of the rotor speed on the drop size diameter. The drop size could be increased with increasing dispersed phase flow rate, but the continuous phase flow rate does not have a significant effect. Drop size distributions measured by image analysis were suitably fitted to the Weibull probability distribution function. The empirical expressions were derived to predict the parameters of the distribution curve as a function of operating variables and physical properties for different probability density functions. Also, empirical correlation for the Sauter mean diameter was proposed with the experimental data in ARDC column.[23]**

# **Drop Behavior in a Pilot Plant Oldshue-Rushton Extraction Column for Three Various Liquid-Liquid Systems**

## **2.1. Description of pilot plant extractor**

A pilot plant Oldshue-Rushton column contactor, 113 mm in diameter, a working height of 700 mm with nine compartments, was used in the experiments. The stirrer is located in the center of each compartment with 6-blade impellers of 50 mm diameter. All internal parts of the column and the blade impellers were made of AISI 316 stainless steel. The blade impellers are mounted on a shaft, which is driven by an electric motor via a variable speed gear box. The speed of rotation could be measured and indicated by an electronic digital rotation speed meter adjusted by regulating the D.C voltage of the source. The specific column geometries studied are summarized in Table 1. Nine sampling valves are provided at 67 mm intervals along the column length. The organic phase is fed into the column through a distributor situated at the bottom. The continuous phase is introduced on the top of the column in a countercurrent mode with respect to the dispersed phase flow. Four stainless steel tanks with 85 L capacity were used to store the liquid feeds, and to collect the extract, and raffinate streams. Centrifugal pumps (Penax model) were used to circulate both liquid phases through the column. Two flow meters are employed to supply and monitor the fixed flow rates of the continuous and dispersed phases. The interface is maintained at the required level by using an optical sensor as previously described by Torab-mostaedi et al.[19].

## **2.2. Determination of drop size**

All experiments are carried out far from flooding conditions. A photographic technique was used to measure the drop diameter Nikon D5000 digital camera. Drop diameters were recorded at different positions of the column and different rotational speeds for available chemical systems. From these photographs the reading of the diameter of the drops was commenced with the Autocad2014 software. Using an optional reference in the picture like the thickness of stators, a simple proportional relationship between these two values would be produced and then the relative real size of the drops would be obtained. It is found that the curved surface of the glass extraction column and significant differences between air and the glass refractive indices leads to a parallax deformation of the objects photographed in the extraction column. In order to omit this phenomenon, a container which filled with water was attached to the extraction column and the photographic approach was used to calculate the size of stator thickness served as the reference for drop size measurements. A minimum of 1000 drops was analyzed for each experimental condition in order to guarantee the statistical significance of the determined size distributions. In the case of non-spherical droplets, the major and minor axes, d<sub>1</sub> and d<sub>2</sub>, were measured and the equivalent diameter, d<sub>e</sub>, was calculated from Eq. 1:

$$d_e = (d_1^2 d_2)^{1/3} \quad (1)$$

Eventually, the Sauter mean diameter was calculated from the following equation:

$$d_{32} = \frac{\sum_{i=1}^N n_i d_i^3}{\sum_{i=1}^N n_i d_i^2} \quad (2)$$

where  $n_i$  denotes the number of drops of diameter  $d_i$ .

The total holdup of the dispersed phase was assessed using the shutdown method. In this method, at the end of an experiment, when the conditions are steady, the inlet and outlet valves and agitation are shut at the same time and the dispersed phase was permitted to disengage from the interface on the top of the extraction column. A period of 10-15 min was allocated to settle the dispersed phase. The holdup was defined as the ratio of the displaced dispersed phase to the total volume of the extraction region. The variation in the interface height between operation and after settling was determined and then converted into the corresponding volume to estimate the holdup. Measurements were made in triplicate to verify experimental reproducibility.

### 2.3. Chemical Systems

Three various systems with different interfacial tensions consisting of n-butanol–water, toluene– water, n-butyl acetate–water were used in these experiments. Two systems involving tolueneacetone-water and n-butyl acetate–acetone-water were used for experiments with two directions of mass transfer. In experiments with mass transfer, dilute solutions were investigated with

approximately 3.5 wt% acetone as transferred solute in the organic or aqueous phase. The European Federation of Chemical Engineering (E.F.C.E) has adopted these systems as Recommended Systems [20]

The technical grade of toluene; n-butyl acetate and n-butanol from Tehran petroleum refinery with 99.5 % purity were used as the dispersed phase and distilled water was used as the continuous phase. The physical properties for three systems are listed in Table 1. After each run, the column was first cleaned using a solution of non-surface-active detergent, then thoroughly washed with tap water, and finally cleaned with distilled water.

**Table 1.** Technical description of the Oldshue-Rushton column and physical properties of systems studied at 20°C [20]

	Physical property	Toluene-water	n-Butyl acetate-water	n-Butanol-water
<b>Experimental systems</b>	$\rho_c$ [kg/m <sup>3</sup> ]	998.2	997.6	985.6
	$\rho_d$ [kg/m <sup>3</sup> ]	865.2	880.9	846.0
	$\mu_c$ [mPa.s]	0.963	1.027	1.426
	$\mu_d$ [mPa.s]	0.854	0.734	3.364
	$\sigma$ [mN/m]	36	14.1	1.75
<b>Technical description</b>	Column height (H)		700 mm	
	Column internal diameter ( $D_c$ )		113 mm	
	Diameter of the rotor		50 mm	
	No. number of stages		9	
	Height of the stages		67 mm	
<b>Correlation for <math>d_{32}</math></b>	Fractional free cross section area (%)		25	
	Continuous phase flow rate		18-36 l/h	
	Dispersed phase flow rate		18-36 l/h	
	Rotor speed		60-240 rpm	
	$d_{32} = C_1 \left( \frac{N^4 d_R^4 \rho_c}{g \sigma} \right)^{-0.286} \left( \frac{\mu_c^4 g}{\Delta \rho \sigma^3} \right)^{-0.308} \left( 1 + \frac{V_c}{V_d} \right)^{-0.009} e^{C_2} \left( \frac{h_c}{d_R} \right)^{C_3}$			

### 3. Results and discussion

#### 3.1. Drop size distribution investigation

Droplets tend to break up into two or more albeit smaller ones in equipment with a shaft which has several impellers aligned with changing operating

parameters. For this reason, drop size distribution is very important in extraction columns. Three vital operating parameters including aqueous and organic phase flow rates and rotor speed were chosen for investigation of drop size distribution and drop size in the Oldshue-Rushton columns.

### 3.1.1. Effect of agitation on drop size distribution

To investigate the influence of agitation on drop size distribution, the rotor speed was varied for different levels of agitation. The flow rates of continuous and dispersed phases were kept constant during the experiments. The amount of drop size distribution for three different systems vs. rotor speed is shown in Fig.1.

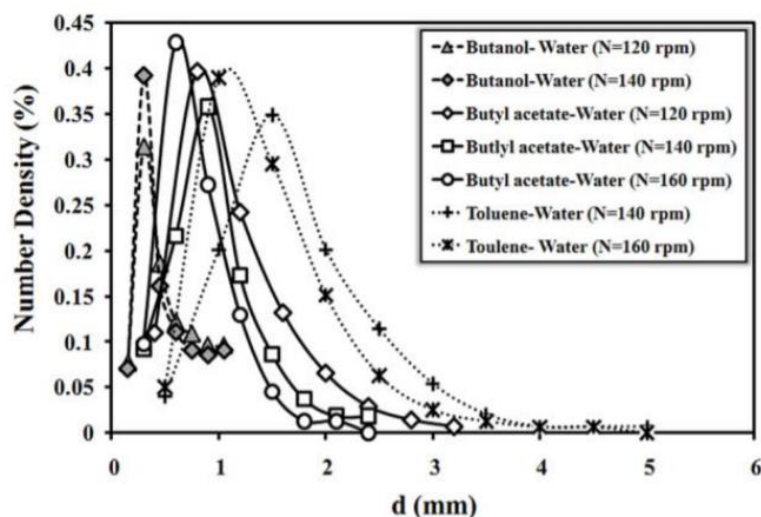


**Fig.1.** Effect of rotor speed on the drop size distribution ( $Q_c=Q_d=24$  l/h).

It was observed that drop size distributions shifted to the left with an increase in agitation, thus evidencing that smaller drops and more homogeneous distributions are obtained in more turbulent conditions, as the same behavior

was observed by Komasawa and Ingham [16]. The explanation for this effect is related to the increase in the frequency of drop collisions against the internal parts of the column in more turbulent environments during their ascending path inside the equipment.

In addition, the drop size distributions are also found to be narrower and more evenly distributed about the mean value for n-butanol-water (lower interfacial tension). When there is no agitation, the ratio of buoyancy to interfacial tension forces is responsible for the breakup of the drops and formation of the smaller drops. Thus, the drop size can be predicted by the following equation:

$$d_{32} = C \left( \frac{\sigma}{\Delta \rho g} \right)^{0.5} \quad (3)$$

where the constant, C, is a function of the column geometry and mass transfer, and may also depend upon the liquid–liquid system employed [21]. According to Eq.3, a decrease in droplet size is expected with a decrease in the interfacial tension of systems.

### **3.1.2. Effect of aqueous and organic phase flow rates on drop size distribution**

The influence of continuous and dispersed phase flow rates on the drop size distribution in the column is presented in Figs.2 and 3.

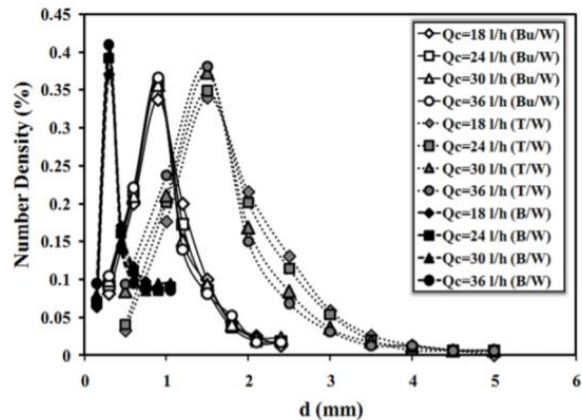


**Fig.2.** Effect of continuous phase flow rate on the drop size distribution at the same rotor speed for the binary systems of toluene- water (T/W), n-butyl acetate- water (Bu/W) and n-butanol- water (B/W) ( $N=140$  rpm ,  $Q_d= 24$  l/h).

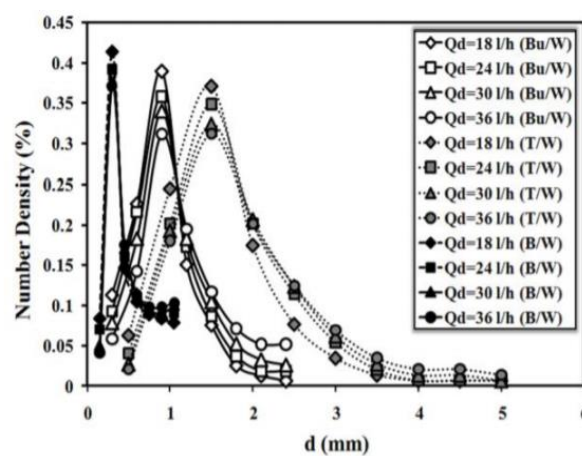


**Fig.3.** Effect of dispersed phase flow rate on the drop size distribution at the same rotor speed for the binary systems of toluene- water (T/W), n-butyl acetate- water (Bu/W) and n-butanol-water (B/W) ( $N=140$  rpm,  $Q_c= 24$  l/h).

### 3.1.3. New correlation for drop size distribution

In order to correlate the experimental drop size distributions, the quantitative analyses, namely the log-normal (plg) and normal (pn) probability density functions were selected. The description of these functions was shown in Table 2. These functions were performed for evaluation of drop size distribution on the basis of experimental data. For some liquid-liquid extraction columns, the probability density was proposed as presented in Table 3. The probability density is the ratio of drops number with a certain diameter to the total drops number. These functions for drop size distribution are given by:

$$P_n = \frac{1}{1.86\pi\alpha} \exp\left(-\frac{(d_i - \beta)^2}{2\alpha^2}\right) \quad (4)$$

$$P_{lg} = \frac{1}{0.33\pi\alpha d_i} \exp\left(-\frac{(\ln(d_i) - \beta)^2}{2\alpha^2}\right) \quad (5)$$

where  $d_i$  denotes the drop diameter and  $\alpha$  and  $\beta$  are constant parameters to be fitted.

For determination of drop size distribution, a nonlinear regression analysis was made to fit the theoretical distribution functions to the experimental data and to obtain the parameters,  $\alpha$  and  $\beta$  for normal and log-normal distribution functions. Further, the evaluated parameters were correlated as a function of operating parameters and physical properties of the systems. The derived correlations are given below:

$$\alpha = 7.684 \left( \frac{N^4 d_R^4 \rho_c}{\sigma g} \right)^{0.147} \left( \frac{\mu_c^4 g}{\Delta \rho \sigma^3} \right)^{0.148} \quad (6)$$

$$\beta = 0.155 \left( \frac{N^4 d_R^4 \rho_c}{\sigma g} \right)^{-0.453} \left( \frac{\mu_c^4 g}{\Delta \rho \sigma^3} \right)^{-0.116} \left( 1 + \frac{V_c}{V_d} \right)^{-0.389} \quad (7)$$

$$\alpha = 5.807 \left( \frac{N^4 d_R^4 \rho_c}{\sigma g} \right)^{0.060} \left( \frac{\mu_c^4 g}{\Delta \rho \sigma^3} \right)^{0.046} \quad (8)$$

$$\beta = 0.0235 \left( \frac{N^4 d_R^4 \rho_c}{\sigma g} \right)^{-0.929} \left( \frac{\mu_c^4 g}{\Delta \rho \sigma^3} \right)^{-0.147} \left( 1 + \frac{V_c}{V_d} \right)^{-0.809} \quad (9)$$

Equations (6) and (7) represent the parameters of normal function and equations (8) and (9) represent the parameters of log-normal function.

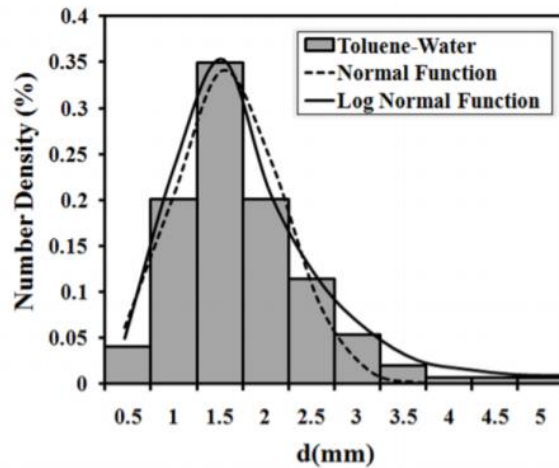
In the latter equations, N, d<sub>R</sub>, ρ<sub>C</sub>, μ<sub>C</sub>, σ, Δρ, V<sub>C</sub>, V<sub>d</sub> and g denote the agitation speed, rotor diameter, density of the continuous phase, viscosity of the continuous phase, interfacial tension, density difference between continuous and dispersed phases, continuous velocity, dispersed velocity and gravity acceleration, respectively. It is observed from the above equations that drop size distribution profiles are strongly affected by rotational speed and surface tension. Each experimental drop size histogram was compared with the normal and log-normal distribution functions and the average absolute relative errors (AARE) were calculated by the following equation:

$$AARE = \frac{1}{n} \sum_{i=1}^n \frac{|p_i(d)(exp) - p_i(d)(theo)|}{p_i(d)(exp)} \quad (10)$$

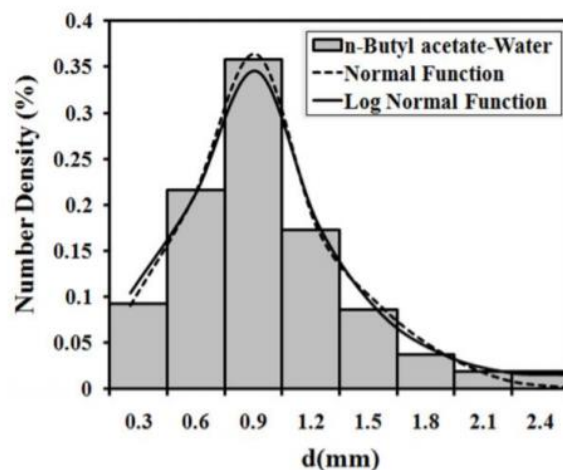
where  $n$  denotes the number of data points, and  $P_i(d)(\text{exp})$  and  $P_i(d)(\text{theo})$  denote the experimental and theoretical number densities of the drops, respectively. The values of AARE are shown in Table 4. A comparison between a typical experimental histogram and the normal and log-normal distribution functions is shown in Figs. 4 and 5. It is observed that the use of normal and log-normal distribution functions was found to result in good agreement with the experimental data. The log-normal distribution function was chosen as the most appropriate for representing the observed drop-size distributions for all the liquid-liquid systems studied.

**Table 4.** The obtained average absolute relative errors for estimation of constant parameters

Function	Parameter of the distribution	AARE (%)
Normal	$\alpha$	10.83
	$\beta$	9.49
Log-Normal	$\alpha$	2.14
	$\beta$	3.54



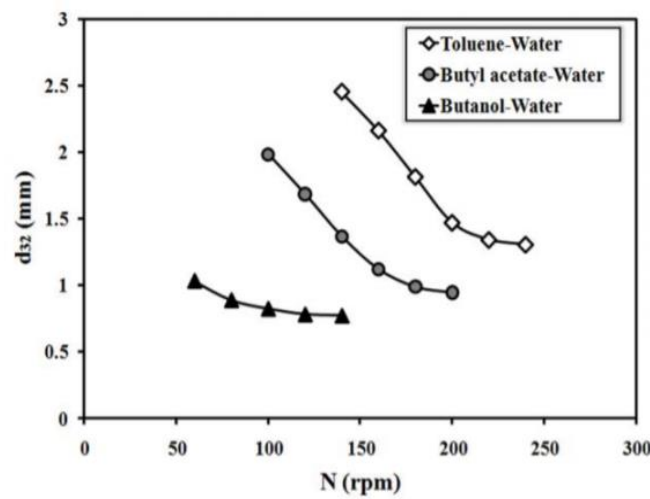
**Fig.4.** Comparison of theoretical distribution functions with a broad drop size distribution for toluene-water ( $N=140$  rpm,  $Q_d=Q_c=24$  l/h).



**Fig.5.** Comparison of theoretical distribution functions with a broad drop size distribution for n-butyl acetate-water ( $N=140$  rpm,  $Q_d=Q_c=24$  l/h).

3.2. Mean drop size Referring to Fig. 6, it is observed that as the agitation rate is increased, the average drop size significantly decreases. For all systems, agitation had a strong effect on the Sauter mean drop diameter. An increase in

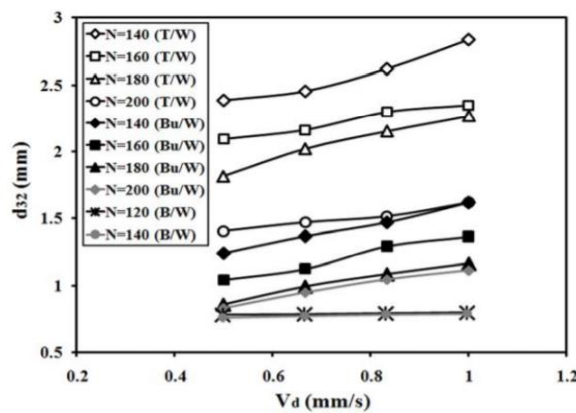
the energy supplied via agitation to the dispersed phase overcomes the interfacial forces of the droplets and, therefore, the droplets break. This phenomenon is predominant in turbulent parts of extraction column. Also, this effect grows in importance as the interfacial tension of the system increases. A similar decrease was reported by Komasawa and Ingham, 1978 [16] and Arnold et al, 1974 [23].



**Fig.6.** The effect of rotor speed on the Sauter mean drop diameter ( $V_c = V_d = 0.66$  mm/s).

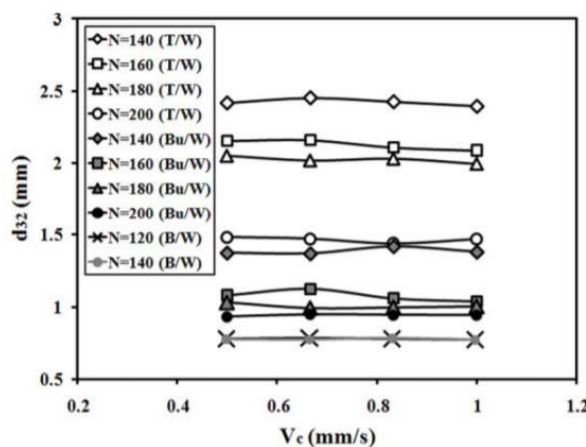
Mean drop size diameter is plotted as a function of continuous and organic phase velocities in Figs. 7 and 8. According to Fig. 7, increasing dispersed phase velocity leads to an increase in the mean drop size, however, it is changed slightly at low interfacial tension. This observation could be attributed to the increasing drop collisions with the acceleration of the dispersed phase velocity and consequently the coalescence frequency among the drops is intensified.

Fig.8 reveals that the continuous phase velocity has a negligible effect on the mean drop size. The experimental results obtained in three systems with Reynolds numbers are given in Tables A.1, A.2 and A.3 in Appendix A.



**Fig.7.** The effect of dispersed phase velocity on the Sauter mean drop diameter for the binary systems of toluene- water (T/W) , n-butyl acetate- water (Bu/W) and n-butanol-water (B/W)

( $V_c = 0.66$  mm/s).



**Fig.8.** The effect of continuous phase velocity on the Sauter mean drop diameter for the binary systems of toluene- water (T/W) , n-butyl acetate- water (Bu/W) and n-butanol-water (B/W)

( $V_d = 0.66$  mm/s).

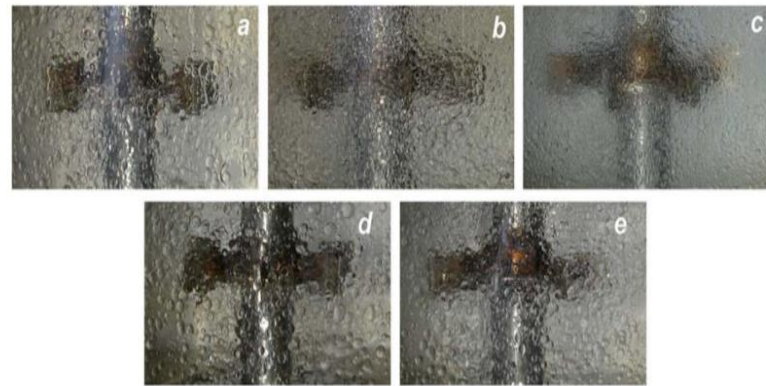


Fig. 8 The photos of drops for three systems without mass transfer conditions, (a) toluene–water, (b) *n*-butyl acetate–water and (c) *n*-butanol–water, and for toluene–acetone–water with mass transfer, (d) d to c transfer and (e) c to d transfer ( $V_c = V_d = 0.66 \text{ mm s}^{-1}$ ,  $N = 140 \text{ rpm}$ ).

The effect of solute transfer (acetone) between two phases for toluene–water and *n*-butyl acetate water is shown in Fig. 9.

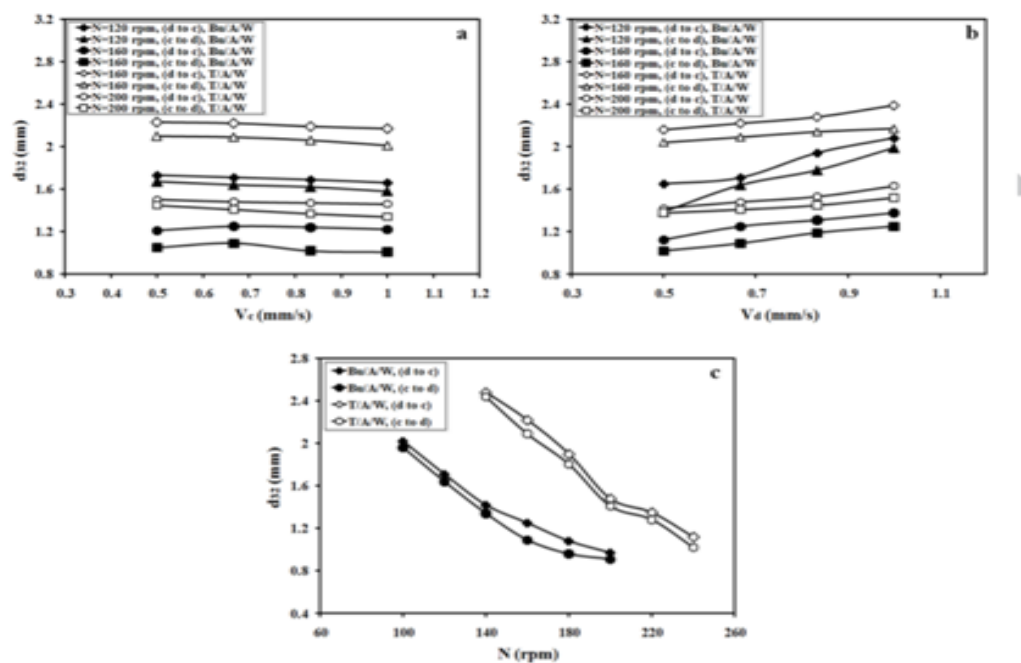


Fig.9. Effect of mass transfer direction on the Sauter mean drop diameter for toluene–acetone–water (T/A/W), *n*-butyl acetate–acetone–water (Bu/A/W) (a) variation with  $V_c$  ( $V_d=0.66 \text{ mm/s}$ ), (b) variation with  $V_d$  ( $V_c=0.66 \text{ mm/s}$ ), (c) variation with rotor speed ( $V_d= V_c=0.66 \text{ mm/s}$ )

The smaller drops were produced from continuous phase to dispersed phase in comparison to the reverse direction. The effect of mass transfer direction on drop coalescence can be interpreted in term of thin film phenomena. The thickness of the film separating an approaching drop from flat interface, or two colliding drops, is not uniform. For mass transfer out of the drops the rate of solute accumulation in the thinner sections of the film will be greater than in their surroundings, thus creating the condition for the appearance of interfacial tension gradients. When the mass transfer happens from the dispersed to the continuous phase, the concentration of the solute in the draining film between the two adjacent drops will be higher than in the surrounding continuous phase. For mass transfer in the opposite direction, the concentration will be correspondingly lower. The resulting gradients of interfacial tension will accelerate the drainage and coalescence in the first case and will retard the drainage and inhibit coalescence in the second case. Therefore, the d→c transfer produces larger drops than those in the opposite direction.

### **3.2.2. New correlation for mean drop size**

It is observed that the previous correlations contain a relatively high error in prediction of  $d_{32}$  for research column. Thus, the following correlation is derived for the mean drop size in the Oldshue-Rushton column based on the operating parameters. The new correlation for mean drop size can be written as:

$$d_{32} = 5.42 \times 10^{-4} \left( \frac{N^4 d_R^4 \rho_c}{g\sigma} \right)^{-0.311} \left( \frac{\mu_c^4 g}{\Delta\rho\sigma^3} \right)^{-0.258} \left( 1 + \frac{V_c}{V_d} \right)^{-0.075} \quad (15)$$

The correlation predicts the results with an average error of 10.7%. In the second correlation, the same variables are considered as for the first correlation and the column geometry term was added. This correlation is derived based on the experimental results of the present work and the data taken from other researchers mentioned in the introduction section.

$$d_{32} = C_1 \left( \frac{N^4 d_R^4 \rho_c}{g \sigma} \right)^{-0.286} \left( \frac{\mu_c^4 g}{\Delta \rho \sigma^3} \right)^{-0.308} \left( I + \frac{V_c}{V_d} \right)^{-0.009} e^{C_2} \left( \frac{h_c}{d_R} \right)^{C_3} \quad (16)$$

The effect of mass transfer and column geometry on the Sauter mean drop diameter is shown by constant parameters, C1, C2, C3 in the above equation, respectively. The values of these parameters are presented in Table 6.

**Table 6.** The constants and AARE values of Eq. 16

	system	C <sub>1</sub>	C <sub>2</sub>	C <sub>3</sub>	AARE%
Experimental					
no mass transfer	Toluene-Water work Tsouris et al. [12]	0.002015	-0.185	-0.734	5.51
	Toluene-Water work Arnold et al. [23]				
	n-Butyl acetate-water work	0.001574	0	0	5.68
c to d transfer	n-Butanol-water work	0.001024	0	0	10.27
	Toluene-acetone-Water work Al-Rahawi [13]	0.001715	-0.2786	-0.823	9.33
	n-Butyl acetate-acetone-water work	0.00142	0	0	6.99
d to c transfer	Clairsol350-acetone-water Al-Aswad [15]	0.02657	0	0	9.61
	Toluene-acetone-Water work	0.002137	0	0	7.21
	n-Butyl acetate-acetone-water work	0.001654	0	0	3.14
	Clairsol350-acetone-water Al-Aswad [15]	0.03112	0	0	9.5

A comparison of the prediction of the proposed correlation was tested, as shown in Fig. 11. Also, a comparison of the experimental data and other researchers with that predicted by the new correlation is illustrated in this Figure. The figures shown correlate the predicted values

with those experimentally measured ones under different operating conditions and the results with other researchers.

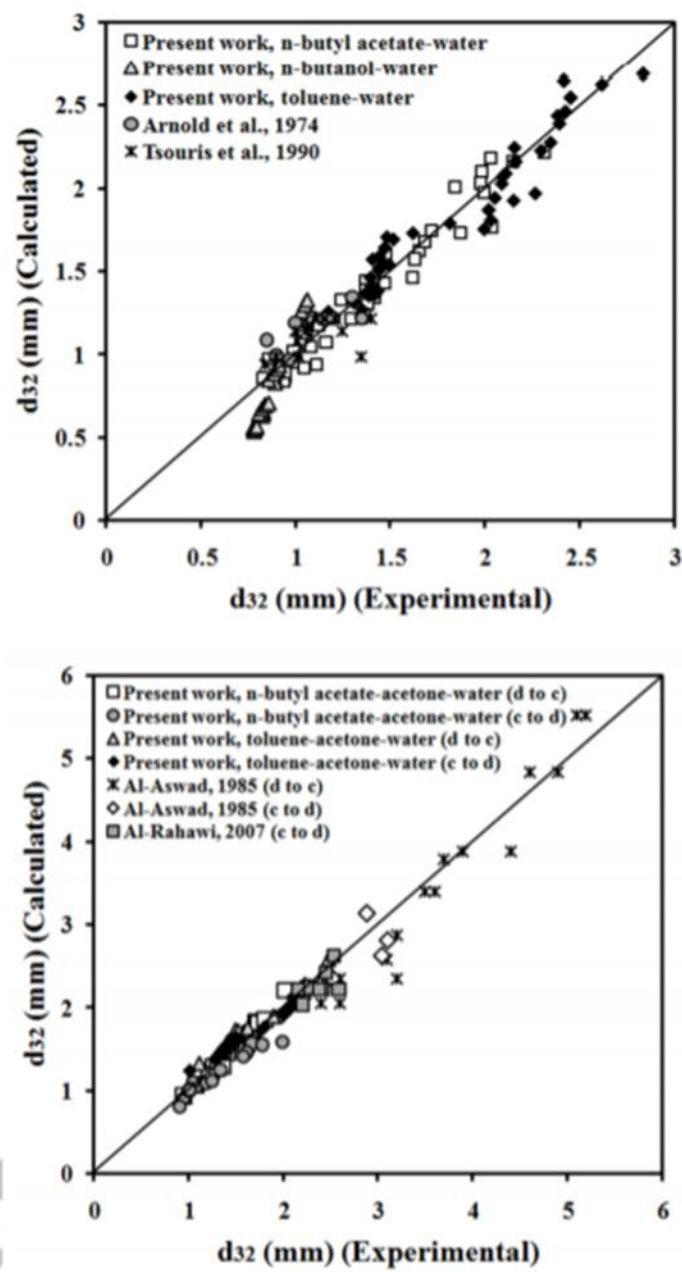


**Fig.11.** Comparison between experimental data and the evaluated values using equation (16).

Equation	Column	Reference
$\frac{d_{32}}{H} = \frac{C_\psi e^n}{\frac{I}{C_\omega \left( \frac{\sigma}{\Delta \rho g H^2} \right)^{1/2}} + \frac{I}{C_H \left[ \left( \frac{\varepsilon}{g} \right) \left( \frac{\rho_c}{g \sigma} \right)^{1/4} \right]^{n_1} \left[ H \left( \frac{\rho_c g}{\sigma} \right)^{1/2} \right]^{n_2}}} \quad (11)$	Rotating disc column Asymmetric rotating disc column Kühni Column Wirtz Column Pulsed column Karr Column	Kumar and Hartland, 1996 [21]
$\frac{d_{32}}{d_R} = 2.44 \left( \frac{h_c}{H} \right)^{-0.06} \left( \frac{V_i^2 d_R \rho_m}{\sigma_i} \right)^{-0.63} \left( \frac{V_k}{V_i} \right)^{0.18} \quad (12)$	Oldshue- Rushton column	Arnold et al., 1974[23]
$\frac{d_{32}}{d_R} = 90.7 \left( \frac{h_c}{H} \right)^{-0.13} \left( \frac{V_i^2 d_R \rho_m}{\sigma_i} \right)^{-0.39} \left( \frac{V_k}{V_i} \right)^{0.40} \varphi^{-0.31} \quad (13)$	Oldshue- Rushton column	Tsouris et al., 1990 [12]
$d_{32} = 0.705 \left( \frac{\sigma}{g \Delta \rho} \right)^{0.5} \frac{d_R^{0.8}}{N^{0.185}} \frac{\left( \frac{Q_c}{Q_d} \right)^{0.15}}{(Q_c + Q_d)^{0.1}} \quad (14)$	Rotating disc column	Al-Rahawi, 2007 [13]

3.2.3. Power dissipation per unit mass In rotary agitated columns, the power dissipation per unit mass ( $\varepsilon$ ) is given in terms of the power input per agitator by:

$$\varepsilon = \frac{4P}{\pi D_c h_c \rho_c} \quad (17)$$

in which P is obtainable from a relationship between the power number,  $N_p$ , and the agitator Reynolds number,  $Re_R$ . The experimental data on the power required to operate the agitated columns can be described by the correlation recently proposed by Kumar and Hartland [24]:

$$N_p = 1.08 + \frac{10.94}{Re_R^{0.5}} + \frac{257.37}{Re_R^{1.5}} \quad (18)$$

$$N_p (N^3 d_R^5 \rho_c) = P \quad (19)$$

The variation of Sauter mean drop diameter with power dissipation per unit mass in the OldshueRushton column for three systems was shown in Fig.12. It was observed that more

energy is required for production of smaller droplets in toluene-water system with higher surface tension.

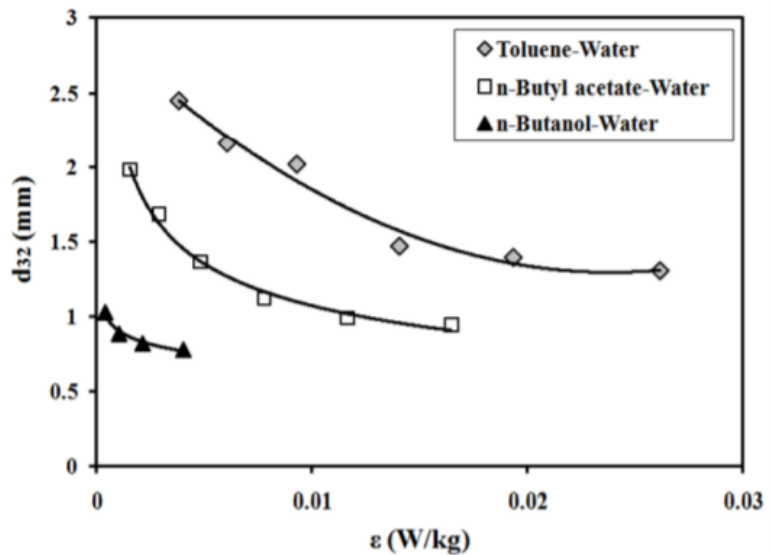


**Fig.12.** Variation of Sauter mean drop diameter with energy dissipation per unit mass

### 3.2.4. Breakage and coalescence rate

The most widely used and quoted model is the approach of the Coulaloglou and Tavlarides (1977) [25]. The breakage frequency derived from this model has the following form:

$$g(d) = k_{1\text{break}} \frac{\epsilon^{1/3}}{(1+\varphi)d^{2/3}} \exp(-k_{2\text{break}} \frac{\sigma(1+\varphi)^2}{\rho_d d^{5/3} \epsilon^{2/3}}) \quad (20)$$

In the above equation,  $k_{1\text{break}}$  and  $k_{2\text{break}}$  is constant parameters in the model,  $d$  is the drop diameter,  $\rho_d$  is the density of the dispersed phase,  $\sigma$  is the interfacial tension and  $\epsilon$  is the energy dissipation per unit mass. Coalescence frequency is defined as the product of the collision frequency ( $h$ ) and the coalescence efficiency ( $\lambda$ ):

$$C(d, d') = h(d, d') \cdot \lambda(d, d') \quad (21)$$

where the collision frequency is given by:

$$h(d, d') = k_{l\text{coal}} \frac{\epsilon^{1/3}}{(1+\varphi)} (d^2 + d'^2) (d^{2/3} + d'^{2/3})^{1/2} \quad (22)$$

and the coalescence efficiency of the collision:

$$\lambda(d, d') = \exp(-k_{2\text{coal}}) \frac{\rho_c \mu_c \epsilon}{\sigma^2 (1 + \varphi)^3} \left( \frac{dd'}{d + d'} \right)^4 \quad (23)$$

where  $k_{1\text{coal}}$  and  $k_{2\text{coal}}$  are constant parameters in the model. These equations with population balance equation were solved with numerical methods. The result of the model for prediction of drop size distribution is shown in Fig.13. It was shown that the experimental results for three systems were successfully simulated with the results of simulation with Coulalglou and Tavlarids model.

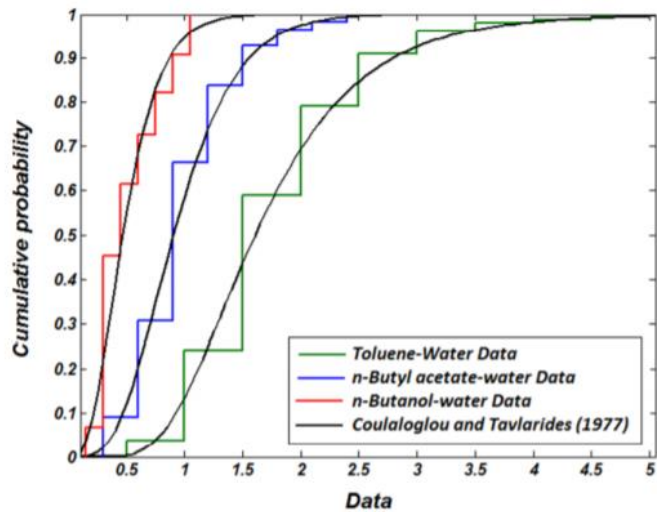


**Fig.13.** Simulated drop size distributions by Coulologlou and Tavlarides model for breakage and coalescence rates, compared with experimental data

3.2.5. Errors of  $d_{32}$  The experimental errors such as errors in measuring droplet size from pictures and errors in taking photos from each experiment may be occurred in the experimental work. Therefore, measurements for determination of Sauter mean drop diameter were made in triplicate to verify experimental reproducibility. The Sauter mean drop diameter for each run was determined by the obtained average results from taking photos.

The average of Sauter mean drop diameter with a standard deviation for one of the experiments is shown in Fig. 14.

The results for toluene-water system at rpm=140 and Vd=Vc=0.66 mm/s show an expected mean value of 2.45 with a standard deviation of 4.81%.[24]

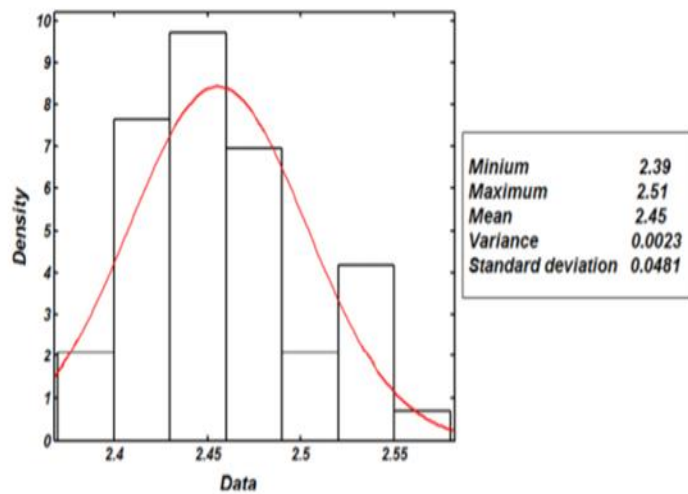


**Fig.14.** Average Sauter mean drop diameter and standard deviation for toluene-water (N=140 rpm,  $V_d = V_c = 0.66 \text{ mm/s}$ ).

**Table A.2**

**Experimental data obtained in the experiments for n-butyl acetate-water**

<b>rpm</b>	<b>holdup</b>	<b>V<sub>d</sub> (mm/s)</b>	<b>V<sub>c</sub> (mm/s)</b>	<b>d<sub>32</sub> (mm)</b>	<b>Re</b>
100	0.078	0.665	0.499	2.031	17.789
100	0.081	0.665	0.665	1.984	17.166
100	0.083	0.665	0.831	1.980	17.124
100	0.092	0.665	0.997	1.997	16.218
120	0.089	0.665	0.499	1.719	13.325
120	0.095	0.665	0.665	1.686	12.645
120	0.100	0.665	0.831	1.657	12.212
120	0.104	0.665	0.997	1.633	11.947
140	0.099	0.665	0.499	1.373	9.729
140	0.104	0.665	0.665	1.369	9.467
140	0.108	0.665	0.831	1.419	9.764
140	0.114	0.665	0.997	1.380	9.297
160	0.117	0.665	0.499	1.080	6.541
160	0.123	0.665	0.665	1.123	6.722
160	0.132	0.665	0.831	1.059	6.180
160	0.139	0.665	0.997	1.039	5.988
180	0.131	0.665	0.499	1.031	5.673
180	0.137	0.665	0.665	0.991	5.428
180	0.145	0.665	0.831	0.996	5.369
180	0.154	0.665	0.997	1.003	5.365
200	0.136	0.665	0.499	0.933	4.955
200	0.146	0.665	0.665	0.948	4.918
200	0.154	0.665	0.831	0.945	4.864
200	0.165	0.665	0.997	0.943	4.788
100	0.077	0.499	0.665	1.844	12.957
100	0.087	0.831	0.665	2.148	21.349
100	0.096	0.997	0.665	2.313	24.928
120	0.088	0.499	0.665	1.478	9.222
120	0.102	0.831	0.665	1.870	16.206
120	0.110	0.997	0.665	2.037	19.489
140	0.098	0.499	0.665	1.242	7.054
140	0.109	0.831	0.665	1.470	11.997
140	0.118	0.997	0.665	1.617	14.403
160	0.116	0.499	0.665	1.042	5.103
160	0.134	0.831	0.665	1.294	8.769
160	0.142	0.997	0.665	1.365	10.323

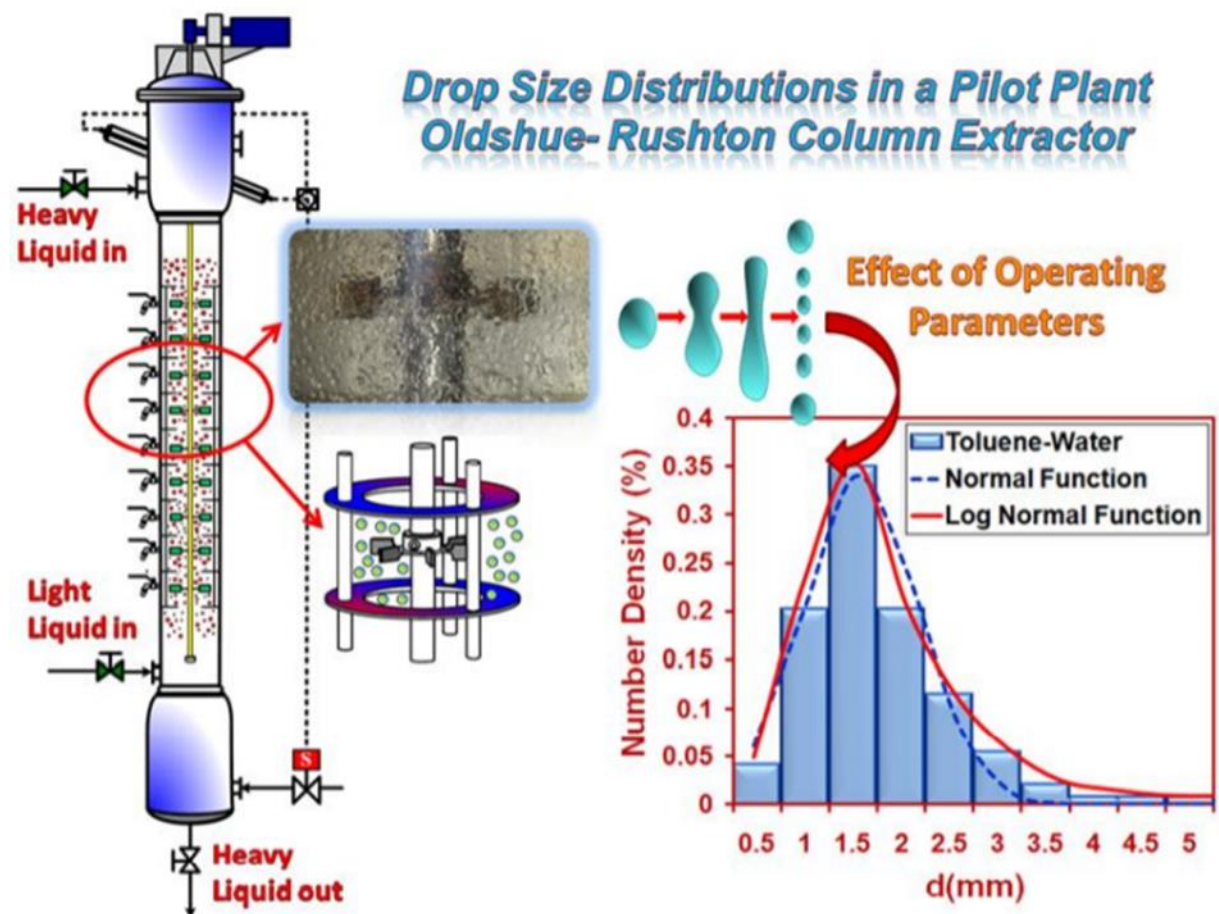
<b>rpm</b>	<b>holdup</b>	<b>V<sub>d</sub> (mm/s)</b>	<b>V<sub>c</sub> (mm/s)</b>	<b>d<sub>32</sub>(mm)</b>	<b>Re</b>
180	0.128	0.499	0.665	0.856	3.873
180	0.148	0.831	0.665	1.084	6.750
180	0.158	0.997	0.665	1.162	8.012
200	0.132	0.499	0.665	0.831	3.665
200	0.158	0.831	0.665	1.045	6.155
200	0.170	0.997	0.665	1.112	7.216

**Table A.3**

**Experimental data obtained in the experiments for n-Butanol-Water**

<b>rpm</b>	<b>holdup</b>	<b>V<sub>d</sub> (mm/s)</b>	<b>V<sub>c</sub> (mm/s)</b>	<b>d<sub>32</sub>(mm)</b>	<b>Re</b>
60	0.077	0.665	0.499	1.051	6.702
60	0.085	0.665	0.665	1.033	6.133
60	0.087	0.665	0.831	1.035	6.107
60	0.099	0.665	0.997	1.041	5.628
80	0.084	0.665	0.499	0.900	5.246
80	0.098	0.665	0.665	0.889	4.622
80	0.102	0.665	0.831	0.891	4.602
80	0.109	0.665	0.997	0.894	4.479
100	0.094	0.665	0.499	0.841	4.452
100	0.107	0.665	0.665	0.825	3.967
100	0.111	0.665	0.831	0.835	3.994
100	0.125	0.665	0.997	0.828	3.689
120	0.119	0.665	0.499	0.778	3.311
120	0.127	0.665	0.665	0.783	3.246
60	0.073	0.499	0.665	1.015	5.287
60	0.085	0.665	0.665	1.033	6.133
60	0.090	0.831	0.665	1.050	7.224
60	0.102	0.997	0.665	1.062	7.701
80	0.082	0.499	0.665	0.860	4.045
80	0.098	0.665	0.665	0.889	4.622
80	0.103	0.831	0.665	0.905	5.533
80	0.113	0.997	0.665	0.917	6.090
100	0.090	0.499	0.665	0.808	3.520
100	0.107	0.665	0.665	0.825	3.967
100	0.114	0.831	0.665	0.844	4.706
100	0.130	0.997	0.665	0.861	5.026
120	0.113	0.499	0.665	0.773	3.012
120	0.127	0.665	0.665	0.783	3.246
120	0.133	0.831	0.665	0.791	3.848
120	0.140	0.997	0.665	0.798	4.351

## Graphical abstract



# **Exact hydrodynamic description of pilot plant Oldshue-Rushton contactor: a case study with the introduction of selenium and tellurium into reaction system**

## **ABSTRACT**

In this paper, the hydrodynamic behaviour of the chemical reaction system (selenium, tellurium, and TBP) was interpreted in the Oldshue-Rushton extraction column. The optimum operating parameters for extracting the selenium and tellurium from chloride medium were carried out by using the batch experiments. The feed acidity of 5 molar and solvent phase with 20% (v/v) TBP in kerosene were optimised to examine the hydrodynamic parameters of the mentioned column.

The impacts of operating variables such as rotor speed, inlet aqueous phase velocity, and inlet solvent phase velocity on the dispersed phase hold-up, mean drop size, slip velocity, drop size distribution, and extraction rate were evaluated in the column experiments.

The experimental drop size distributions in the Oldshue-Rushton column were fitted with the two modified functions containing the normal and log-normal. The stable parameters within the mentioned functions were connected with the operating variables, reactive and physical systems. Among the two distribution functions, the modified log-normal is found to accomplish sufficiently in the fitting of the drop size distribution. The

results of extracting the selenium and tellurium with TBP in the extractor indicated the column feasibility with the proper extraction for tellurium and selenium in the chloride solution.

## **Introduction**

The Oldshue-Rushton column has broadly utilised in the chemical reactions, including the solvent extraction process [16,17]. These types of extractors have advantages such as better mass transfer rate, appropriate for heterogeneous phase reaching using small size particles with large hold-up values, comfortable in start-up, high-efficiency, high flexibility.

Unfortunately, the hydrodynamic parameters of the Oldshue-Rushton extractor have rarely been reported by considering the solvent extraction system. Also, the usages of the mentioned column have not been reported in the literature for extracting the selenium and tellurium from sulphide ores and anode slime residue. This investigation is carried out to ensure an adequate understanding of hydrodynamic properties in a multistage column under the reactive extraction system. The impact of operational parameters containing the rotor speed, inlet aqueous and inlet solvent phase velocities on the hold-up, mean drop size, slip velocity, drop size distribution, and extraction percentages were investigated in the mentioned extractor, to acquire additional information.

## **Extraction experiments in the column**

Figure 1 depicts the schematic stream chart of the Oldshue-Rushton column set-up. The column was built of a round and hollow glass segment. It was prepared with impellers with precise speed control, though the inside parts were constructed of stainless steel. This column was utilised with 11.3 cm diameter, the operational section of 70 cm, and nine stages within the extraction experiments. The agitated was seated in the centre of the extractor with 5 cm distance across. The revolution speed has been measured and demonstrated with the electronic computerised turn speed metre balanced by controlling the DC voltage. A settler with 16.8 cm internal diameter has been located at each end of the extractor allowed the fluids to coalesce and decant independently. The inlet aqueous phase velocity and inlet solvent phase velocity were measured by applying calibrated flow metres. The inlet and outlet of the extractor were connected to four stainless steel tanks. The inlet aqueous and solvent phases were filled within the column from the bottom and the top, respectively. An optical sensor was utilised for automatically controlling the interface location of the two phases, as previously described by TorabMostaedi et al. [28]. Based on the batch experiments, 5 M of hydrochloric acid was chosen for the initial acidity of the feed solution as well as the solvent phase contained TBP solution and kerosene diluent of

20% (v/v) and 80% (v/v), respectively. By considering reaction conditions, all of the extraction tests were performed at room temperature and far from flooding rates.

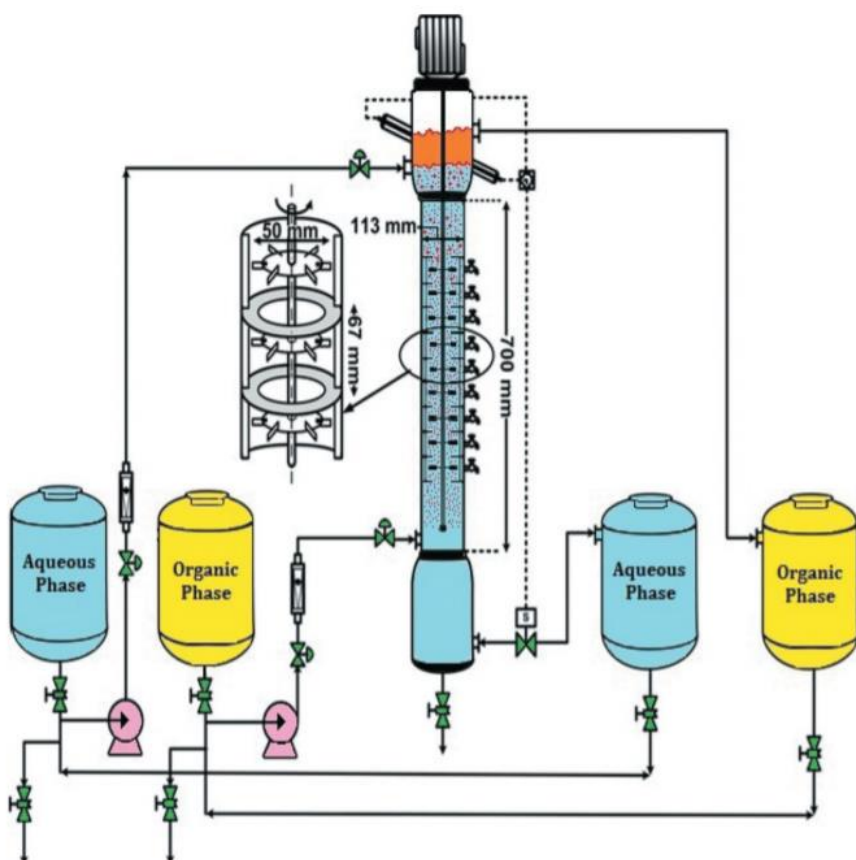


Figure 1. Schematic diagram of Oldshue-Rushton column and flows of light and heavy.

**2.4. Procedure** The ICP analysis was used for determining the concentration of the metals in the aqueous solution. All of the experiments were carried out under the chemical reaction system. The physical properties of the aqueous and solvent phases are given in Table 1.

**Table 1.** Physical properties of the solvent extraction system.

Components	$\mu (\times 10^3 \text{ kg.m}^{-1}\text{s}^{-1})$	$\rho (\text{kg/m}^3)$	$\sigma (\times 10^3 \text{ N/m})$
Aqueous phase	0.951	1012	17.5
Solvent phase	1.162	802	-

In a few cases, non-spherical droplets were apperceived [30]. Therefore, the following equation expressed the drop size with consideration of the equivalent sphere:

$$d_e = \sqrt[3]{(d_1^2 d_2)} \quad (5)$$

After each experiment was completed, the shutdown procedure was utilised to obtain the hold-up values. When the system occurred to steady-state, the outlet and inlet valves of both phases were closed. The inlet and outlet valves of aqueous and solvent phases were closed altogether after steady-state situation. The light phase was allowed to settle. By determining the interfacial height variation, the dispersed phase hold-up has been calculated. The fractional volumetric hold-up ( $\varphi$ ) was defined as follows:

$$\varphi = \frac{V_d}{V_d + V_c} \quad (6)$$

The slip velocity is a significant parameter for calculating the mass transfer

coefficients. The relative movement between the aqueous phase and the solvent phase drops for the countercurrent flow of two phases is defined as follows [31–33]:

$$V_{slip} = \frac{V_d}{\varphi} + \frac{V_c}{(1 - \varphi)} \quad (7)$$

The following equation defined the interfacial surface area per unit volume [34]:

$$a = \frac{6\varphi}{d_{32}} \quad (8)$$

Comparing the experimental data with the anticipated results was done using the AARE which the following equation determines these values:

$$AARE = \frac{1}{NDP} \sum_{i=1}^{NDP} \frac{|Experimental\ value - Predicted\ value|}{Experimental\ value} \quad (9)$$

Also, NDP indicates the number of experimental data.

### **3.2.2. Impact of operational parameters on size of droplets**

Drop size owns an essential influence on the maximum amount of throughput [39–41]. Moreover, d32 and hold-up values utilise for determining the interfacial area. The experimental data for drop size under different rotor

speeds based on the reaction between ions in the aqueous phase and TBP in the solvent phase are shown in Figure 4(a). It is concluded that the average drop size decrements by increasing the mixing effect. Because the droplet breakage intensification happened by the increment of the rotor speed owing to enhancing the collisions between solvent phase droplets and the internal wall. An enhancement in the inlet solvent phase velocity leads to a higher coalescence frequency along the column. Consequently, at high inlet solvent phase velocity, the larger droplets formed (Figure 4(b)). The results from changing the average drop diameter with inlet aqueous phase velocity are depicted in Figure 4(c).

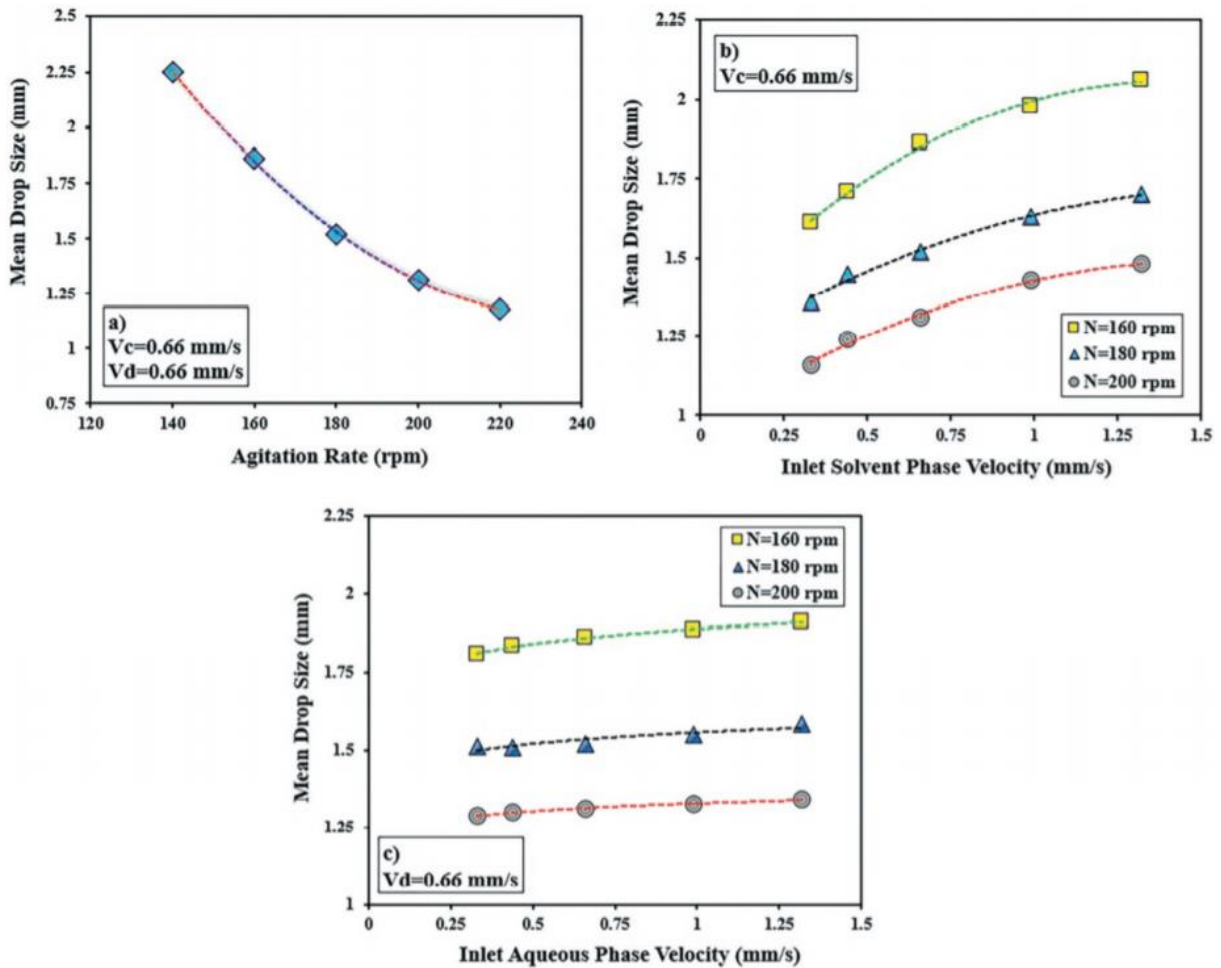


**Figure 4.** Impact of rotor speed and inlet phase velocities on mean drop sizes.

A variation in the inlet aqueous phase velocity has no critical effect on the drop diameter. It is indicated that drop size is generally influenced by the rotor speed as well as inlet solvent phase velocity under chemical reaction conditions. However, Asadollahzadeh et al. observed that the inlet aqueous phase velocity has an ordinarily impact on the drop size for the toluene/water framework in the high rotor speed [42].

### **3.2.3. Impact of operational parameters on slip velocity**

In this research, equation (7) is utilised for obtaining the slip velocity. The results of changing the slip velocity with the rotor speed are shown in Figure 5(a). The raise of the rotor speed leads to more shear forces and the formation of small droplets. Thus, slip velocity decreases with increasing the agitation rates. As demonstrated in Figure 5(b), the residence time of solvent phase droplets reduces with increasing the inlet solvent phase velocity that causes the slip velocity enhances [43]. The hold-up values increase with an increment in the inlet aqueous phase velocity. But, a change in the inlet aqueous phase velocity has no importantly influenced the average droplet size, and the dispersed phase hold-up impact is more significant than the drop size. As a result, with increasing the inlet aqueous phase velocity, the slip velocity slightly decreases (Figure 5(c)).

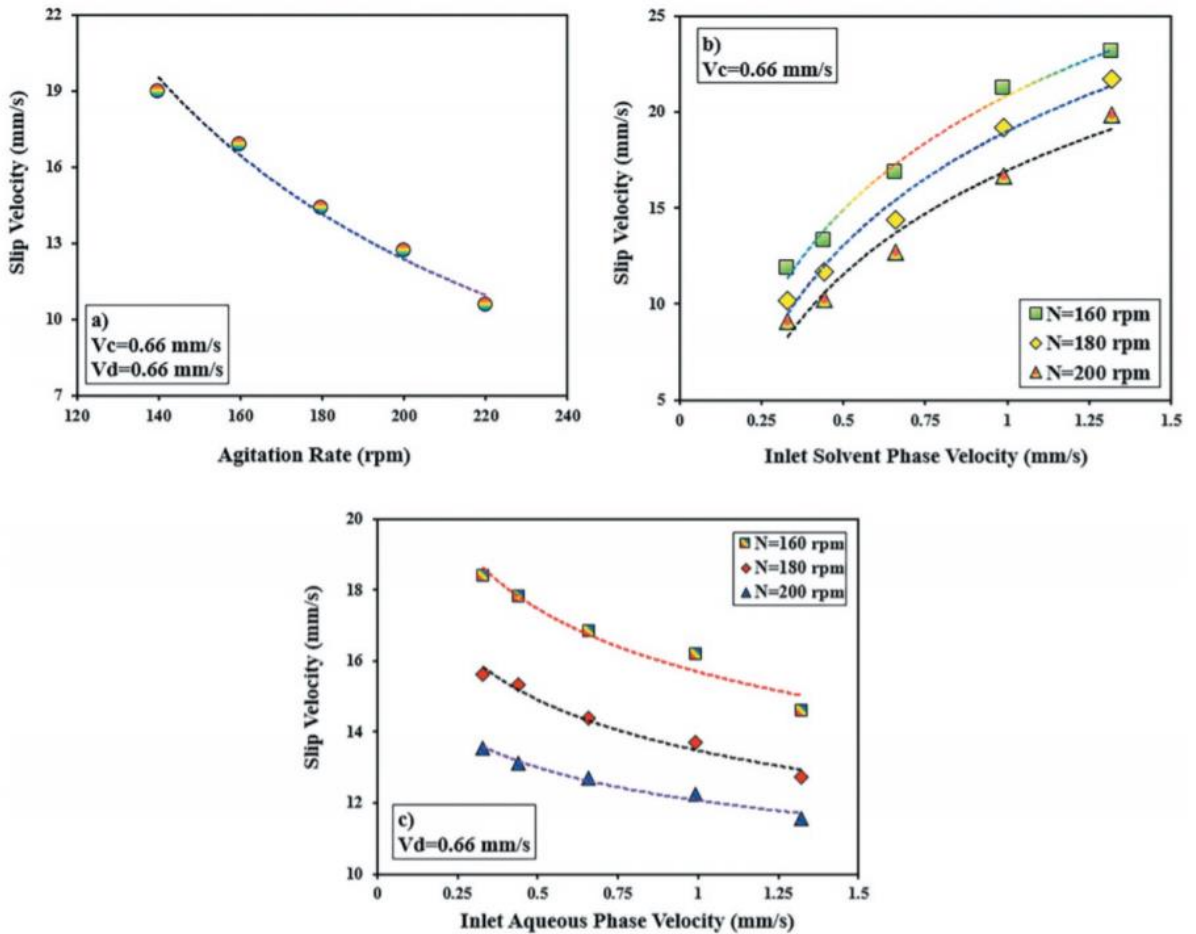


**Figure 5.** Impact of rotor speed and inlet phase velocities on slip velocity.

### 3.2.4. Impact of operational parameters on drop size distribution

In a device with a fomenter, droplets habitually propagate at the vortexes. The outcomes of collisions are capable of the drops break up into several smaller droplets. That is why this function is an essential parameter in the columns. In this study, the impact of changing the operational variables is interpreted on the drop size distribution in the extractor. To examine the impact of interfacial tension on drop size distribution, the experimental results detailed by Asadollahzadeh et al. [44] for three systems without reaction conditions were compared with the experimental data under the

reactive extraction system. To better indicate the changes of the drop size distribution, the experimental tests were performed at the various ranges of agitation levels. Figure 6(a) demonstrated the drop size distribution curves for four various systems with the agitation rate. In the constant inlet phase velocities, this parameter moved to the left side with enhancing the rotor speed evidencing that droplet break-up is gotten in the intensification of turbulent situations, as previously this phenomenon was apperceived by Komasawa and Ingham [24]. The clarification for this impact is dependent on the increment within the frequency of drop collisions against the inside parts of the extractor in an escalation of turbulent situations amid their ascendant direction. It is clearly seen from Figure 6(b), the variation of this function was scanty with the inlet solvent phase velocity. As demonstrated in Figure 6(c), no reasonable shifts within the tendency of the curves were apparent in a way that the inlet aqueous phase velocities had nearly the same dissemination points. It should be noted that the impacts of inlet aqueous and solvent phase velocities in comparison with the rotor speed and interfacial tension are insignificant on the drop size distribution under the physical system or chemical reaction system in the Oldshue-Rushton column.

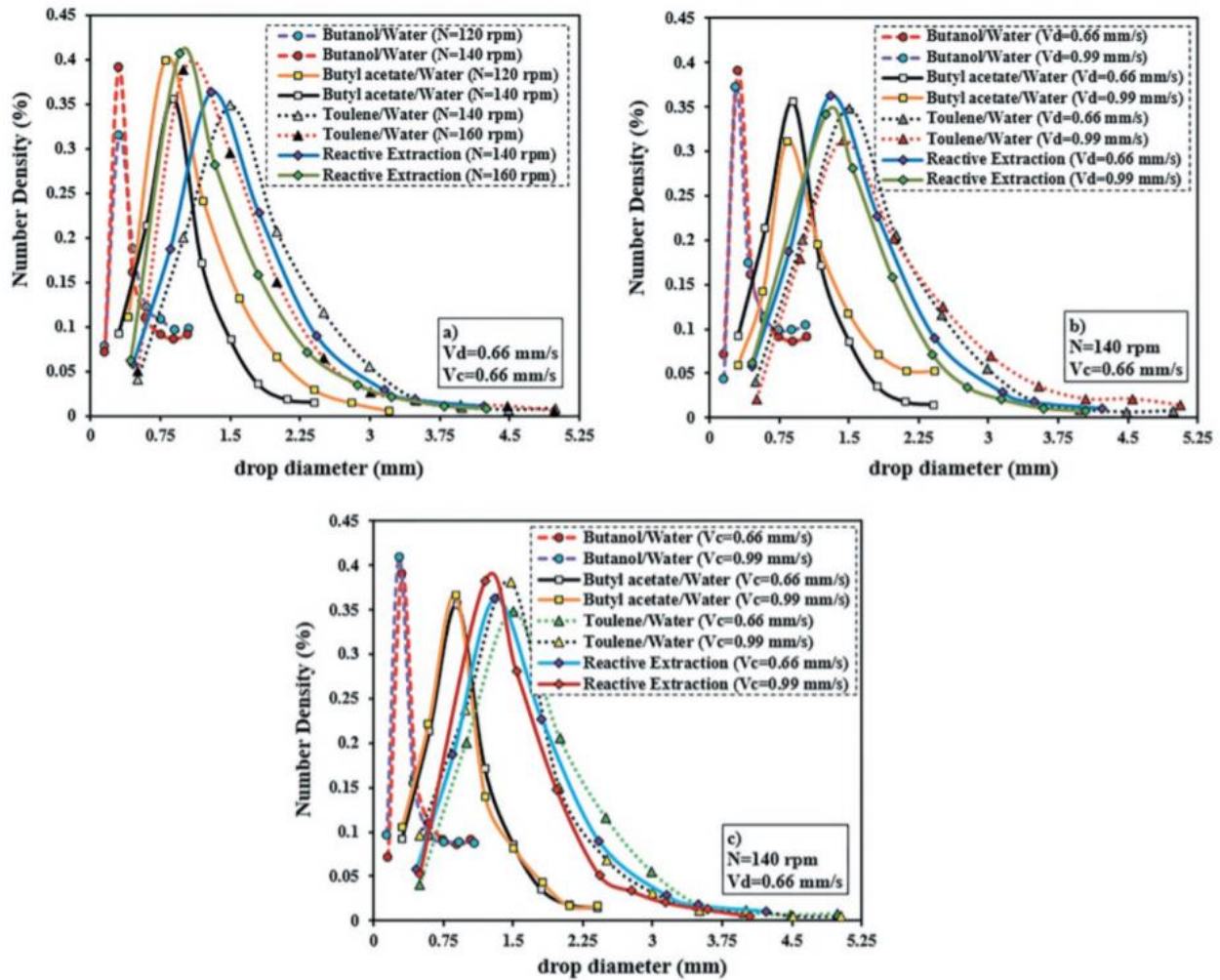


**Figure 6.** Impact of rotor speed and inlet phase velocities on drop size distribution.

### 3.2.5. Previous models for hold-up, mean drop size and slip velocity

Shakib et al. studied the performance of an Oldshue-Rushton column for molybdenum extraction from sulphate solution by implies of synergistic extractants [45]. They interpreted experimental data and proposed a model for estimating the hold-up values under the reactive extraction system as follows:

$$\varphi = 0.059 \left( 1 + \frac{V_c}{V_d} \right)^{1.4} \left( \frac{N^4 d_R^4 \rho_c}{g\sigma} \right)^{0.23} \left( \frac{V_d^4 \rho_c}{g\sigma} \right)^{0.26} \left( \frac{\Delta\rho}{\rho_c} \right)^{-0.7} \left( \frac{\rho_c V_c^2 D_c}{\sigma} \right)^{-0.25} \quad (12)$$

In this research, the mentioned model is recommended for calculating the hold-up values under extraction with chemical reaction. Figure 7(a) indicates the present data comparison with the predicted values by using correlation (12) that the AARE equal to 7.82% indicates the compromise of this model with the experimental results.

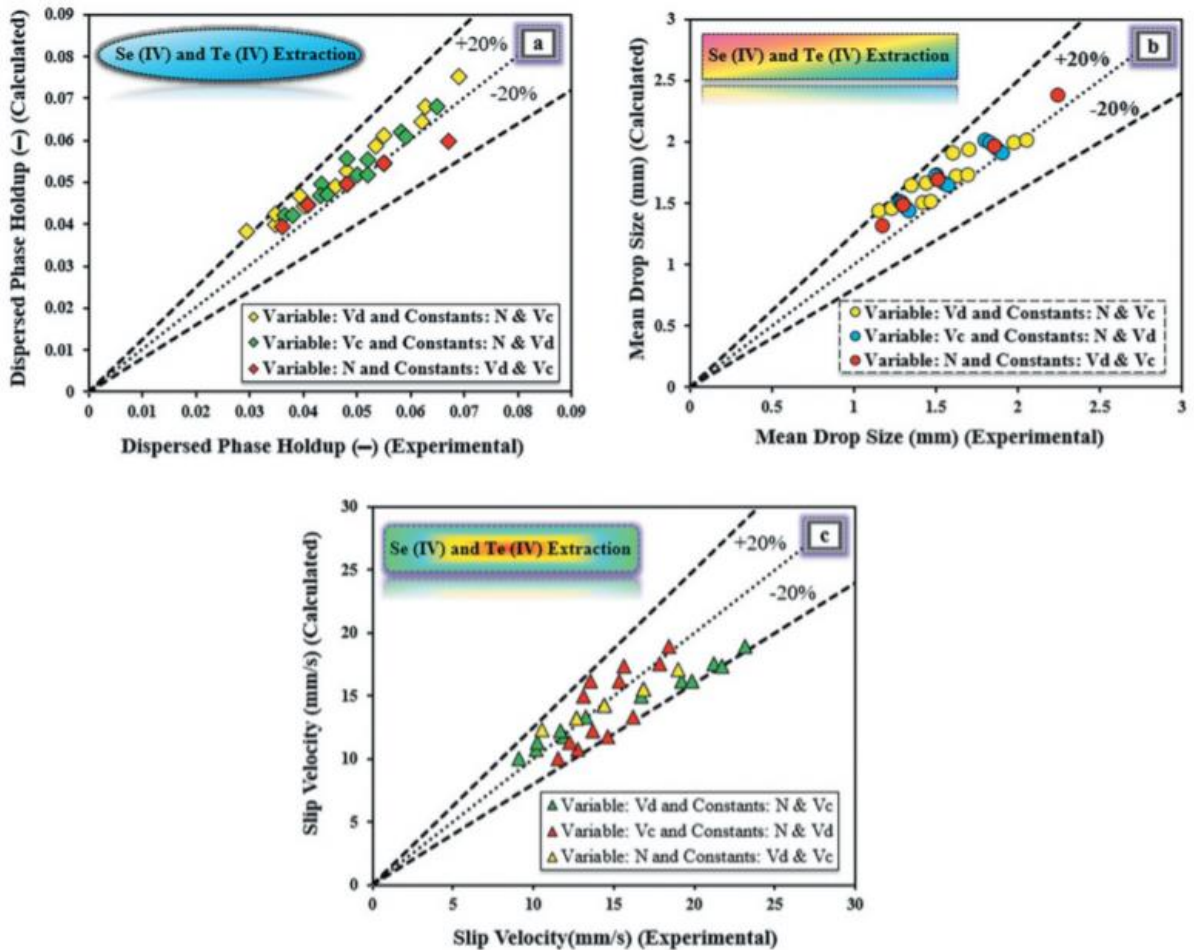


**Figure 7.** Comparison of experimental data with calculated values by the previously model for (a) dispersed phase hold-up using Eq. (12) (b) mean drop size using Eq. (13) (c) slip velocity using Eq. (14).

By considering the physical and reactive systems, the feasibility of the

OldshueRushton scale-up column for the selective extraction of cobalt with the mixture of D2 EHPA and TBP was evaluated by Torkaman et al. [46]. Also, they proposed a developed model based on the dimensionless groups that written as follows:

$$d_{32} = 2.97 \times 10^{-4} \left( \frac{N^4 d_R^4 \rho_c}{g \sigma} \right)^{-0.311} \left( \frac{\mu_c^4 g}{\Delta \rho \sigma^3} \right)^{-0.258} \left( 1 + \frac{V_c}{V_d} \right)^{-0.075} \quad (13)$$

The estimation of  $d_{32}$  is counselled by this model for extracting the selenium and tellurium in this column. This modified model anticipates mean drop size with an AARE of 9.49% for transporting the selenium and tellurium into the solvent phase that the experimental data comparison with the mentioned model is illustrated in Figure 7(b). Torkaman et al. investigated the slip velocity in the pilot plant Oldshue-Rushton column for the reactive system with consideration of the samarium and gadolinium elements [47]. Furthermore, they concluded that the slip velocities for chemical reaction conditions were more significant than the physical systems that the present experimental outcomes were justified this phenomenon, and the developed model was presented as follows:

$$\frac{V_{slip} \mu_c}{\sigma} = 0.02671 \left( \frac{N^2 d_R}{g} \right)^{-0.357} \left( \frac{\rho_d}{\rho_c} \right)^{-5.277} \left( 1 + \frac{V_c}{V_d} \right)^{-0.698} \left( \frac{\mu_c g^{0.25}}{\rho_c^{0.25} \sigma^{0.75}} \right)^{1.037} \quad (14)$$

Figure 7(c) displays the results of the slip velocity comparison between the present data and estimated values of the mentioned model. The value of

AARE for the predicted data applying correlation (14) and the slip velocity data was equal to 9.64%. Therefore, this empirical model is closely matched for predicting the slip velocity performance in the multistage column based on the solvent extraction system.

### **3.2.6. Modified model for drop size distribution**

In this extractor, two models of probability density functions containing the normal and log-normal functions were proposed by Asadollahzadeh et al. for the system lacking in the reaction conditions with the low, medium, and high interfacial tensions [44]. The proportion of the number of droplets with a specified distance across to the number of the overall droplets is defined as a function of the probability density. The mentioned functions were interpreted for studying the drop size distribution based on the experimental data of physical and chemical systems and presented as follows:

$$P_n = \frac{1}{1.86\pi a} \exp\left(-\frac{(d_i - \beta)^2}{2a^2}\right) \quad (15)$$

$$P_{Log} = \frac{1}{0.33\pi ad_i} \exp\left(-\frac{(\ln d_i - \beta)^2}{2a^2}\right) \quad (16)$$

It should be noted that  $d$ ,  $\alpha$  and  $\beta$  denote the drop diameter and constant parameters, respectively. Based on the data of this research and the data

taken from Asadolahzadeh et al. [44], at the first step, the values of di in terms of number density were utilised in the fitting of distribution functions for the data set with the aid of the LABFIT software.

Determination of the parameters  $\alpha$  and  $\beta$  for each set has been studied based on the operating parameters such as the rotor speed and the inlet phase velocities. Then constant parameters are correlated for mentioned distribution functions. After a trial series, correlations of the theoretical distribution functions were calculated by the multiple linear regressions, in which the modified  $\alpha$  and  $\beta$  for normal and log-normal distribution functions under both physical and reactive systems were obtained as follows:

$$\alpha = C_1 \left( \frac{N^4 d_R^4 \rho_c}{\sigma g} \right)^{0.163} \left( \frac{\mu_c^4 g}{\Delta \rho \sigma^3} \right)^{0.171} \quad (17)$$

$$\beta = C_2 \left( \frac{N^4 d_R^4 \rho_c}{\sigma g} \right)^{-0.314} \left( \frac{\mu_c^4 g}{\Delta \rho \sigma^3} \right)^{-0.101} \left( 1 + \frac{V_c}{V_d} \right)^{-0.262} \quad (18)$$

$$\alpha = C_3 \left( \frac{N^4 d_R^4 \rho_c}{\sigma g} \right)^{0.074} \left( \frac{\mu_c^4 g}{\Delta \rho \sigma^3} \right)^{0.031} \quad (19)$$

$$\beta = C_4 \left( \frac{N^4 d_R^4 \rho_c}{\sigma g} \right)^{-0.822} \left( \frac{\mu_c^4 g}{\Delta \rho \sigma^3} \right)^{-0.167} \left( 1 + \frac{V_c}{V_d} \right)^{-0.659} \quad (20)$$

Equations (17) and (18) are the constant parameters of the normal function as well as equations (19) and (20) are the constant parameters of the log-

normal function. It is clearly shown in the theoretical modelling that the distribution profiles are essentially influenced by the rotor speed and type of the system. Based on the type of used system, the AARE values of the constant parameters and the values of constant parameters are given in Table 2. The experimental histogram comparison with the mentioned distribution functions under the reactive extraction system is displayed in Figure 8. The modified log-normal function was selected for predicting the drop size distributions in this column due to a good agreement with the data of both systems.[25]

**Table 2.** Values of constant parameters and AARE values of equations (17), (18), (19) and (20).

System	Values of constants				AARE%			
	C <sub>1</sub>	C <sub>2</sub>	C <sub>3</sub>	C <sub>4</sub>	Eq. (17)	Eq. (18)	Eq. (19)	Eq. (20)
Physical system	8.276	0.454	6.201	0.051	10.73	9.95	3.02	5.22
Reactive system	7.041	0.741	3.989	0.072	9.13	8.27	2.79	4.18

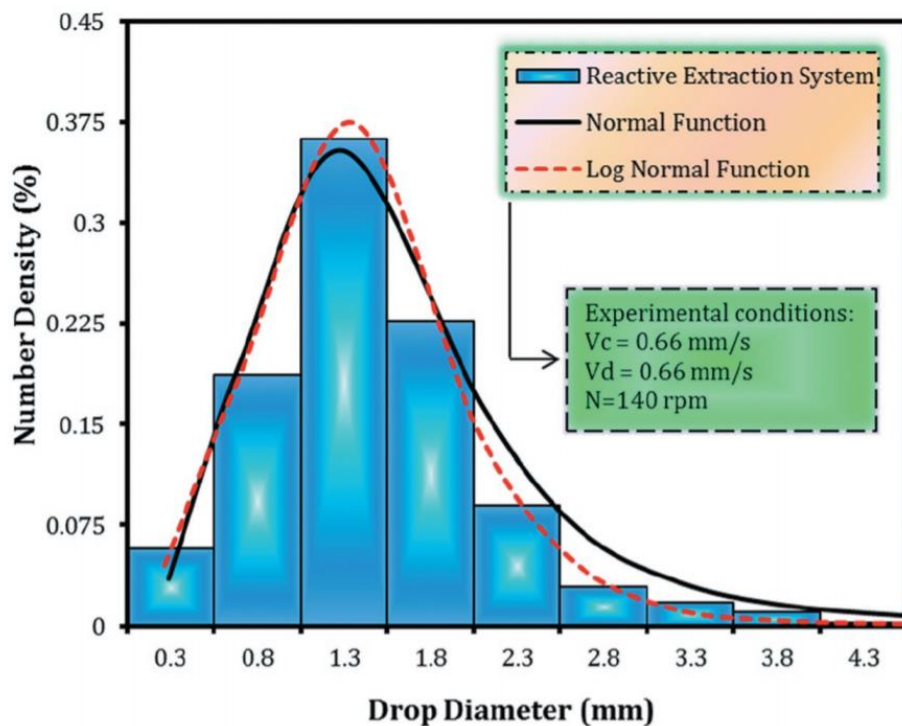


**Figure 8.** Comparison of theoretical distribution function and probability distribution functions under reactive extraction system.

---

[M]	concentration of metal ion
a	Interfacial area ( $\text{m}^{-1}$ )
AARE	Average absolute relative error (-)
D	Distribution coefficient
d	Drop diameter (m)
$d_{32}$	Sauter mean drop diameter (m)
$D_c$	Column diameter (m)
$d_e$	Equivalent diameter (m)
$d_R$	Rotor diameter (m)
E%	Extraction percentage (-)
g	acceleration due to gravity ( $\text{m}/\text{s}^2$ )
N	Rotor speed ( $\text{s}^{-1}$ )
SF	Separation factor (-)
V	Volume ( $\text{m}^3$ )
$V_{\text{slip}}$	slip velocity (m/s)
<b>Greek</b>	
$\mu$	Viscosity (pa.s)
$\alpha$	constant parameter of probability of density function
$\beta$	constant parameter of probability of density function
$\Delta\rho$	density difference between phases ( $\text{kg}/\text{m}^3$ )
$\rho$	Density ( $\text{kg}/\text{m}^3$ )
$\sigma$	Interfacial tension (N/m)
$\varphi$	Dispersed phase holdup (-)
<b>Subscripts</b>	
aq	Aqueous phase
org	Organic phase
c	Continuous phase
d	Dispersed phase

---

## **A study of drop size distribution and mean drop size in a perforated rotating disc contactor (PRDC)**

The present study has examined the influence of operating variables including the rotor speed, continuous and dispersed phase flow rates on Sauter mean drop size and drop size distribution behavior in a pilot scale perforated rotating disc contactor. In addition, empirical correlations have been proposed for the Sauter mean drop diameter and drop size distribution as a function of operating conditions and physical properties of the liquid systems.

## **2. Experimental**

2.1. PRDC pilot scale unit A pilot plant was constructed comprising a 113 mm internal diameter perforated rotating disc contactor having 43 stages, and accessory equipment including storage tanks, pumps and rotameters. The rotor shaft carries perforated disc with a diameter of 0.07 m and drilled with 30 holes of 0.015 cm diameter. A schematic of the PRDC pilot-scale unit used in this study is shown in Figure 1. The geometrical data of the investigated column are given in Table 1.

**Table 1 – The main dimensions of the PRDC column.**

Item	Symbol	Column dimensions (m)
Column internal diameter	$D_c$	0.113
Stator ring diameter	$D_s$	0.08
Disc diameter	$D$	0.07
Compartment height	$h_c$	0.03
Column active height	$Z$	1.43

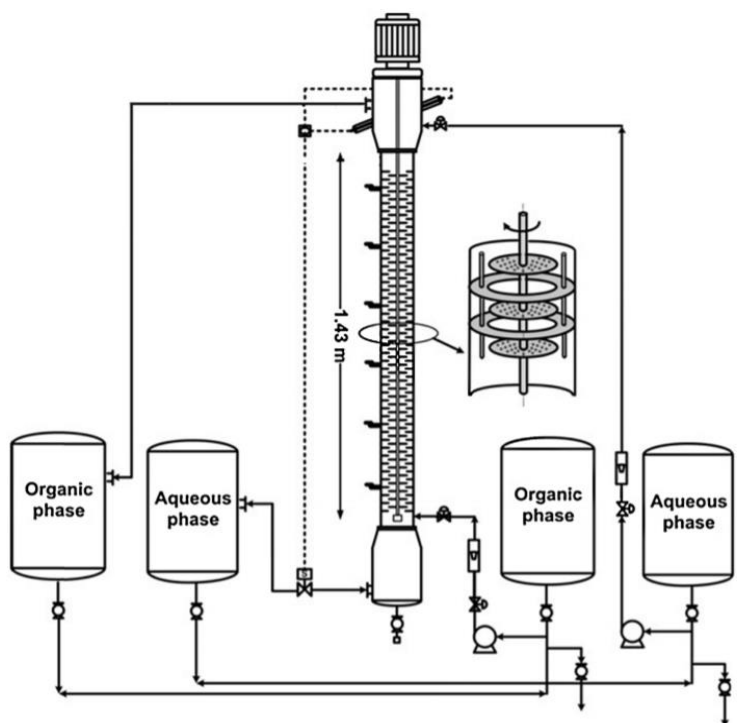


Fig. 1 – A schematic diagram of the perforated rotating disc contactor (PRDC).

**2.2. Liquid–liquid systems** All experiments were carried out in the absence of mass transfer at room temperature, using three liquid–liquid systems to cover a wide range of interfacial tension values according to the recommendations of the European Federation of Chemical Engineering (Misek et al., 1985). The systems were toluene–water (high interfacial tension), butyl acetate–water (medium interfacial tension) and butanol–water (low interfacial tension). Distilled water was used as continuous phase in all experiments. The physical properties of these systems are listed in Table 2.

**Table 2 – Physical properties of systems studied at 20 °C  
(Mišek et al., 1985).**

Physical property	Toluene–water	n-Butylacetate–water	n-Butanol–water
$\rho_c$ (kg/m <sup>3</sup> )	998.2	997.6	985.6
$\rho_d$ (kg/m <sup>3</sup> )	865.2	880.9	846
$\mu_C$ (mPa s)	0.963	1.0274	1.426
$\mu_d$ (mPa s)	0.584	0.734	3.364
$\sigma$ (mN/m)	36	14.1	1.75

2.3. Image analysis procedure In order to determine drop size, taking a digital photo of the column contents using a Nikon D3100 digital camera that was put away 7 cm from the extraction column wall. The photographs of the two-phase mixture were then taken at operating condition. It is found that the curved surface of the glass extraction column and significant differences between air and the glass refractive indices leads to a parallax deformation of the objects photographed in the extraction column. In order to omit this phenomenon, a container which filled with water was attached to the extraction column and the photographic approach was used to calculate the size of the discs or stators thickness served as the reference for the drop size measurements. To determine the size of the drops, the recorded photos were analyzed by Digimizer image analysis software. More than 300 drops were analyzed for each experimental condition at three points of the active column to guarantee the statistics significance of the determined Sauter mean drop diameter. According to

interphases tension energy definition, drop shape tends to change to the state which has been had a minimum amount of surface to volume. Moreover, In the PRDC extraction column, monotonous drops are created due to presence of perforated plates. The predominant of drops are spherical on the basis of empirical observations and also the diameter of measured drops was equal. For this reason, it was assumed that the drop is spherical. For elliptical drops both the vertical and horizontal axes were measured and following equation was used to calculate the mean drop size of drops.

$$d_e = (d_1^2 d_2)^{1/3} \quad (1)$$

The major and minor axes,  $d_1$  and  $d_2$ , are measured and the equivalent diameter,  $d_e$ , determined. The drops photos of three various systems are shown in Fig. 2. The hold-up was defined as the ratio of the dispersed phase to the total volume of the extraction region. At the end of each run, displacement method is used to determine hold-up of dispersed phase in the extraction column (Rincon-Rubio et al., 1993). The values of hold-up in the column are less than 11%.

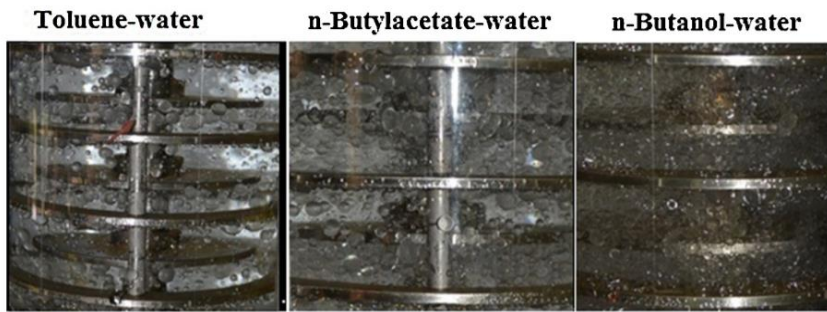


Fig. 2 – The photos of drops in three different systems. ( $V_c = V_d = 6.67 \times 10^{-4}$  m/s,  $N = 240$  (rpm)).

In this study, three operational parameters were examined including rotor speed and volumetric flow rates of continuous and dispersed phases. For each liquid-liquid system the operating variables were systematically varied to determine their influence of the mean drop size and the drop size distribution. The investigated operating conditions are given in Table 3.

**Table 3 – Investigated ranges of operating variables.**

Liquid system	Rotor speed (rpm)	Continuous flow rate (l/h)	Dispersed flow rate (l/h)
Toluene–water	180–240–300–360–420	18–24–30–36	18–24–30–36
n-Butylacetate–water	120–180–240–300–360	18–24–30–36	18–24–30–36
n-Butanol–water	60–120–180–240–300	18–24–30–36	18–24–30–36

3. Results and discussion The influence of various parameters on the drop size distribution and mean drop size was investigated. The operating parameters including rotor speed, dispersed phase flow rate and continuous phase flow rate were selected for investigation of drop size distribution in the extraction column.

3.1. Drop size distribution To measure the number density or drop size distribution at each run,

the size of drops was divided into seven ranges.  $(d_i \pm \frac{\Delta d_i}{2})$

The number of drops was then determined in the each part and using following equation:

$$p_n = \frac{\text{number of drops of class } i}{\text{total number of drops}} \quad (2)$$

An important parameter that influence the drop size distribution is the rotor speed. As it can be seen in Table 3 for each system, 5 different rotor speeds were tested that the drop size distributions determined for two different rotor speeds are depicted in Fig.3. The size distribution in each system clearly shifts towards the left ahead with an increase in the rotor speed, because an increase in the rotor speed cause drop breakup based on three different mechanisms that play a very important role. The first one is collision of drops with eddy, by increasing rotor speed, higher turbulency is induced to the flow which in turn results in reduction of eddy size also by increasing rotor speed, drag force increases and pressure loss increases as well. The latter increases energy dissipation and causes turbulent velocity fluctuation. Therefore, kinetic energy exerted on the surface of drops increases, consequently, results in breakup. Secondly, increasing

rotor speed results in enhancement of drop velocity, and the drops collide to the internal parts with higher intensity. It means that higher force from internal parts is exerted on the surface of drops and results in drop break-up and finally, in PRDC towers, due to existence holes on the trays, shear force is exerted on the drops during passage of drop through the holes, and results in drop break-up (Soltanali et al., 2009; Drumm et al., 2009; Samani et al., 2014). The difference between distribution curves of different liquid systems decreases when the rotor speed increase due to a distinguished effect of rotor against the interfacial tension. Moreover the drop size distributions are also found to be narrower and more evenly distributed about the mean value for systems of lower interfacial tension at a given rate of agitation.

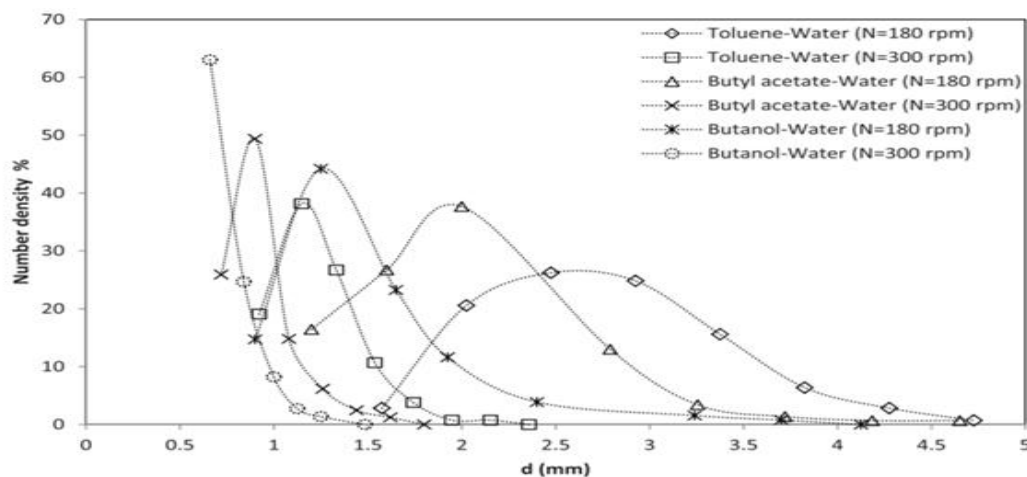
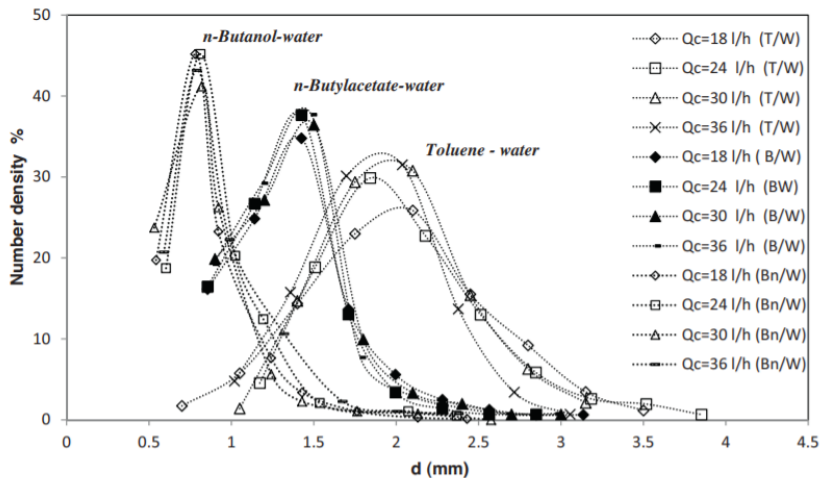


Fig. 3 – Effect of rotor speed on the drop size distribution ( $V_c = V_d = 6.67 \times 10^{-4}$  (m/s)).

The effect of continuous phase flow rate on the drop size distributions is shown in Fig.4. As it is clear in this figure, there are no sensible changes in the trend of the curves and all flow rates had almost the same distribution points.



**Fig. 4 – Effect of continuous phase flow rate on the drop size distribution at the same rotor speed for the systems of toluene–water (T), butyl acetate–water (B) and butanol–water ( $B_n$ ) ( $N = 240$  rpm,  $V_d = 6.67 \times 10^{-4}$  (m/s)).**

Fig. 5 shows the effect of flow rate of the dispersed phase on the drop size distribution. It is seen from Fig.5 that the drop size distribution has no significant change with the dispersed phase flow rate for liquid system with a low interfacial tension contrary to the toluene–water system, the drop size distribution curve becomes wider and clearly shifts towards the right because increase of the dispersed phase flow rate increases the coalescence frequency. Therefore, the distribution function is dependent of to the phase flow rates. The results obtained in this work were similar to those described by Moreira et al. (2007) in a RDC column.

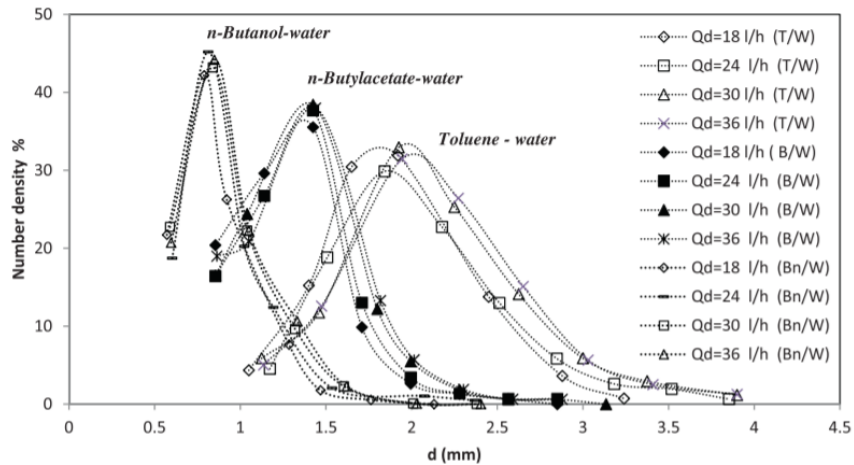


**Fig. 5 – Effect of dispersed phase flow rate on the drop size distribution at the same rotor speed for the systems of toluene–water (T), butyl acetate–water (B) and butanol–water ( $B_n$ ) ( $N = 240$  rpm,  $V_c = 6.67 \times 10^{-4}$  (m/s)).**

### 3.2. Predictive correlation for drop size distribution

Apart from the qualitative analysis of the effects of operating conditions on the drop size distributions, an attempt was made to enable some quantitative representation of these effects. In order to do so, two probability distribution functions, namely the normal ( $p_n$ ) and the log-normal ( $p_{lg}$ ) functions, were tested for reproduction of the experimental drop size distributions. Table 4 summarizes these functions presented in the literature for liquid–liquid extraction systems. In this study these functions are given by the following equations:

$$P_n = \frac{1}{0.27\pi\alpha} \exp\left(\frac{(d_i - \beta)^2}{2\alpha^2}\right) \quad (3)$$

$$P_{lg} = \frac{1}{0.27\pi\alpha d_i} \exp\left(\frac{(\ln(d_i) - \beta)^2}{2\alpha^2}\right) \quad (4)$$

In which  $d_i$  is the drop diameter and  $\alpha$  and  $\beta$  are parameters to be fitted.

**Table 4 – Probability distribution functions presented in the literature for liquid-liquid extraction systems.**

Name	Function	Reference
Normal	$F(d) = \frac{1}{\sqrt{2\pi}\sigma_d} \exp \left[ -\frac{\left(\frac{d-d_i}{\sigma_d}\right)^2}{2} \right]$	Chen et al. (2013)
Log-normal	$F(d) = \frac{1}{d\sigma_{\ln(d)}\sqrt{2\pi}} \exp \left[ -\frac{1}{2} \left( \frac{\left(\ln d - \ln d_i\right)^2}{\sigma_{\ln(d)}^2} \right) \right]$	Chen et al. (2013)
Normal	$f(0, 0, \tau, L) = \frac{U}{\sqrt{4\pi E_D \tau}} \exp \left[ \left( \frac{(L-U)^2}{4E_D^2} \right) \right]$	Zhang et al. (2009)
Log-normal	$P_n(d) = \frac{1}{\sqrt{2\pi}\alpha} \exp \left[ \left( \frac{(\ln d - \beta)^2}{\sqrt{2}\alpha} \right) \right]$	Oliveira et al. (2008)
Normal	$P_n(d) = \frac{1}{\sqrt{2\pi}\alpha} \exp \left[ \left( \frac{(d - \beta)^2}{\sqrt{2}\alpha} \right) \right]$	Moreira et al. (2005)
Log-normal	$P_n(d) = \frac{1}{\sqrt{2\pi}\alpha} \exp \left[ \left( \frac{(\ln d - \beta)^2}{\sqrt{2}\alpha} \right) \right]$	Moreira et al. (2005)
Log-normal	$P_n(d) = \frac{\alpha}{d\sqrt{\pi}} \exp \left[ -\left( \alpha \ln \frac{(d)^2}{d_q} \right) \right]$	Rincon-Rubio et al. (1994)

At first the values of  $d_i$  as a function of number density were used in the fitting of normal and log-normal distributions for the data set with the aid of the software LABFIT, determining the parameters  $\alpha$  and  $\beta$  for each set of studied operating conditions and then constant parameters are correlated with Eqs. (6 and 7) and (8 and 9) for normal and log-normal distributions respectively.

$$\alpha = 6.477 \left( \frac{N^4 D_R^4 \rho_c}{\sigma g} \right)^{-0.093} \times \left( \frac{\mu_c^4 g}{\Delta \rho \sigma^3} \right)^{-0.018} \quad (5)$$

$$\beta = 6.493 \left( \frac{N^4 D_R^4 \rho_c}{\sigma g} \right)^{-0.11} \times \left( \frac{\mu_c^4 g}{\Delta \rho \sigma^3} \right)^{-0.003} \times \left( 1 + \frac{V_c}{V_d} \right)^{-0.151} \quad (6)$$

$$\alpha = 0.072 \left( \frac{N^4 D_R^4 \rho_c}{\sigma g} \right)^{0.227} \times \left( \frac{\mu_c^4 g}{\Delta \rho \sigma^3} \right)^{-0.051} \quad (7)$$

$$\beta = 3.084 \left( \frac{N^4 D_R^4 \rho_c}{\sigma g} \right)^{-0.174} \times \left( \frac{\mu_c^4 g}{\Delta \rho \sigma^3} \right)^{-0.013} \times \left( 1 + \frac{V_c}{V_d} \right)^{0.162} \quad (8)$$

As it can be seen the four fitted parameters are given in dimensionless numbers that calculated by Buckingham's pi-theorem (Hanche, 2007) where N is the rotor speed,  $\mu_c$  and  $\rho_c$  are viscosity and density of the continuous phase  $\sigma$  and  $\Delta\rho$  are the interfacial tension and density difference between two phases,  $V_c$  and  $V_d$  are volumetric flow rates of the continuous and dispersed phases, and  $g$  is the acceleration due to gravity (9.8 m/s<sup>2</sup>). In this fitting, Average Absolute Relative Error (AARE) was used as an objective function to calculate the fitted parameters.

$$AARE = \frac{1}{n} \sum_{i=1}^n \frac{|p_i(d)(exp) - p_i(d)(cal.)|}{p_i(d)(exp)} \quad (9)$$

where n is the number of data points, and  $P_i(d)(exp)$  and  $P_i(d)(cal.)$  represent the experimental and theoretical number densities of the drops,

respectively. Both functions for each distribution represented the data well within the investigated range of operating parameters. In Table 5 AARE numbers were listed.

**Table 5 – Comparison between ARRE numbers.**

Function	Fitted parameter	AARE (%)
Normal ( $p_n$ )	$\alpha$	7.8
	$\beta$	8.2
Log-normal ( $p_{lg}$ )	$\alpha$	9.79
	$\beta$	9.74

Comparative data shown in Table 5 indicate that both distribution functions suitably reproduce parameters  $\alpha$  and  $\beta$  with deviations lower than 10% for PRDC extraction column. It is important to emphasize that, for both fitted functions the acceleration of gravity, density and viscosity of the continuous phase are constant in all of the equations presented here so the main variations of these correlations are then to be related to the rotor speed and the interfacial tension. These indicate that a combination of the two variables in Equations play the key role in determining the drop size distributions.

### 3.3. Predictive correlation for mean drop size

It is well known that the mean drop size is an important factor that effect on the study and design of the liquid-liquid extraction column (Ayham and Ismail, 2007) The Sauter mean drop diameter,  $d_{32}$ , was calculated at the

exerted experimental conditions as follows:

$$d_{32} = \frac{\sum n_i d_i^3}{\sum n_i d_i^2} \quad (10)$$

Where  $n_i$  is the number of droplets of mean diameter  $d_i$  with in a narrow size range i. The effect of disc speed on the mean drop sizes is illustrated in Fig. 6. For all runs carried out the mean drop size diameters generated in the PRDC column were strongly affected by the rotor speed so that increasing the disc speed reduced the drop diameter. The explanation for this effect is related to the increase in the frequency of drop collisions against the internal parts of the column in more turbulent environments.

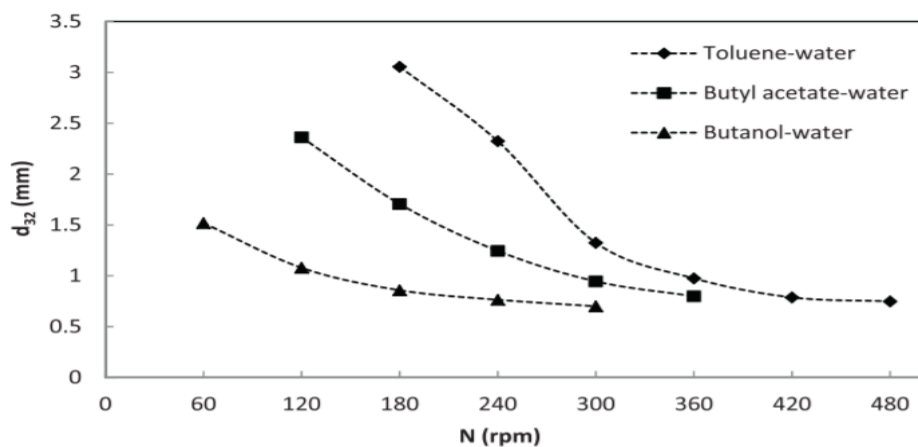


**Fig. 6 – The effect of rotor speed on the Sauter mean diameter ( $V_c = V_d = 6.67 \times 10^{-4}$  (m/s)).**

The influence of the flow rate on the mean drop diameter has been investigated in order to resolve the overlap of the variables, and to help in the interpretation of the hydrodynamic behavior of flow rate in a PRDC column. The effects of increasing the dispersed phase velocity on the mean drop diameter were tested

and are illustrated in Fig. 7

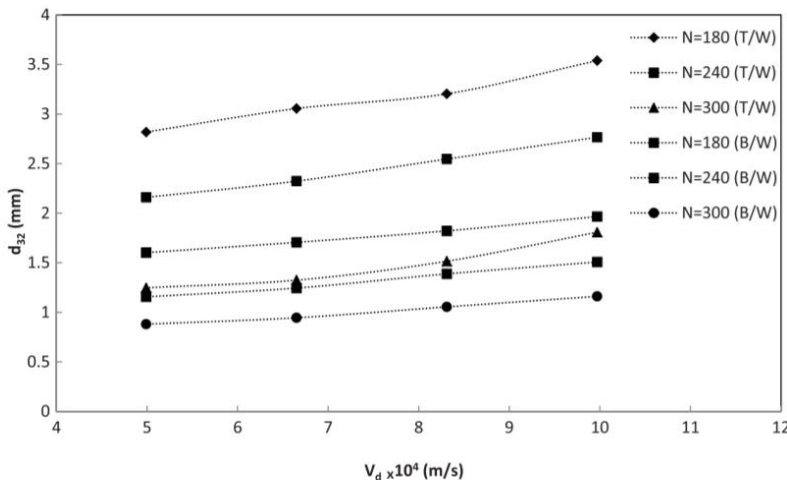


Fig. 7 – The effect of dispersed phase velocity on the Sauter mean diameter at  $V_c = 6.67 \times 10^{-4}$  (m/s).

The mean drop diameter increased with increasing flow rate and varied slightly at low interfacial tension. For this reason, dispersed flow rates increased at constant volume leads to increase the number of drops and consequently coalescence frequency increases by the collision of drops (E. Moreira et al., 2007, M.G. Samani et al., 2014). Moreover, an increase hold-up causes the enhancement of the coalescence probability based on the film drainage model and energy model (Y. Liao and D. Lucas, 2010). On this basis, the mean drop size increases with an increase in coalescence of the drops.

Typical variations in the mean drop size with continuous phase velocity are given in Fig.8. As seen in this figure, in the case of continuous phase velocity, no significant change in mean drop size is verified for the operating range studied.

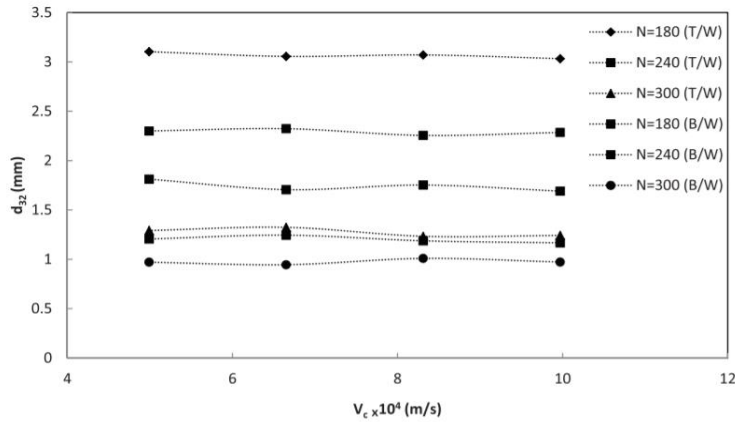
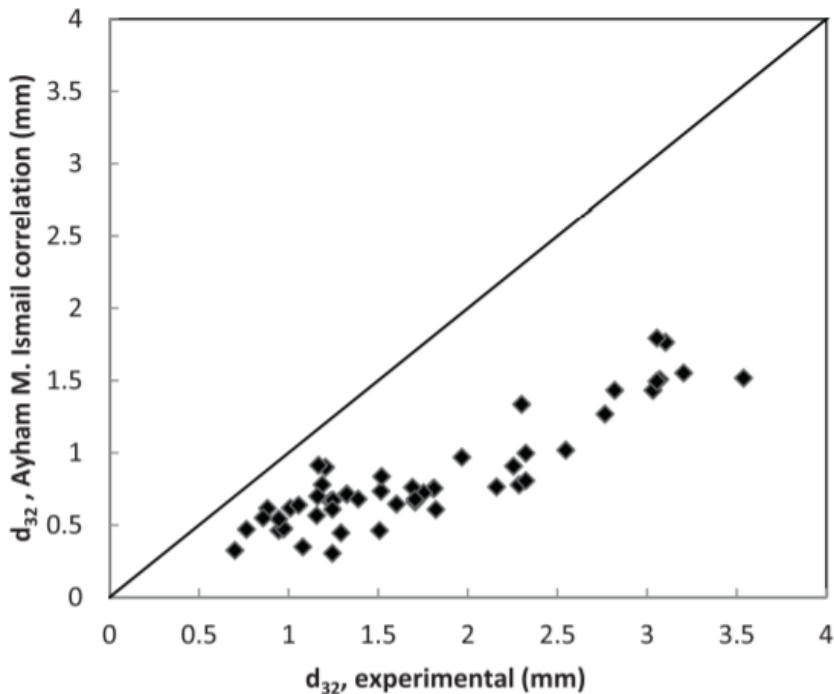


Fig. 8 – The effect of continuous phase velocity on the Sauter mean diameter at  $V_d = 6.67 \times 10^{-4}$  (m/s).

A number of correlations have been proposed to predict the mean drop size in liquid-liquid extraction columns using different columns and systems. Ayham and Ismail (2007) correlated the mean drop diameter,  $d_{32}$ , could be useful to collect drop size data for the RDC columns.

$$d_{32} = 0.705 \left( \frac{\sigma}{g\Delta\rho} \right)^{0.5} \frac{D_h^{0.8}}{N^{0.185}} \frac{(Q_c/Q_d)^{0.15}}{(Q_c + Q_d)^{0.1}} \quad (11)$$

It was observed that if the model (Eq. 12) was plotted with the experimental data, the predicted values of  $d_{32}$  were more than 51.03% out.



**Fig. 9 – Comparison between experimental data and Ayham M. Ismail correlation.**

Kumar and Hartland (1986) proposed two correlations for RDC column, one at low disc Reynolds number ( $Re_{DR} \leq 50,000$ ) another at higher ( $Re_{DR} \geq 50000$ )

$$\frac{d_{32}}{D_R} = 0.18(Re_R)^{-1.12} \left( \frac{\mu_C}{(\sigma \rho_C D_R)^{0.5}} \right)^{-1.38} \left( \frac{\Delta \rho}{\rho_C} \right)^{-0.24} \times \left( \frac{D_R \rho_C g}{\sigma} \right)^{-0.05} \left( \frac{h_c}{D_R} \right)^{0.42} \quad (12)$$

$$\frac{d_{32}}{D_R} = 7.01 \times 10^{-3} (Re_R)^{-0.55} \exp [-0.23 (Fr_R)] \times \left( \frac{\mu_C}{(\sigma \rho_C D_R)^{0.5}} \right)^{-1.3} \left( \frac{\rho_d}{\rho_C} \right)^{-0.75} \left( \frac{D_R^2 \rho_C g}{\sigma} \right)^{-0.3} \left( \frac{h_c}{D_R} \right)^{0.2} \quad (13)$$

A comparison between predicted and experimental values using Eq.(13) is shown in Fig.10. The value of AARE in the predicted value of  $d_{32}$  by

using this correlation is 45.81%

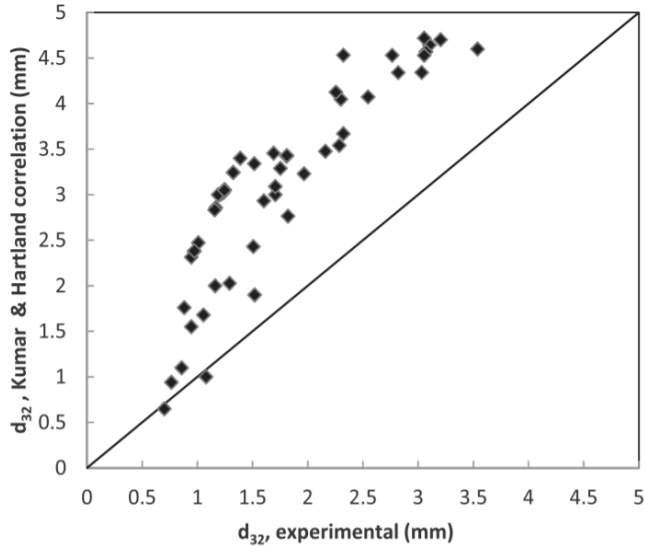


Fig. 10 – Comparison between experimental data and Kumar & Hartland correlation.

As it known most existing  $d_{32}$  correlations were derived from dependent variables and physical properties. One of the main objectives of this study is proposed a correlation to represent the Sauter mean diameter of drops in a PRDC column. The correlation, presented below, was mainly based upon the operating variables, i.e., rotor speed, dispersed and continuous flow rates, and the system physical properties:

$$d_{32} = 10 \left( \frac{N^4 D_R^4 \rho_c}{\sigma g} \right)^{-0.296} \left( \frac{\mu_c^4 g}{\Delta \rho \sigma^3} \right)^{-0.087} \left( 1 + \frac{V_c}{V_d} \right)^{-0.402} \quad (14)$$

The correlation reliability and accuracy increased with integrating the relationships between interfacial tension, ( $\sigma$ ), and physical properties, mainly density difference, ( $\Delta\rho$ ). This equation excluded the column geometry term so could be used for design purposes. As portrayed in

Fig.11, with the aid of Equation (15), most of the experimental data are predicted with an AARE equal 6.8%.[26]

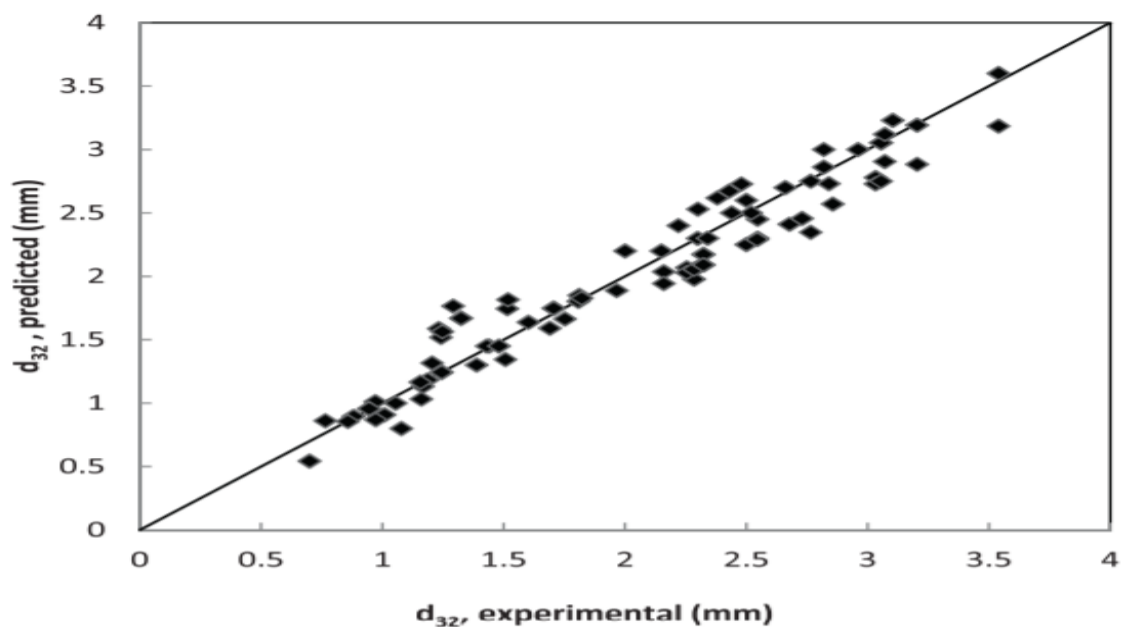


**Fig. 11 – Comparision between experimental data and correlation predictions.**

## Nomenclature

$d_{32}$	Sauter mean drop diameter (m)
$d_i$	drop diameter (mm)
$D$	disc diameter (m)
$G$	acceleration due to gravity ( $=9.81\text{ m/s}^2$ )
$n_i$	number of droplets of mean diameter $d_i(-)$
$P$	probability of number density (-)
$G$	acceleration due to gravity ( $\text{m/s}^2$ )
$h_c$	compartment height (m)
$N$	rotor speed (1/s)
$Q$	flow rate of the continuous or dispersed phase ( $\text{m}^3/\text{s}$ )
$Re$	Reynolds number (-)
AARE	average absolute relative error (-)
$V$	superficial velocity (m/s)

### Greek letters

$A$	constant parameter of probability of density function
$B$	constant parameter of probability of density function
$\rho$	density ( $\text{kg/m}^3$ )
$\Delta\rho$	density difference between two phases ( $\text{kg/m}^3$ )
$\mu$	viscosity (Pa s)
$\sigma$	interfacial tension between two phases (N/m)

### Subscripts

$c$	continuous phase
$d$	dispersed phase
$n$	normal probability density function
ln	log-normal probability density function

# **Revealing mass transfer and hydrodynamic efects in a PRDC column by using the integration of extraction and separation for molybdenum and tungsten ions from aqueous solution**

## **Introduction**

Molybdenum and tungsten are the hard-headed metallic component utilized mainly as the alloying operator in cast press, steel, and alloys to improve hardenability, quality, durability, as well as within the oil industry. In the extraction of molybdenum and tungsten from primary and secondary resources, hydrometallurgy is preferred over pyrometallurgy (Nguyen and Lee 2016). The molybdenum separation from tungsten has continuously been an issue within the hydrometallurgy process. Their adjoining positions in the periodic table result in the fuid to some degree comparable chemical behavior, but contrasts do exist (Elwell and Wood 2013).

the present research focuses on the study of extracting the molybdenum and tungsten from sulfate medium by coupling of acid and solvating extractants as well as the stripping of loaded organic phase by ammonium hydroxide in a perforated rotating disk contactor. Furthermore, the holdup values, mean drop size, drop size distribution, and continuous phase mass transfer coefcients were interpreted with changing the variables such as agitation rate and inlet phase velocities for two various reactive systems. The comparison between the values of available models and experimental

data in the mentioned column for the physical systems were investigated that caused to present the modified models for anticipating the hydrodynamic parameters as well as the new model for predicting the mass transfer coefficients under reactive systems.

## **Experimental**

Materials In the present work, the commercial grade of D2EHPA and TBP was utilized without any further purification from Sigma-Aldrich and Merck, respectively. Kerosene was supplied from the Tehran refinery as a diluent for the organic phase. Based on the leach solution, the concentration of molybdenum and tungsten in the aqueous solution was adjusted in 1000 ppm and 100 ppm, respectively (Zhao et al. 2010). Commercial salts ( $\text{Na}_2\text{MoO}_4 \cdot 2\text{H}_2\text{O}$  and  $\text{Na}_2\text{WO}_4 \cdot 2\text{H}_2\text{O}$ ) were purchased from Sigma-Aldrich. Furthermore,  $\text{NH}_4\text{OH}$  supplied from Merck was used as a stripping reagent.

## **Apparatus**

ICP-AES instrument and digital pH meter were used for measuring the concentration of the metals and hydrogen ions of the initial aqueous phase in the aqueous solution, respectively. All of the solvent extraction processes were performed at room temperature and atmospheric pressure. The physical properties of the aqueous and solvent phases are given in Table 2. Furthermore, Wilke and Chang (1955) equation was utilized for

calculating the molybdenum and tungsten difusivities in the aqueous and solvent phases. In the liquid–liquid extraction by chemical reaction, a degree of uncertainty along the column affected the measurement of physical properties, especially interfacial tension. Therefore, the physical properties of the aqueous and solvent phases have been calculated by considering the average values at the inlet and outlet of the mass transfer device.

**Table 2** Physical properties of the solvent extraction systems, at room temperature and atmospheric pressure

Properties		$\rho$ (kg/m <sup>3</sup> )	$\mu$ ( $\times 10^3$ kg/m s)	$\sigma$ ( $\times 10^3$ N/m)
Extraction stage	Continuous phase	1003	0.958	15.3
	Dispersed phase	793	1.34	
Stripping stage	Continuous phase	994	0.956	16.4
	Dispersed phase	801	1.35	

## Determination of mean drop size

A Nikon D5000 digital camera was used to take the digital photo from the active section of the column. The taken photographs were obtained from three sides of the active section, and they were analyzed by ImageJ software for calculating the size of droplets. Almost 500 droplets were analyzed in any picture to investigate the factual importance of the determined  $d_{32}$

$$d_{32} = \frac{\sum_{i=1}^n n_i d_i^3}{\sum_{i=1}^n n_i d_i^2} \quad (22)$$

where  $n_i$  is the number of mean diameter size. The tension energy leads to a

change of drop shape based on the least amount of surface to the volume, which the overwhelming of solvent droplets is spherical. In this column, the structure of punctured plates causes the uniform droplets (Soltanali et al. 2009). In a few cases, non-spherical droplets were observed in which the vertical and horizontal axes were calculated by the following equation:

$$d_e = \sqrt[3]{(d_1^2 d_2)} \quad (23)$$

In the above equation, d1 and d2 are assumed the major and minor axes, respectively. Moreover, the interfacial surface area per unit volume was determined as follows (Seader et al. 1998):

$$a = \frac{6\varphi}{d_{32}} \quad (24)$$

$\emptyset$ : holdup

The AARE was utilized to compare the experimental data with the anticipated results. The objective function was obtained according to the following equation:

$$AARE = \frac{1}{NDP} \sum_{i=1}^{NDP} \frac{|Experimental Value - Predicted Value|}{Experimental Value} \quad (25)$$

Impact of operating variables on the mean drop size Drop size owns an essential

influence on the maximum amount of throughput. Moreover, d32 and holdup values were utilized for determining the interfacial area (Kadam et al. 2009). The experimental results for the mean drop sizes of the reactive systems in both directions are shown in Fig. 6a. The comment for this phenomenon is related to an increase in the energy supplied by agitation at higher speeds. It leads to an increment in the collision and breakage of droplets. Moreover, the average drop size in the  $d \rightarrow c$  transfer is higher than in the  $c \rightarrow d$  transfer due to the difference in the interfacial tension and mass transfer direction. The variation of d32 with inlet solvent phase velocity at different pulsation intensities is demonstrated in Fig. 6b. An enhancement in the inlet solvent phase velocity leads to a higher coalescence frequency along the column. Consequently, the larger droplets formed in higher inlet solvent phase velocity. The impact of inlet aqueous phase velocity on the mean drop size at the different agitation speeds based on the reaction between ions such as molybdenum (VI) and tungsten (VI) in the aqueous phase and the mixture of D2EHPA and TBP in the solvent phase is shown in Fig. 6c. In the case of inlet aqueous phase velocity, no fundamental impact was confirmed for d32 in the operational range considered.

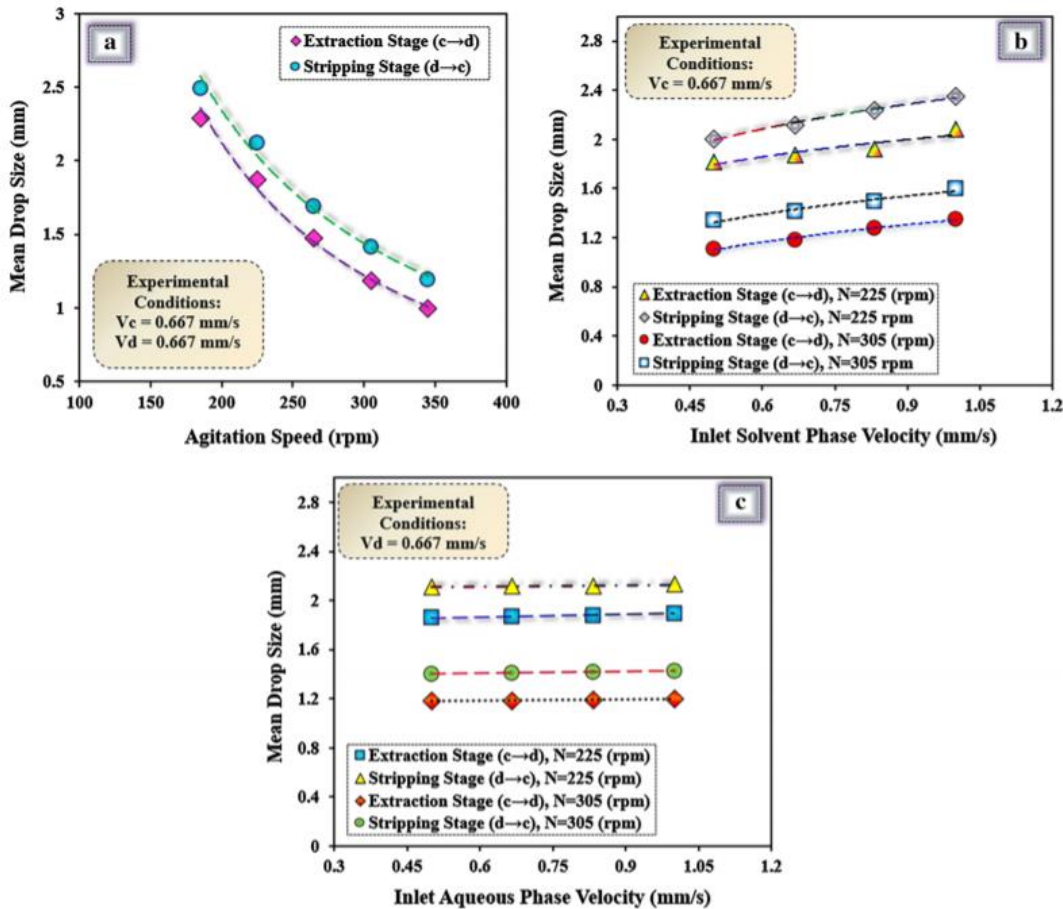


**Fig. 6** Impact of agitation speed and inlet phase velocities on mean drop size

Impact of operating variables on the drop size distribution The droplets frequently propagate at the vortexes in an agitator device. The drop size distribution due to the breakage into several smaller droplets is a vital parameter in the mass transfer devices. The experiment of reactive systems focuses on the study of changing the operational parameters containing the agitation speed as well as inlet phase velocities on the drop size distribution in the PRDC column. The experimental results reported by Hemmati et al. (2015b) in the three different physical systems were compared with the experimental data of the reactive extraction systems for investigating the interfacial tension impact on the drop size distribution.

The drop size distribution curve for five different systems with two agitation speeds is indicated in Fig. 7a.

In the constant inlet phase velocities, the drop size distribution moved to the left side with enhancing the agitation speed evidencing that droplet breakup and higher turbulence are gotten in the intensification of agitation rates. An increase in the energy losses and turbulent speed oscillation leads to the increment of the dynamic energy applied on the surface of droplets and consequently results in the droplets decomposition (Asadollahzadeh et al. 2018). Also, the shear force was applied on the drops amid the droplet transit through the available gaps on the plates of the mentioned column. The distribution data of the used systems have become narrower in the higher agitation rates as well as the distinction between the distribution curves of the physical and reactive systems reduces. The impact of inlet solvent phase velocity on the drop size distribution for physical and chemical systems is shown in Fig. 7b

The distribution curves as a function of the inlet solvent phase velocity have a little change for systems with the medium and low interfacial tensions. However, the differences of the curves in the stripping stage and the toluene/water have been observed, which moved to the right side with enhancing the inlet solvent phase velocity due to the coalescence frequency. By considering the physical and reactive systems in this

column, the drop size distribution curves in terms of inlet aqueous phase velocity are shown in Fig. 7c. No considerable alterations in the propensity of the curves were apparent, so the inlet aqueous phase velocities had nearly the same dissemination points.

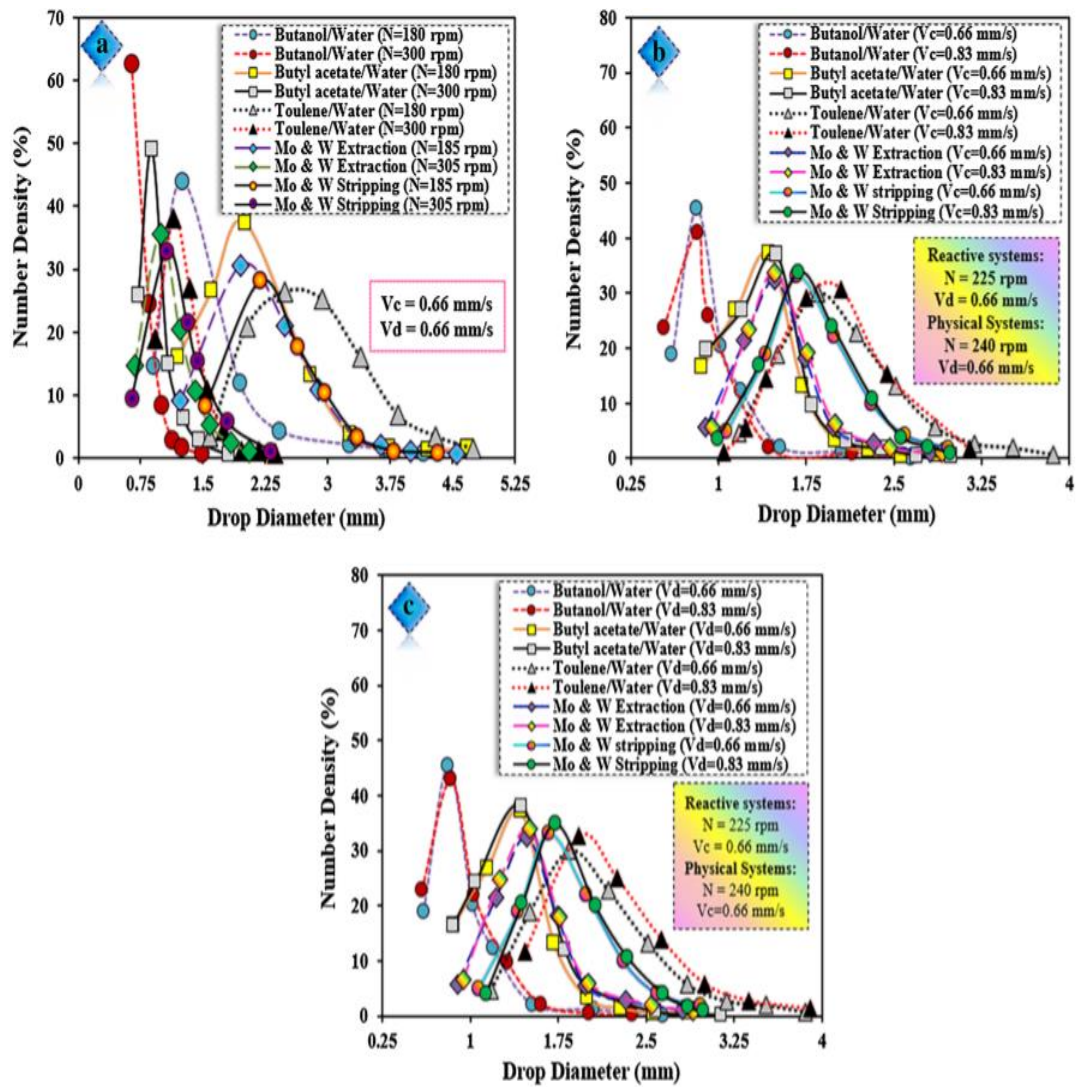


**Fig. 7** Impact of agitation speed and inlet phase velocities on drop size distribution

## **Modified models for hydrodynamic parameters**

Precise predicting the hydrodynamic parameters of reactive systems in the PRDC column is exceptionally troublesome due to the lack of experimental data in the available literature as well as presented models. Hemmati et al. (2015a) fitted the experimental data for three different physical systems in the PRDC column, the agitation speeds of 60 to 420 rpm, as well as the variations of flow rates, were 18–36 L/h. The following model is presented for predicting the holdup values in the mentioned column:

$$\varphi(-) = 0.089 \left( \frac{N^2 D_R}{g} \right)^{0.254} \left( \frac{\mu_d}{\mu_E} \right)^{0.272} \left( \frac{D_R}{h_c} \right)^{0.256} \left( 1 + \frac{V_c}{V_d} \right)^{-1.04} \quad 0.75 < \varphi < 0.12 \quad (32)$$

The AARE values between the experimental data of solvent extraction systems and the presented model were 21.14%. The interpretation of this error is relevant to the performance of the proposed model for physical systems. Still, the present data have been taken based on the chemical reaction between molybdenum and tungsten with the mixture of D2EHPA and TBP. Therefore, the following modified model for decreasing the errors of the presented equation has been derived based on the physical and reactive systems:

$$\varphi(-) = C_1 \left( \frac{N^4 D_R^4 \rho_c}{g\sigma} \right)^{0.074} \left( 1 + \frac{V_c}{V_d} \right)^{0.079} \left( \frac{\mu_d}{\mu_c} \right)^{-0.218} \left( \frac{\rho_d V_d^2 D_c}{\sigma} \right)^{0.137} \quad 0.06 < \varphi < 0.12 \quad (33)$$

Hemmati et al. (2015b) suggested the following model for calculating the mean drop size for high/medium/low interfacial tension systems in this extractor:

$$d_{32} = 10 \left( \frac{N^4 D_R^4 \rho_c}{g\sigma} \right)^{-0.296} \left( \frac{\mu_c^4 g}{\Delta \rho \sigma^3} \right)^{-0.087} \left( 1 + \frac{V_c}{V_d} \right)^{-0.402} \quad 0.7 < d_{32} < 3.5 \quad (34)$$

This model estimates the experimental data with an AARE of 20.08%.

Consequently, the presented model was unsuccessful to properly predict the experimental data due to the  $d_{32}$  variations in the interfacial properties of D2EHPA and TBP. When the ions such as molybdenum (VI) and tungsten (VI) with a mixture of extractants participated in the surface reaction, a reduction in the concentration of D2EHPA, as well as TBP at the interface, leads to enhancing the drop diameter. Therefore, a modified model has derived for anticipating the  $d_{32}$  based on the physical systems (toluene/water, butyl acetate/water, and butanol/water) as well as the reactive systems (extraction and stripping stages) that defined as follows:

$$\frac{d_{32}}{\sqrt{\frac{\sigma}{\Delta \rho g}}} = C_2 \times 10^{-5} \left( \frac{N^2 D_R}{g} \right)^{-0.58} \left( 1 + \frac{V_c}{V_d} \right)^{0.005} \left( \frac{\mu_d}{\mu_c} \right)^{0.38} \left( \frac{\mu_c g^{0.25}}{\rho_c^{0.25} \sigma^{0.75}} \right) \left( \frac{\rho_d V_d^2 D_c}{\sigma} \right)^{0.165} \quad 0.7 < d_{32} < 3.5 \quad (35)$$

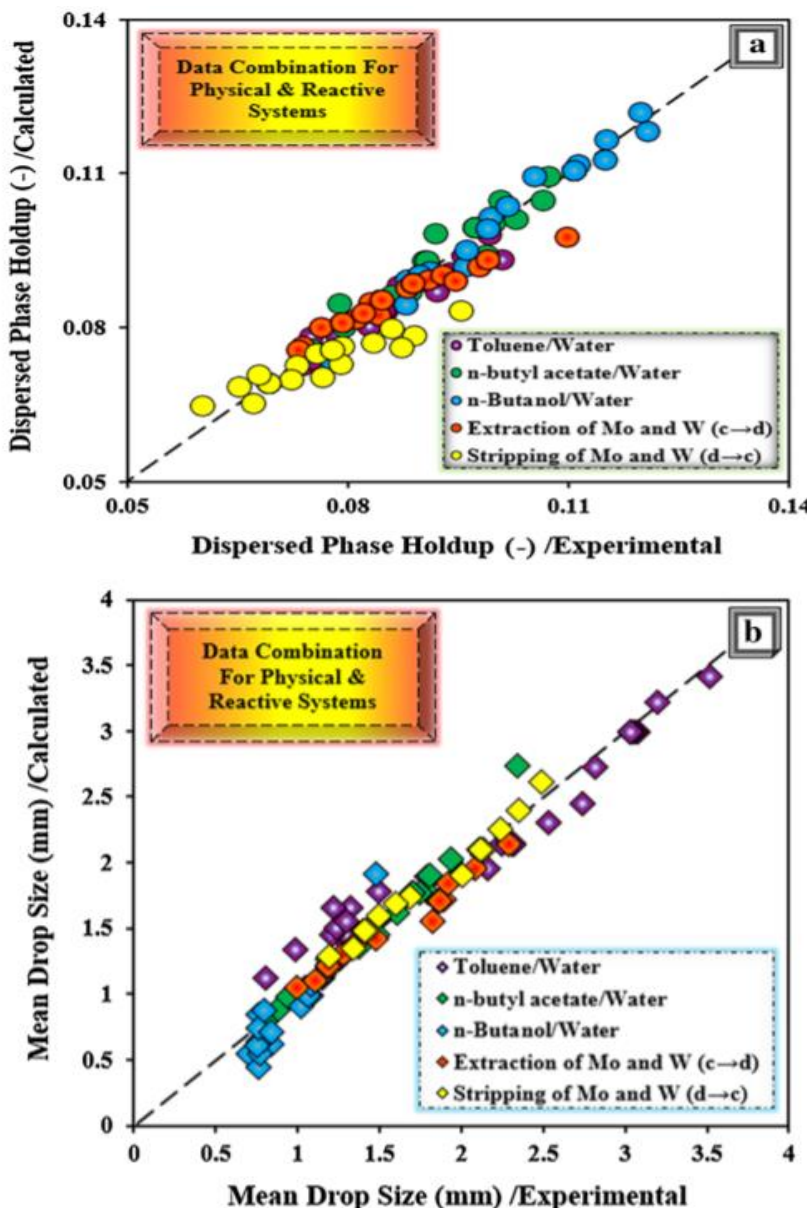
The impact of reaction conditions within this column is indicated by the

constant parameters of C1 and C2 in the modified models. The error of models and the values of constant parameters for physical and reactive systems are given in Table 4.

**Table 4** Values of constant parameters and AARE values of Eq. (33) and Eq. (35)

Reaction conditions	Values of constant		AARE%	
	C <sub>1</sub>	C <sub>2</sub>	Eq. (33)	Eq. (35)
Physical system	0.136	1.16	2.01	9.23
Reactive system	(c → d)	0.144	1.05	2.82
	(d → c)	0.125	1.23	5.22
			5.22	3.44

Figure 8 demonstrates the comparison results between obtained data of the solvent extraction system and calculated values of these models. The experimental data based on the chemical reaction systems and data taken from Hemmati et al. (2015a, b) in the punctuated rotating disk contactor showed the excellent precision of the proposed models.



In addition to the experimental investigation of the impacts of operating parameters, column geometry, and reactive systems on the drop distributions, an endeavor has also performed to empowering some analytical methods of these impacts. In recent decades, many researchers have utilized the probability functions such as the normal and log-normal

functions for the analysis of distribution data in the extraction columns (Liu et al. 2013; Oliveira et al. 2008; Samani et al. 2012). The ratio of the number of droplets with a specified distance across to the number of the overall droplets is defined as a function of the probability density. These functions examined for analyticity the drop distribution data for the physical and chemical systems and presented as follows:

$$P_n = \frac{1}{0.27\pi\alpha} \exp\left(-\frac{(d_i - \beta)^2}{2\alpha^2}\right) \quad (36)$$

$$P_{\log} = \frac{1}{0.27\pi\alpha d_i} \exp\left(-\frac{(\ln d_i - \beta)^2}{2\alpha^2}\right) \quad (37)$$

In the above equation,  $d_i$  is denoted the function of number density, which utilized for fitting the data set of distribution functions. After a trial series, correlations of the theoretical distribution functions were calculated by the multiple linear regressions with consideration of the solvent extraction data as well as the data taken from Hemmati et al. (2015b). By considering the physical and reactive systems, the modified parameters of  $\alpha$  and  $\beta$  for each operational condition were correlated and have given below:

$$\alpha = C_3 \left( \frac{N^4 D_R^4 \rho_c}{\sigma g} \right)^{-0.093} \left( \frac{\mu_c^4 g}{\Delta \rho \sigma^3} \right)^{-0.018} \quad (38)$$

$$\beta = C_4 \left( \frac{N^4 D_R^4 \rho_c}{\sigma g} \right)^{-0.11} \left( \frac{\mu_c^4 g}{\Delta \rho \sigma^3} \right)^{-0.003} \left( 1 + \frac{V_c}{V_d} \right)^{-0.151} \quad (39)$$

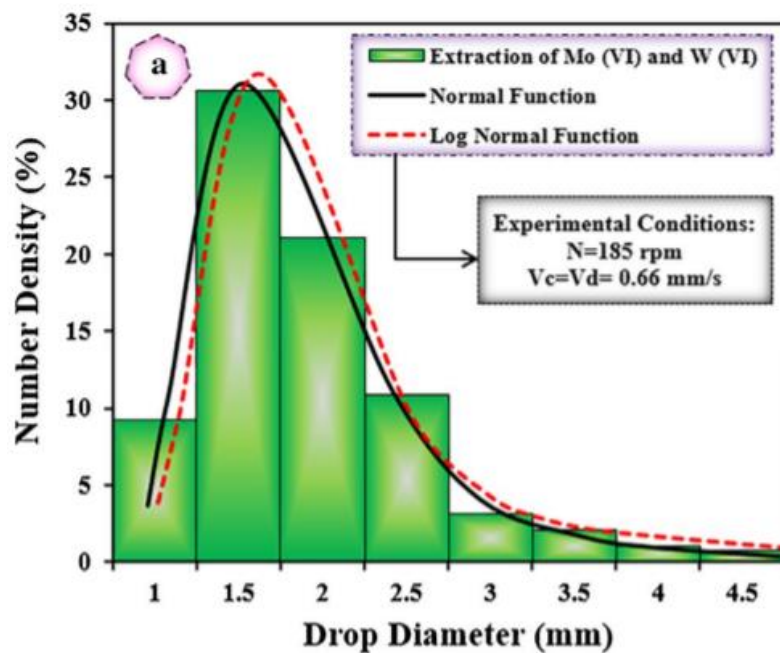
$$\alpha = C_5 \left( \frac{N^4 D_R^4 \rho_c}{\sigma g} \right)^{0.227} \left( \frac{\mu_c^4 g}{\Delta \rho \sigma^3} \right)^{-0.051} \quad (40)$$

$$\beta = C_6 \left( \frac{N^4 D_R^4 \rho_c}{\sigma g} \right)^{-0.174} \left( \frac{\mu_c^4 g}{\Delta \rho \sigma^3} \right)^{-0.013} \left( 1 + \frac{V_c}{V_d} \right)^{0.162} \quad (41)$$

Equations (38–39) and (40–41) have derived for the normal and log-normal functions, respectively. It should be noted that the Buckingham's pi-theorem has been used for obtaining the dimensionless numbers. The values of constant parameters (C3–C6) and their AARE are presented in Table 5 for the physical and reactive systems in the PRDC column.

System	Values of constants				AARE%			
	$C_3$	$C_4$	$C_5$	$C_6$	Eq. (38)	Eq. (39)	Eq. (40)	Eq. (41)
Physical system	6.125	5.836	0.089	2.794	8.03	8.77	10.27	10.46
Extraction stage	6.523	5.987	0.069	2.395	5.85	6.24	10.64	11.96
Stripping stage	5.698	5.548	0.096	2.878	5.26	6.06	10.96	12.68

The impact of agitation speed and interfacial tension on the drop distribution has larger than inlet phase velocities. A comparison of the experimental histograms for extraction and stripping stages with the mentioned distributions functions is indicated in Fig. 9



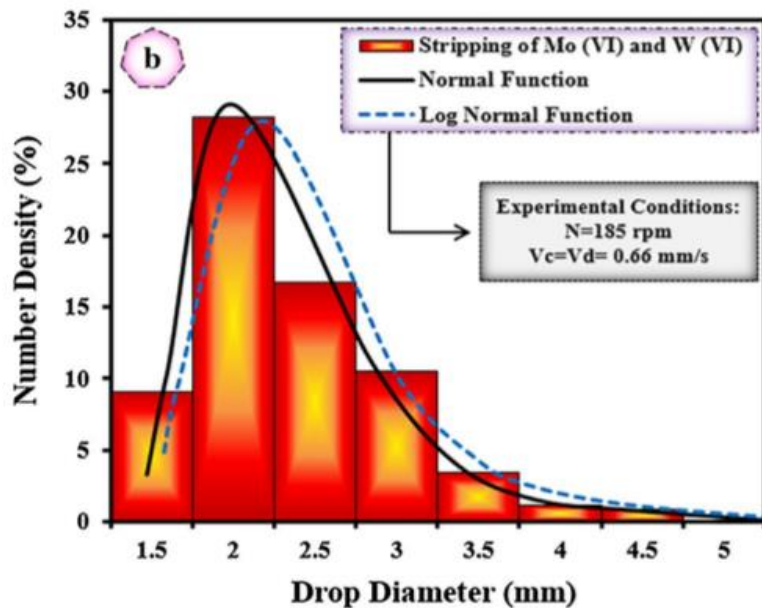


**Fig. 9** Comparison between theoretical distribution function and probability distribution functions in **a** extraction stage ( $c \rightarrow d$ ) and **b** stripping stage ( $d \rightarrow c$ )

## Conclusion

The agitation speed and type of the physical or reactive systems had a substantial influence on the drop size distribution, but weaker were the influences of phase velocities. A comparison of the previous models with the experimental data of solvent extraction systems was performed for predicting the holdup values, mean drop size, and drop size distribution, and the modified models were proposed for physical and reactive systems in the mentioned column. By considering the reactive systems, the evaluation of mass transfer data by the axial dispersion model was studied in the various ranges of agitation speed and inlet phase velocities in this column. It was found that the agitation speed and the ions transfer in the extraction and stripping stages had a significant impact on the column.

performance. Still, the inlet phase velocities had little impact on the volumetric overall mass transfer coefficients. The present experimental results were provided substantial information on the holdup values, mean drop size and drop size distribution, and mass transfer performance in the PRDC extractor under the chemical reaction systems.[27]

### List of symbols

AARE	Average absolute relative error (-)
$a$	Interfacial area ( $\text{m}^2/\text{m}^3$ )
$d_{32}$	Sauter mean drop diameter (m)
$D$	Distribution coefficient (-)
$D_{\text{col}}$	Column diameter (m)
$D_c$	Molecular diffusivity of continuous phase ( $\text{m}^2/\text{s}$ )
$D_R$	Disk diameter (m)
$D_S$	Stator ring diameter (m)

$E$	Axial mixing coefficient ( $\text{m}^2/\text{s}$ )
$E\%$	Extraction efficiency (-)
$g$	Acceleration due to gravity ( $\text{m}/\text{s}^2$ )
$H$	Effective height of the column (m)
$h_c$	Compartment height (m)
$K_{\text{oc}}$	Overall continuous mass transfer coefficient ( $\text{m}/\text{s}$ )
$K_c$	Continuous mass transfer coefficient ( $\text{m}/\text{s}$ )
$K_d$	Dispersed mass transfer coefficient ( $\text{m}/\text{s}$ )
$m$	Distribution ratio (-)
$N$	Agitation speed (l/s)
$N_{\text{oc}}$	Number of 'true' transfer unit (-)
$\text{Re}$	Reynolds number (-)
$\text{Sc}$	Schmitt number (-)
$P$	Péclet number (-)
$P_{n \text{ org log}}$	Probability of number density (-) for normal or logarithmic function
$\text{Pe}_c$	Continuous-phase Péclet number ( $= d_{32} V_s / D_c$ )
$[M]$	Concentration of metal ions (mg/L)

$[M]_{\text{aq, s}}$	Concentration of metal ions in the stripping solution (mg/L)
$V_{\text{org}}$	Volume of organic phase (ml)
$V_{\text{aq}}$	Volume of aqueous phase (ml)
$V_{\text{aq, s}}$	Volume of aqueous phase in the stripping solution (ml)
$d_e$	Equivalent diameter (m)
$d_i$	Droplet diameter (m)
$n_i$	Number of droplets of mean diameter $d_i$ (-)
SF	Separation factor (-)
SEF	Synergistic enhancement factor (-)
Sh	Sherwood number (-)
$S\%$	Stripping efficiency (-)
NDP	Number values of data points
$V$	Superficial velocity (m/s)
$\forall$	Specific volume ( $\text{m}^3$ )
$\overline{V}_c$	Continuous phase true velocity (m/s)
$V_s$	Slip velocity (m/s)
$x$	Mass fraction of elements in continuous phase (-)
$x^*$	Equilibrium mass fraction (-)
$y$	Mass fraction of elements in dispersed phase (-)

#### Greek letters

$\alpha$	Constant parameter of probability of density function (-)
$\beta$	Constant parameter of probability of density function (-)
$\rho_c$	Density of continuous phase ( $\text{Kg/m}^3$ )
$\rho_d$	Density of dispersed phase ( $\text{Kg/m}^3$ )
$\mu_d$	Viscosity of dispersed phase (pa.s)
$\mu_c$	Viscosity of continuous phase (pa.s)
$\varphi$	Dispersed phase holdup (-)
$\sigma$	Interfacial tension (N/m)
$\kappa$	Viscosity ratio of $\mu_d/\mu_c$

## References:

- [1] G. W. Stevens, T. C. Lo, and M. H. I. Baird, “Extraction, liquid-liquid,” *Kirk-Othmer Encycl. Chem. Technol.*, 2000.
- [2] R. Torkaman, M. Torab-Mostaedi, and M. Asadollahzadeh, “Studies of drop behavior and prediction of Sauter mean drop diameter in various rotary agitated extraction columns,” *Int. J. Eng.*, vol. 29, no. 8, pp. 1047–1055, 2016.
- [3] A. Kumar and S. Hartland, “Unified correlations for the prediction of drop size in liquid–liquid extraction columns,” *Ind. Eng. Chem. Res.*, vol. 35, no. 8, pp. 2682–2695, 1996.
- [4] D. Ramkrishna, *Population balances: Theory and applications to particulate systems in engineering*. Elsevier, 2000.
- [5] H. B. Jildeh, M. W. Hlawitschka, M. Attarakih, and H. J. Bart, “Solution of inverse problem with the one primary and one secondary particle model (OPOSPM) coupled with computational fluid dynamics (CFD),” *Procedia Eng.*, vol. 42, no. August, pp. 1692–1710, 2012, doi: 10.1016/j.proeng.2012.07.562.
- [6] H.-J. Bart, H. Jildeh, and M. Attarakih, “Population Balances for Extraction Column Simulations—An Overview,” *Solvent Extr. Ion Exch.*, vol. 38, no. 1, pp. 14–65, 2020.
- [7] S. Kumar and D. Ramkrishna, “On the solution of population balance equations by discretization - II. A moving pivot technique,” *Chem. Eng. Sci.*, vol. 51, no. 8, pp. 1333–1342, 1996, doi: 10.1016/0009-2509(95)00355-X.
- [8] J. Su, Z. Gu, and X. Y. Xu, “Advances in numerical methods for the solution of population balance equations for disperse phase systems,” *Sci. China Ser. B Chem.*, vol. 52, no. 8, pp. 1063–1079, 2009.
- [9] Jildeh, H. Liquid-Liquid Extraction Columns. Parameter Estimation, Dissertation, TU Kaiserslautern, Germany, “No Title,” 2015.

- [10] L. N. Gomes, M. L. Guimaraes, J. Stichlmair, and J. J. Cruz-Pinto, “Effects of Mass Transfer on the Steady State and Dynamic Performance of a Kühni Column—Experimental Observations,” *Ind. Eng. Chem. Res.*, vol. 48, no. 7, pp. 3580–3588, 2009.
- [11] H. J. Bart, H. Jildeh, and M. Attarakih, “Population Balances for Extraction Column Simulations—An Overview,” *Solvent Extr. Ion Exch.*, vol. 38, no. 1, pp. 14–65, 2020, doi: 10.1080/07366299.2019.1691136.
- [12] M. M. TORAB, J. Safdari, and M. Asadollahzadeh, “Mean drop size and drop size distribution in a hanson mixer-settler extraction column,” 2012.
- [13] J. O. Hinze, “Fundamentals of the hydrodynamic mechanism of splitting in dispersion processes,” *AIChE J.*, vol. 1, no. 3, pp. 289–295, 1955.
- [14] M. Abdelbasit and N. Salih, “Liquid-Liquid Equilibrium for the Design of Extraction,” *Eur. J. Eng. Technol.*, vol. 5, no. 4, pp. 18–36, 2017.
- [15] A. Ghaemi, “Experimental Investigation of Flooding and Drop Size in a Kuhni Extraction Column,” vol. 29, no. 3, pp. 288–296, 2016.
- [16] N. S. Oliveira, D. M. Silva, M. P. C. Gondim, and M. B. Mansur, “A Study of the drop size distributions and hold-Up in short kühni columns,” *Brazilian J. Chem. Eng.*, vol. 25, no. 4, pp. 729–741, 2008, doi: 10.1590/S0104-66322008000400010.
- [17] A. H. Tahershamsi, A. Ghaemi, and M. Shirvani, “Modeling and Simulation of Kuhni Extraction Column Using a Rate-based Model,” *Iran. J. Oil Gas Sci. Technol.*, vol. 5, no. 4, pp. 53–67, 2016.
- [18] A. H. Tahershamsi, A. Ghaemi, and M. Shirvani, “Modeling and Simulation of Kuhni Extraction Column Using a Rate-based Model,” vol. 5, no. 4, pp. 53–67, 2016.
- [19] M. Asadollahzadeh, M. Torab-Mostaedi, and R. Torkaman, “Drop behavior in a pilot plant asymmetric rotating disc extraction column for three various liquid–liquid systems,” *Chem. Eng. Res. Des.*, vol. 138, pp. 366–373, 2018, doi: 10.1016/j.cherd.2018.03.013.

- [20] M. . L.-L. E. C. D. C. Slater, “No Title,” *J. Chem. Eng.*, vol. 63, pp. 1004–1007, 1985.
- [21] M. Torab-Mostaedi, M., Ghaemi, A., Asadollahzadeh, “No Title,” *Chem. Eng. Res. Des.*, vol. 89, p. 2742-2751., 2011.
- [22] J. Mišek, T., Berger, R., Schroter, “No Title,” *Stand. test Syst. Liq. Extr. Stud.*, vol. Ser., EFCE, 1985.
- [23] M. Asadollahzadeh, M. Torab-Mostaedi, R. Torkaman, and J. Safdari, “A new model for prediction of drop size distribution in a liquid–liquid extraction column,” *RSC Adv.*, vol. 6, no. 86, pp. 82496–82504, 2016.
- [24] Mehdi Asadollahzadeh, Shahrokh Shahhosseini, Meisam Torab-Mostaedi, Ahad Ghaemi, “Drop Behavior in a Pilot Plant Oldshue-Rushton Extraction Column for Three Various Liquid-Liquid Systems ”, Separation and Purification Technology ,2015.
- [25] Benyamin Shakib , Rezvan Torkaman , Meisam Torab-Mostaedi & Mehdi Asadollahzadeh, “Exact hydrodynamic description of pilot plant Oldshue-Rushton contactor: a case study with the introduction of selenium and tellurium into reaction system”,2020
- [26] Alireza Hemmati, Meisam Torab-Mostaedi, Mansour Shirvani Ahad Ghaemi , “A study of drop size distribution and mean drop size in a perforated rotating disc contactor (PRDC)” ,2015
- [27] Benyamin Shakib, Rezvan Torkaman , Meisam Torab-Mostaedi,Mehdi Asadollahzadeh, “Revealing mass transfer and hydrodynamic efects in a PRDC column by using the integration of extraction and separation for molybdenum and tungsten ions from aqueous solution”,2020